

VARIABILITY AND PATHOGENESIS OF NEURODEVELOPMENTAL DEFICITS IN NOONAN SYNDROME

Dissertation

zur Erlangung des akademischen Grades

doctor rerum naturalium

(Dr. rer. nat.)

genehmigt durch die Fakultät für Naturwissenschaften

der Otto-von-Guericke-Universität Magdeburg

von: Franziska Altmüller, M.Sc.

geboren am: 05. März 1987 in Bad Hersfeld

Gutachter: Prof. Dr. med. Martin Zenker

Prof. Ype Elgersma, PhD

Eingereicht am: 19. Mai 2017

Verteidigt am: 15. November 2017

Summary

RASopathies comprise a group of disorders clinically characterized by short stature, heart defects, facial dysmorphism, varying degrees of intellectual disability and cancer predisposition. They are caused by germline mutations in genes encoding key components or modulators of the highly conserved RAS-MAPK signaling pathway and lead in general to dysregulation of cell signal transmission. For example, germline mutations in the genes encoding members of the RAS subfamily of GTPases are associated with variable phenotypes of the RASopathy spectrum, ranging from Costello syndrome (*HRAS* mutations) to Noonan and Cardiofaciocutaneous syndromes (*KRAS* mutations). Only a small number of cases with germline *NRAS* mutations have been reported previously. Affected individuals exhibited features fitting Noonan syndrome, and the observed germline mutations differed from the typical oncogenic *NRAS* mutations occurring as somatic events in tumors. The first part of this thesis describes the genotype and phenotype spectrum of 19 previously unpublished individuals with a RASopathy due to mutations in *NRAS*. Importantly, three of them harbored missense mutations affecting G12, which was previously described to occur exclusively in cancer. The phenotype in our cohort was variable but well within the RASopathy spectrum. Further, one of the patients (p.G12D) had a myeloproliferative disorder, and one individual (p.G12R) exhibited an uncharacterized brain tumor. This part of the thesis expands the genotype and phenotype spectrum of germline *NRAS* mutations and provides evidence that *NRAS* mutations do not spare the cancer-associated mutational hotspots.

Noonan syndrome is the most common type of RASopathies. Approximately 50% of cases of Noonan syndrome are caused by mutations in *PTPN11*. While the knowledge about mutations causing Noonan syndrome is steadily increasing, the molecular mechanism underlying the cognitive impairment seen in patients with Noonan syndrome is still poorly understood. In the second part of this thesis the generation of a new mouse model of Noonan syndrome is described that expresses the hyperactivated protein Shp2^{D61Y} from an endogenous locus in a restricted manner in excitatory neurons and astrocytes of the forebrain. Unlike mice with a global expression of this mutation, this strain is viable and without severe systemic impairments. Using dissociated hippocampal neurons, we found changes in the release of neurotransmitters from the presynapses and alterations in the surface expression of synaptic glutamate receptors, suggesting deficits in synaptic transmission and neuroplasticity in the hippocampus. Furthermore, we show that the basal ERK phosphorylation level is increased and that the activity-induced activation of ERK as well as the consequent regulation of gene expression is perturbed. This study uncovers the impaired activity-induced ERK phosphorylation and downstream gene expression in murine neurons expressing the hyperactive Shp2^{D61Y} and proposes that the aberrant activity-dependent gene expression contributes to the pathophysiology of cognitive deficits observed in Noonan syndrome.

Zusammenfassung

RASopathien umfassen eine Gruppe kongenitaler genetischer Störungen, die durch Kleinwuchs, Herzfehler, faziale Dysmorphie und einen unterschiedlichen Schweregrad kognitiver Beeinträchtigung sowie eine gewisse Tumorprädisposition gekennzeichnet sind. Keimbahnmutationen in Genen, die für Signalkomponenten oder –modulatoren des hochkonservierten RAS-MAPK Signalwegs kodieren, werden für dessen zelluläre Dysregulation und die Entstehung von RASopathien als ursächlich angesehen. Seltener sind Keimbahnmutationen in Genen, die für die Familie der RAS GTPasen codieren und sind mit einem eher variablen Phänotyp des RASopathie-Spektrums assoziiert. Dabei reicht das Spektrum von Costello-Syndrom (*HRAS* Mutationen) über Noonan-Syndrom und Cardio-facio-cutanes-Syndrom (*KRAS* Mutationen). Die bisherigen Berichte über Keimbahnmutationen in *NRAS* sind rar. Betroffene zeigen Noonan-typische Merkmale und die gefundenen *NRAS*-Keimbahnmutationen unterscheiden sich von dem bekannten onkogenen Spektrum der somatischen Mutationen in Tumoren ab. Der erste Teil dieser Dissertation beschreibt 19 neue RASopathie-Fälle mit Mutationen in *NRAS*. Dabei haben drei der beschriebenen Patienten eine Mutation an Position G12, eine Position, an der zuvor Mutationen ausschließlich in Tumoren gefunden wurde. Der Phänotyp der Kohorte erweist sich als variabel, liegt aber innerhalb des RASopathie-Spektrums. Dieser Teil der Dissertation soll das bekannte Genotyp-Phänotyp-Spektrum an *NRAS* Mutationen erweitern und zeigt, dass *NRAS* Mutationen ebenfalls an bekannten Krebs-assoziierten Hotspots vorkommen können und nicht wie bisher angenommen mit dem Leben unvereinbar sind.

Noonan-Syndrom gehört ebenfalls zur Gruppe der RASopathien. In circa 50 Prozent der Fälle von Noonan-Syndrom werden kausale Mutationen in *PTPN11* gefunden. Jedoch sind die molekularen Mechanismen, die zu den kognitiven Beeinträchtigungen in NS führen noch weitestgehend unbekannt. Im zweiten Teil dieser Dissertation wird ein neues Mausmodell mit einer *Ptpn11* Mutation charakterisiert, welche die überaktivierende Mutation von einem endogenen Locus und exklusiv in exzitatorischen Neuronen und Astrozyten des Vorderhirns exprimiert. Im Gegensatz zur globalen Expression dieser Mutation führt dies zu einem lebensfähigen Phänotyp ohne schwere systemische Beeinträchtigung. Anhand von dissoziierten neuronalen Kulturen dieses Mausmodells fanden wir Hinweise für Veränderungen in der Ausschüttung präsynaptischer Vesikel sowie eine veränderte synaptische Oberflächenexpression von Glutamat-Rezeptoren. Dies sind Mechanismen, die für die aktivitätsabhängige neuronale Plastizität von elementarer Bedeutung ist. Weiterhin ist die aktivitätsabhängige Phosphorylierung von ERK gestört und die darauffolgende Regulation der Genexpression ebenfalls beeinträchtigt. Diese Studie ist eine der ersten, die die

Folgen der gestörten RAS-MAPK Signalkaskade im Gehirn analysiert und spricht dafür, dass die aberrante prä- und postsynaptische Komposition sowie die Beeinträchtigung der Genregulation durch die ERK Dysregulation durchaus zu möglichen Pathomechanismen zählen, die zur kognitiven Beeinträchtigung in NS führen können.

Table of Contents

Summary	I
Zusammenfassung	II
1. Introduction	1
1.1. Noonan syndrome	2
1.1.1. Characteristic features and physical signs	2
1.1.2. Neurodevelopmental deficits	4
1.1.3. Genotype-phenotype correlations in NS	5
1.2. RASopathies	6
1.3. SHP2 and the RAS-MAPK signaling cascade	8
1.3.1. RAS-MAPK signaling cascade	8
1.3.2. ERK nuclear translocation and regulation of gene expression	12
1.4. <i>NRAS</i> mutations in human disorders	13
1.5. Molecular functions of SHP2	14
1.6. <i>PTPN11</i> mutations and SHP2 dysregulation in human disease	17
1.7. NS-associated animal models	18
1.8. Function of the RAS-MAPK pathway in neurons	21
1.9. Synaptic vesicle pools	23
1.10. Glutamate receptors	24
1.10.1. AMPA receptors	24
1.10.2. NMDA receptors	25
2. Material and Methods	28
2.1. Analysis of the <i>NRAS</i> mutations in a cohort of RASopathy patients	28
2.1.1. Subjects and phenotyping	28
2.1.2. Molecular analysis	28
2.2. <i>Shp2</i> ^{D61Y} animals	30
2.2.1. Breeding	30
2.2.2. Genotyping	31
2.2.3. Breeding statistics	34
2.2.4. SHP2-specific Protein Tyrosine Phosphatase Activity assay	34
2.2.5. Antibodies and chemicals	36
2.2.6. Primary hippocampal culture	37
2.2.7. Immunocytochemistry	39
2.2.8. BDNF pI+pII-EGFP and Synapto-pHlourin lentiviruses	41
2.2.9. Immunohistochemistry	43
2.2.10. Image analysis	44

2.2.11. Statistical Analysis.....	45
3. Results	46
3.1. Clinical and molecular spectrum of <i>NRAS</i> mutations	46
3.1.1. Spectrum of <i>NRAS</i> mutations.....	46
3.1.2. Clinical presentation of patients with <i>NRAS</i> mutations	46
3.2. Characterization of <i>Shp2</i> ^{D61Y} animals	54
3.2.1. Generation of <i>Shp2</i> ^{D61Y} mouse strain	54
3.2.2. Morphometric analyses of <i>Shp2</i> ^{D61Y} neurons	55
3.2.3. Surface expression of glutamate receptors in <i>Shp2</i> ^{D61Y} neurons	58
3.2.4. Reorganization of synaptic vesicle pools in <i>Shp2</i> ^{D61Y} neurons	61
3.2.5. Impairments of activity-induced phosphorylation of ERK in <i>Shp2</i> ^{D61Y} neurons	65
3.2.6. Impairments of activity-induced gene regulation in <i>Shp2</i> ^{D61Y} neurons	69
4. Discussion	72
4.1. Clinical and molecular spectrum of <i>NRAS</i> mutations	72
4.1.1. Spectrum of <i>NRAS</i> mutations.....	72
4.1.2. Conclusion	76
4.2. Characterization of the cognitive phenotype in <i>Shp2</i> ^{D61Y} animals	77
4.2.1. Generation of the <i>Shp2</i> ^{D61Y} mouse model	77
4.2.2. Absence of morphological alterations in <i>Shp2</i> ^{D61Y} neurons	78
4.2.3. Changes in the vesicle pool size in <i>Shp2</i> ^{D61Y} neurons.....	79
4.2.4. Alteration in the glutamate receptor abundancies in <i>Shp2</i> ^{D61Y} neurons	80
4.2.5. Disturbed activity-induced phosphorylation of ERK in <i>Shp2</i> ^{D61Y} neurons	83
4.2.6. Aberrant activity-dependent regulation of <i>BDNF</i> gene transcription and the transcriptional co-repressor CtBP1	84
4.2.7. Outlook and conclusion	85
5. Bibliography	89
5.1. References	89
5.2. Online references.....	106
6. Supplements	106
6.1. Supplementary figure.....	106
6.2. Supplementary table	107
6.3. List of abbreviations	108
6.4. List of Publications	111
6.5. Erklärung zur eigenständigen Verfassung der Arbeit	112

1. Introduction

In 1962, Dr. Jacqueline Noonan first described nine patients with similar facial features, pulmonary valve stenosis and multiple anomalies at a meeting of the Society for Pediatric Research. At that time, the designation “male Turner syndrome” was prevailing for males resembling this phenotype she described on the meeting. In 1968, she was the first to define this as a new syndrome associated with congenital heart defects, which also affects females and is clinically and etiologically different from Turner syndrome (Noonan 1968). In the same year, Kaplan and colleagues were the first ones to report a patient with “Noonan’s syndrome” (Kaplan et al. 1968). At that time the knowledge about Noonan syndrome (NS) was still in its very infancy but research has strongly progressed to the present time.

NS is a congenital developmental disorder and one of the most common monogenic diseases. It is not without reason that NS is called ‘the most common syndrome you’ve never heard of’ by the NS family support groups. During the last 15 years, many achievements of basic molecular genetic research have increased the knowledge about the pathogenesis of NS and many causative mutations have already been identified. However, the knowledge about the detailed pathogenesis of NS is still sparse. To investigate the genotype-phenotype correlations and especially the mechanisms behind the disease-specific organ dysfunctions still remains a challenging task for basic research. Gaining deeper insight into pathogenesis is still of great importance for the establishment of possible clinical treatment trials. The aim of my thesis was to combine these two important research fields: the first part outlines the clinical and molecular spectrum in patients with a RASopathy phenotype caused by a germline mutation in *NRAS*, which was published in Altmüller et al. (2017a) “Genotype and phenotype spectrum of *NRAS* germline variants” in the European Journal of Human Genetics. The second part of my thesis focusses on neuronal alterations caused by a gain-of-function mutation in *Ptpn11* investigated in a newly established mouse model. Parts of this study were published in Altmüller et al. (2017b) “Aberrant neuronal activity-induced signaling and gene expression in a mouse model of RASopathy” in PLoS Genetics.

1.1. Noonan syndrome

1.1.1. Characteristic features and physical signs

NS is an autosomal dominant congenital disorder with an estimated prevalence of 1:1000 to 1:2500 livebirths. NS belongs to a class of developmental disorders, collectively named RASopathies, which is linked to overactivating mutations in genes encoding for components of the RAS mitogen-activated protein/extracellular signal-regulated kinase (RAS-MAPK) signaling cascade (Zenker 2011). Clinical manifestations include typical craniofacial appearance, congenital heart defects, webbed neck, and postnatal reduced growth, cryptorchidism in males, eye abnormalities, hypotonia, and skeletal anomalies. A variable degree of developmental delay and intellectual disability, which is described in more detail in section 1.1.2, belongs to the key features of NS, too. The typical facial features include low-set posteriorly rotated ears, hypertelorism, low posterior hairline, broad forehead, and ptosis (see Figure 1.1). These very distinctive appearances tend to fade with age making diagnosis more difficult in adulthood. NS characteristics are variable in expression and can manifest in almost all organs (Romano et al. 2010, Tartaglia et al. 2010).



Figure 1.1: Clinical photograph documenting the craniofacial phenotype of NS. NS patient with an I24N mutation in *NRAS* at the age of 10 years. Note the broad forehead, down slanting palpebral fissures, ocular ptosis, hypertelorism and low-set ears that belong to the main characteristics of facial features in NS. Moreover, he has a short and broad (webbed) neck and widely spaced nipples. This image is exemplarily taken from the patient cohort described in Part 1 of this thesis and adapted from Altmüller et al. (2017a). Written consent from the patient's legal guardian for publication of the image was obtained.

First possible hints for the clinical diagnosis of NS are prenatal findings like an increased nuchal translucency, pleural effusions, a fetal heart defect, and/or polyhydramnios seen in ultrasound, which can also complicate pregnancy (Roberts et al. 2013). Children regularly also present with feeding difficulties, failure to thrive, recurrent vomiting, and gastroesophageal reflux making tube-feeding necessary in severe cases. Typically the period of severe feeding problems is limited and resolves after 18 months (Romano et al. 2010). After trisomy 21, NS is the second most common syndrome with congenital heart defects. The heart defects itself vary in severity and characteristics with pulmonary stenosis and hypertrophic cardiomyopathy being most frequently found (Prendiville et al. 2014). A wide range of other lesions, including atrioventricular septal defects and aortic stenoses, are also observed (Tartaglia et al. 2010). Usually birth weight and body length are normal, but a postnatal onset of growth retardation and subsequent short stature with relative macrocephaly is common in NS (Roberts et al. 2013). Puberty is usually delayed in both sexes and is characterized by a diminished pubertal growth spurt (Romano et al. 2010). However, a delay in the pubertal growth spurt does not necessarily lead to short stature in adulthood, possibly because the time span when growth occurs is also prolonged. Growth hormone deficiency can also occur. Growth retardation can be caused by abnormalities in growth hormone (GH) and IGF1 signaling since elevated serum GH levels and low serum IGF-I levels are found in some NS patients suggesting GH insensitivity (Noonan and Kappelgaard 2015). Skeletal malformations associated with NS typically include scoliosis and pectus deformities. The latter are observed in the vast majority, but usually do not require surgical intervention. Scoliosis occurs in approximately 10% of patients. Other bony defects, such as vertebral anomalies, occur at low frequency (Tartaglia et al. 2010). More than 80% of the affected individuals display abnormalities in their visual function. Hearing loss is reported less frequently but data are variable (Cremers and van der Burgt 1992, Qiu et al. 1998, Tartaglia et al. 2010). Ectodermal anomalies and lymphatic dysplasia are also common. The cutaneous involvement can include keratosis pilaris/hyperkeratotic skin, sparse eyebrows (Tartaglia et al. 2010). Lymphatic issues in NS are estimated to occur in about 20% of the cases including peripheral lymphedema, hydrops, and lymphangiectasis, complicating the management of these conditions (Romano et al. 2010). The typical facial features and other characteristics like the webbed neck (pterygium colli), widely-spaced nipples and cryptorchidism in males are believed to result from lymphatic obstructions or dysfunction during embryonic development (Roberts et al. 2013). Infants with NS often also present with hematological disorders, like easy bruising and bleeding diathesis due to coagulation defects (Kratz et al. 2011, Kratz et al. 2015). Individuals with NS also have a slightly increased risk to develop neoplasias, depending on the

specific gene mutation. Recurrently observed NS-associated neoplasias include juvenile myelomonocytic leukemia (JMML), giant cell lesions of the jaws, rhabdomyosarcoma and brain tumors (Tartaglia et al. 2011, Zenker 2011, Strullu et al. 2014, Kratz et al. 2015). JMML, a severe myeloproliferative disorder of infancy, is particularly associated with mutations of the RAS-MAPK pathway, with somatic mutations in *PTPN11*, *KRAS* and *NRAS*, and loss of neurofibromin function accounting for a majority of cases (Niemeyer 2014). Somatic *PTPN11*, *KRAS*, and *NRAS* mutations found in JMML are assumed to have a stronger impact on cellular physiology, which implies their incompatibility with life, if these mutations occur in germline (Tartaglia and Gelb 2010).

1.1.2. Neurodevelopmental deficits

In an early study in 1992 that included 151 individuals with clinical signs of NS, a delay in achieving motor milestones was commonly described: Unsupported sitting is reported with 10 months and walking with 21 months of mean age (Sharland et al. 1992). This can be attributed at least in part to hypotonia often observed in these children (Tartaglia et al. 2010). Individuals with NS tend to be clumsier and have a poor coordination (Wood et al. 1995).

Language impairments are common among individuals with NS. First spoken two-word-sentences occur a mean age of 31 months (Sharland et al. 1992). The verbal abilities are usually slightly impaired, while the visual and spatial domains of learning and memory are relatively preserved (Lee et al. 2005, Alfieri et al. 2011). This makes childhood intelligence an important predictor of adult intelligence. While the cognitive performance of individuals with NS in general can reach a normal level in adulthood, the verbal IQ does not develop proportionately and requires additional support for the improvement of verbal skills. However, most of the difficulties during childhood tend to ease in adulthood (Roelofs et al. 2016). Most affected individuals have normal to low IQs between 70 and 120, with a mean IQ of 84. Of note, 10% to 40% of individuals with NS require special education and IQ is usually about 10 points lower than the familial background (van der Burgt et al. 1999, Lee et al. 2005). Memory tasks depending on prefrontal-hippocampal networks are more challenging for individuals with NS than tasks depending on cortical regions (Pierpont et al. 2013). Attention deficit/hyperactivity disorder (ADHD) has been reported, too (Verhoeven et al. 2008). Social interaction impairments, alexithymia (the inability express its own emotions), and problems in emotional perception have been reported, too (Verhoeven et al. 2008). Children with NS often show stubbornness. Individuals with NS can also have a poor self-esteem, depression, and social

inadequate behavior, but reported data are limited (Romano et al. 2010). Lack of social life and the inability to fit into it represent the main problem. However, most individuals describe their quality of life as satisfactory or good. The majority of adults with NS finishes high school and has paying jobs, contributing to a good quality of life (Shaw et al. 2007, Romano et al. 2010).

1.1.3. Genotype-phenotype correlations in NS

Up to now 13 genes are already identified to cause NS: *PTPN11*, *SOS1*, *RAF1*, *RIT1*, *KRAS*, *CBL*, *NRAS*, *SOS2*, *BRAF*, *LZTR1*, *SHOC2*, *MEK1*, and *RRAS* (in descending frequency according to the NSEuroNet Database)(Nava et al. 2007, Aoki et al. 2013, Roberts et al. 2013, Flex et al. 2014, Yamamoto et al. 2015). Importantly, all genes encode for members or modulators of the RAS-MAPK signaling cascade. More than 50% of the mutations causing NS are found in *PTPN11*, encoding for the Protein Tyrosine Phosphatase SHP2. These mutations are typically gain-of-function (GOF) mutations clustering in important regulatory domains of SHP2 that shift the protein conformation towards a constitutively active state (Tartaglia and Gelb 2010).

Distinct genotype-phenotype correlations emerged in NS during the past decade (Figure 1.2). Mutations in *PTPN11* usually cause the “classical” NS associated with distinct facial features, short stature and heart defect (typically pulmonary valve stenosis or atrial septal defects), pectus deformities, bleeding disorders, and predisposition for JMML. Interestingly, *PTPN11*^{N308} mutations were found to be less frequently associated with cognitive impairments in comparison to other *PTPN11* mutations that are associated with stronger cognitive impairments (Pierpont et al. 2009, Roberts et al. 2013). In contrast, mutations in *KRAS* are considered to be generally more variable including more severe intellectual impairment (Carta et al. 2006). Mutations in *SOS1* are linked to marked skin abnormalities as found in Cardiofaciocutaneous syndrome (CFCS) and pulmonary valve stenosis, but patients usually show linear growth and a low prevalence of cognitive impairment (Tartaglia et al. 2007, Lepri et al. 2011). Hypertrophic cardiomyopathies frequently occur in NS patients with *RAF1* mutations (Pandit et al. 2007, Lee et al. 2011). Mutations in *BRAF* are typically associated with CFCS (see paragraph 1.2.), but are also found in severe forms of NS with neonatal growth failure, variable feeding difficulties, short stature, dysmorphic facial features, mild-to-moderate cognitive deficits, developmental delay, skeletal anomalies and hypotonia (Sarkozy et al. 2009, Lee et al. 2011).

Genotype-phenotype-correlations of rarer mutations are still preliminary and call for further investigations, especially subtypes of NS that are not caused by mutations in *PTPN11* a much lower general prevalence. Thus, only a limited number of cases were studied and it is not possible yet to draw reliable conclusions.

1.2. RASopathies

RASopathies have recently been introduced as a collective term to describe the group of genetic disorders with dysregulation of the RAS-MAPK pathway as the common underlying mechanism (see Figure 1.2)(Tidyman and Rauen 2009), of which NS is the most frequent one (Rauen 2013). The other congenital disorders are rare but especially in the first years of life, the phenotypic overlaps are high between the single conditions and a clear distinction between the single conditions is not always possible. However, each syndrome is characterized by its own features. Interestingly, the comparison of cognitive abilities in all RASopathies shows a clear trend that mutations in components of the RAS-MAPK pathway located upstream of RAS in the cascade have only a milder effect on cognitive abilities. Mutations in signaling molecules downstream of RAS show more severe impairments in cognitive abilities (Cesarini et al. 2009).

Cardiofaciocutaneous syndrome (CFCS, OMIM: 115150) is a very rare condition caused by mutations in *BRAF*, *KRAS*, *MEK1*, and *MEK2*. Epidemiological studies providing a clear prevalence in Europe are lacking, as it is true for most of the RASopathies. CFCS is characterized by distinctive facial appearance, cardiac malformations, ectodermal, gastrointestinal, ocular, and musculoskeletal abnormalities, and short stature. Affected individuals have very thin and usually curly hair and dystrophic nails. Cognitive delay ranges from mild to severe but is typically significantly more severe than in NS (Rauen 1993, Tidyman and Rauen 2009).

Costello syndrome (CS, OMIM: 218040) is characterized by severe postnatal feeding difficulties and resulting failure to thrive during infancy, short stature, developmental delay, intellectual disability, heart defect, macrocephaly, and increased risk for the development of neoplasias. The typical NS-like facial features are present, but the traits are coarser and affected individuals usually have loose soft skin with deep palmar and plantar creases. Mutations are exclusively found in *HRAS* (Gripp and Lin 1993, Tidyman and Rauen 2009).

Noonan syndrome with loosen anagen hair (NSLAH, OMIM: 607721) is caused exclusively by mutations in *SHOC2*, also known as Mazzanti syndrome. Affected individuals

present with facial features typical of NS, short and webbed neck, redundant skin, hypernasal voice, enlarged cerebrospinal fluid spaces, mild psychomotor delay, hyperactivity, and ectodermal abnormalities with generally darkly pigmented and hairless skin. The hair is easily pluckable, sparse, thin, slow growing and usually silver-blond. Growth hormone deficiency is frequent. Developmental delay and intellectual disability tend to be slightly more pronounced than in NS in general (Mazzanti et al. 2003, Cordeddu et al. 2009).

Noonan syndrome with multiple lentigines (NSML, OMIM: 151100), formerly known as LEOPARD syndrome is a rare autosomal dominant disorder. The acronym stands for multiple **L**entigines, **E**KG abnormalities, **o**cular hypertelorism, **p**ulmonary valve stenosis, **a**bnormal genitalia, **r**etardation of growth, and **d**eafness and together with mild intellectual disability describe the main characteristics. Distinct mutations in *PTPN11* and *RAF1* are known to cause NSML. In contrast to NS, mutations in *PTPN11* causing NSML result in reduced SHP2 catalytic activity (Gelb and Tartaglia 1993, Tidyman and Rauen 2009).

Neurofibromatosis type 1 (NF1, OMIM: 162200) is an autosomal dominant disorder caused by heterozygous loss of Neurofibromin. NF1 is characterized by the presence of six or more café au lait macules, axillary freckling, and later on the development of multiple cutaneous neurofibromas and iris Lisch nodules. The NS-like facies, scoliosis, learning disabilities, macrocephaly, and a certain tumor predisposition are accompanying the skin abnormalities (Friedman 1993, Tidyman and Rauen 2009).

Legius syndrome (LS, OMIM: 611431) or NF1-like syndrome is associated with the heterozygous loss of *SPRED1* and a very rare autosomal dominant condition. An exact prevalence is not known. Its characteristics comprise multiple café au lait spots without neurofibromas or other tumor manifestations typical for NF1. Additional clinical manifestations include freckling, lipomas, macrocephaly, and learning disabilities and developmental delay (Stevenson et al. 1993, Tidyman and Rauen 2009).

Neurofibromatosis-Noonan syndrome (NFNS, OMIM: 601321) harbors traits of both syndromes, but patients normally have a single *NF1* mutation. Double-heterozygosity for *NF1* and *PTPN11* mutations rarely cause NFNS. Usually patients present with lower incidence of plexiform neurofibromas, skeletal anomalies, internal tumors, the NS-typical facies and congenital heart defect (Tartaglia et al. 2010).

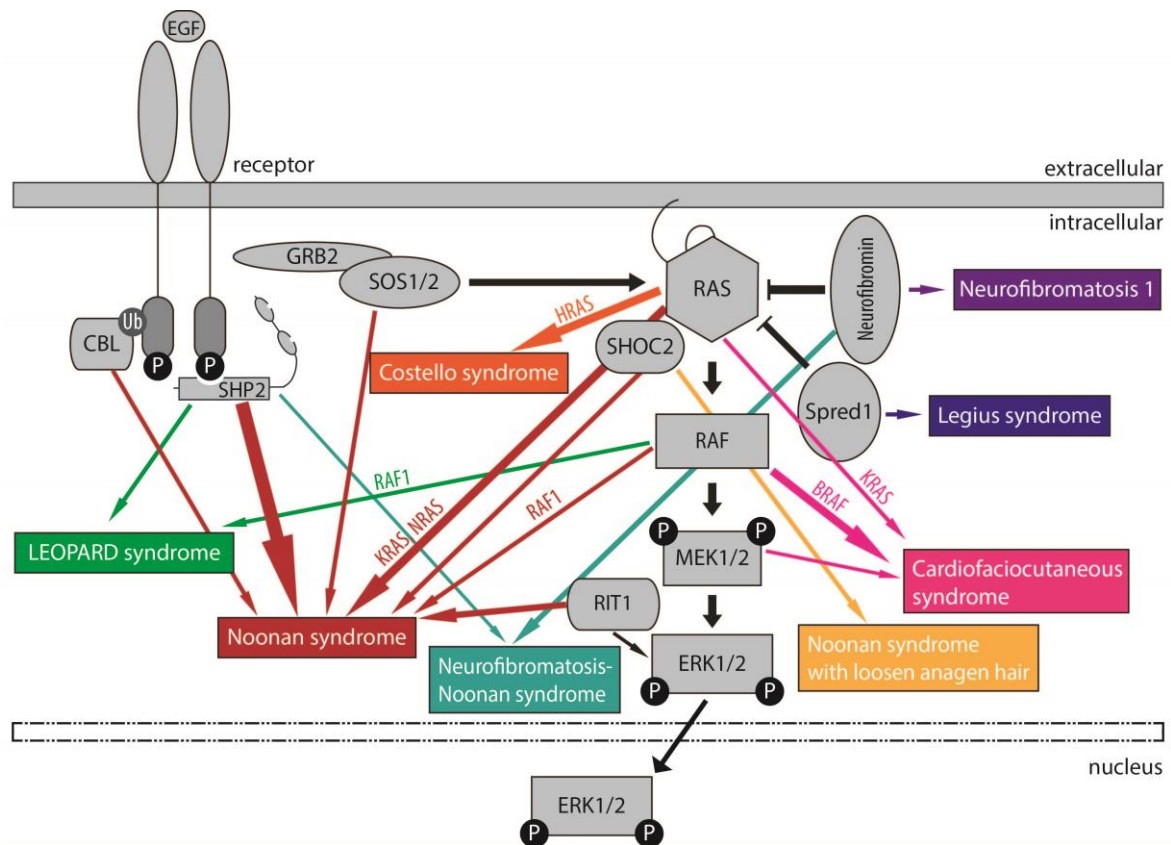


Figure 1.2: Genotype-Phenotype correlation of RASopathies. Each disorder is linked to mutations in genes of the respective members of the RAS-MAPK signaling cascade. Of note, only the major members of RAS-MAPK signaling causing RASopathies are depicted here. Colors represent the different syndromes. The thickness of the arrow is related to the frequency of mutations causing the respective syndrome. This figure is adapted from Prof. Dr. Martin Zenker.

1.3. SHP2 and the RAS-MAPK signaling cascade

In the following, more details about the molecular functions of SHP2 and the RAS-MAPK signaling cascade are provided and depicted in Figures 1.3 and 1.4.

1.3.1. RAS-MAPK signaling cascade

In general, the MAPK signaling cascade is a highly conserved pathway that transduces extracellular stimuli via cytoplasmic signaling proteins to the nucleus. It is involved in the control of many cellular processes such as growth, proliferation, differentiation, migration, and apoptosis. MAPK signaling can be activated in response to cytokines, hormones, and growth factors binding to cell surface receptors and interacts with other cellular signaling pathways resulting in its complex regulation. Dysregulation of this cascade is associated with RASopathies and, most prominently, various forms of cancer. MAPK pathways are constituted of a three-

tier kinase module in which a MAPK is activated upon phosphorylation by a mitogen-activated protein kinase kinase (MAPKK), which in turn is activated when phosphorylated by a mitogen-activated protein kinase kinase kinase (MAPKKK). There are several MAPK pathways known, and the best studied mammalian cascade is the RAS-RAF-ERK pathway (see Figure 1.4) (Dhillon et al. 2007). All MAPK pathways can be divided into five steps that are explained in detail in the following for the RAS-RAF-ERK pathway.

Activation of the cascade:

Ligand binding to the extracellular domain of the transmembrane tyrosine kinase receptors on the cell surface leads to the dimerization and auto-phosphorylation of the intracellular domains of the receptor. This autophosphorylation is required for the recruitment of the signaling complex composed of guanine nucleotide exchange factors (GEFs) Son of sevenless 1 or 2 (SOS1/2) and the growth factor receptor-bound protein 2 (GRB2). GEFs at the plasma membrane catalyze the release of guanosine diphosphate (GDP) from the nucleotide-binding pocket of RAS. Free RAS rapidly binds guanosine triphosphate (GTP), which is in excess in the cytoplasm. The GTP-bound RAS as the active form can interact with its downstream target RAF and activate it (Quilliam et al. 1995, Tartaglia et al. 2010).

The G-Protein: RAS

More than three decades ago, the Rat Sarcoma Virus (RAS) genes were first described and identified as key players in tumorigenesis. Harvey-, Kirsten- and neuroblastoma-RAS (*HRAS*, *KRAS*, and *NRAS*) encode for the three highly homologous members of the mammalian RAS subfamily of small monomeric GTPases (Barbacid 1987). However, the entire RAS superfamily consists of more than 30 human genes (Wennerberg et al. 2005). RAS proteins belong to the group of small GTPases, which possess a low intrinsic GTP hydrolysis activity and thus are capable of the dephosphorylation of a GTP molecule bound to their nucleotide-binding pocket to GDP. These small GTPases act as molecular switches (see Figure 1.3), as specific changes in their three-dimensional conformation depending on the binding of either GTP or GDP determine their capacity to bind and activate downstream signaling molecules like RAF. The major conformational changes involve the Switch I and Switch II regions of RAS that bind to the γ -phosphate of GTP. After GTP hydrolysis, the switch regions return to a relaxed conformation. RAS activity is regulated by two different classes of enzymes that regulate cycling of RAS proteins between a GDP-bound inactive conformation and a GTP-bound active form: GEFs that induce the exchange of GDP by GTP (see above), thereby promoting RAS

activation, and GTPase activating proteins (GAPs) that accelerate the relatively low intrinsic GTPase activity of RAS, thereby returning to its inactive conformation. The interaction of RAS with receptor associated GEFs is significantly facilitated by RAS prenylation, which leads to its targeting to the plasma membrane. Activated RAS then promotes the translocation of RAF to the plasma membrane, where additional phosphorylation events promote the full activation of RAF (Vetter and Wittinghofer 2001, Tartaglia and Gelb 2010, Tartaglia et al. 2010).

Neurofibromin and Spred1 are involved in negative feedback loops regulating RAS-MAPK signaling by increasing the GTPase activity of RAS. Neurofibromin contains a GAP-related domain and is known to act as a brake on cellular signaling through the RAS-MAPK cascade through its function as GAP for RAS. The loss or inactivation of neurofibromin can lead to an unconstrained cell proliferation (Trovo-Marqui and Tajara 2006). Spred1 acts in a similar way as a brake on RAS-MAPK signaling (Figure 1.4D). Spred proteins can form a complex with RAS and in this way suppress the phosphorylation and activation RAF (Wakioka et al. 2001).

MAPKKK: RAF

RAF1 (CRAF), ARAF and BRAF are serine-threonine kinases that function downstream of RAS. Under basal conditions, the inactive state of RAF is maintained by the binding of 14-3-3 dimers. The recruitment of RAF to the plasma membrane, which is initiated by activated (GTP-bound) RAS, is an essential step in its activation and depends on the concerted action of the RAS-Binding domain (RBD) and the cysteine-rich domain CRD of RAF. Via the RBD RAF can interact with the effector loop of RAS isoforms that are themselves anchored to the plasma membrane. Once recruited to the plasma membrane the inhibitory 14-3-3 binding dissociates. Then RAF is phosphorylated at its activation loop, undergoes conformational changes, and dimerizes, leading to its full activation at the plasma membrane. RAF kinases phosphorylate and thereby activate the dual specificity kinases MEK1 and MEK2 as their main downstream targets (Baljuls et al. 2013, Lavoie and Therrien 2015).

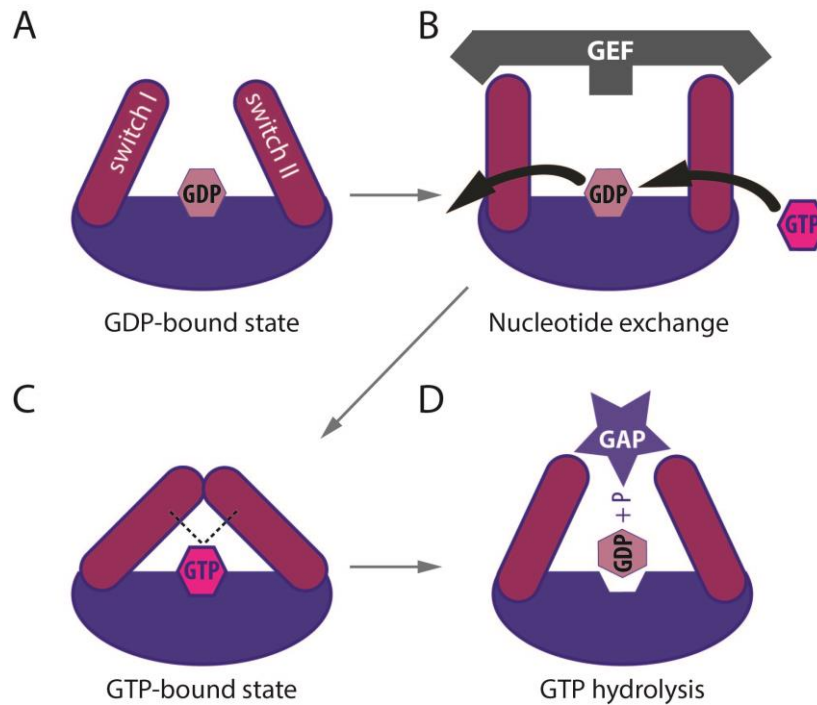


Figure 1.3: Schematic diagram of RAS activation and deactivation. (A) In the inactive state has bound GDP and the switch I and switch II regions, displayed as the small arms, remain in a relaxed conformation. **(B)** A GEF is needed for GDP to be released. A new GTP molecule can bind to the active site. **(C)** The GTP-bound state is stabilized by backbone interactions of the γ -phosphate of GTP in two sequence motifs located in the switch I and switch II region and. **(D)** The intrinsic GTP hydrolysis of RAS and a GAP function together to eject the GTP molecule and to return the protein to an inactive state. The release of the γ -phosphate (P) after GTP hydrolysis allows the switch regions to return to the relaxed conformation. This figure is based on Vetter and Wittinghofer (2001).

MAPKK: MEK

MEK1 and MEK2 are dual-specificity protein kinases that are activated by phosphorylation of two Serine residues (S218 and S222 in MEK1) in their activation loop. Upon activation, MEK mediates the phosphorylation and activation of human ERK1/2 at Tyr204/187 and then Thr202/185. Interestingly, ERKs are so far the only known physiological substrates of MEK (Shaul and Seger 2007). Moreover, MEK functions as a cytoplasmic anchor and nuclear export shuttle for ERK (Fukuda et al. 1997).

MAPK: ERK

ERK1 and 2 are serine/threonine protein kinases and modulate the activity state of many cytoplasmic and nuclear proteins. MEK1 and 2 catalyze the phosphorylation of ERK1/2, which is required for the enzymatic activation of ERK1/2. Whereas RAF and MEK have narrow substrate specificities, ERK1/2 have hundreds of cytoplasmic and nuclear substrates including

regulatory molecules and transcription factors (Busca et al. 2016). ERKs function and downstream signaling targets are explained in more detail in the following chapter.

1.3.2. ERK nuclear translocation and regulation of gene expression

The transient nuclear translocation of ERK is required for the regulation of gene expression in response to growth factor stimulation (Brunet et al. 1999). The MEK-dependent phosphorylation of ERK is necessary, but still not sufficient for the nuclear translocation of ERK and a phosphorylation-independent event or component is needed additionally (Caunt and McArdle 2010). MEK and many ERK substrates contain a Docking (D) domain or DEF (docking site for ERK and FXFP) that are made of a cluster of positively charged residues with two or more hydrophobic residues and serve as specificity determinants in ERK signaling (Raman et al. 2007). MEK functions as a cytoplasmic anchor for inactive ERK (Fukuda et al. 1997). Due to its nuclear export signal (NES), MEK is mainly cytosolic. Upon activation by phosphorylation, MEK phosphorylates ERK enabling their dissociation and translocation of ERK into the nucleus (Fukuda et al. 1997, Adachi et al. 1999). ERK does not contain intrinsic nuclear localization or export signals and depends on the dynamic association with a huge variety of proteins for its proper subcellular targeting (von Kriegsheim et al. 2009). ERK activated by phosphorylation (pERK) can either translocate into the nucleus as a monomer by passive diffusion or as a dimer requiring active transport through Ran GTPase and β -importins or direct interaction with the nuclear pore complex (NPC) (Torii et al. 2004). The passive transport is energy- and transport factor-independent and involves ERK binding to phenylalanine-repeats of nucleoporins in the NPC (Raman et al. 2007). Whether ERK has a nuclear anchor is still under debate (Torii et al. 2004). The nuclear export of ERK is primarily not based on new protein synthesis. Furthermore, MEK, the upstream partner of ERK is also able to shuttle between the cytosol and the nucleus and is suggested to be involved in the nuclear export of ERK. It is suggested, that the nuclear export of ERK involves a MEK-dependent, active export mechanism. Inactivated ERK preferentially binds to MEK, which is one way to rapidly export ERK from the nucleus (Adachi et al. 2000). Targets of pERK include transcription factors, cytoskeletal proteins, regulatory enzymes, and other kinases. pERKs are capable of modulating gene expression by phosphorylating transcription factors and other activating kinases, which then phosphorylate proteins involved in gene expression (Pearson et al. 2001). There is a huge variety of possibilities of ERK activation and modulating gene transcription, as well as other nuclear and cytoplasmic downstream effects of ERK activation.

1.4. *NRAS* mutations in human disorders

RAS genes are frequently mutated in malignancies. While mutations in individual *RAS* genes have a different prevalence in human cancers, their oncogenic mutations almost invariably affect codons 12, 13, and 61, leading to constitutive activation of the transducer and upregulation of downstream signaling pathways (Bos 1989). *NRAS* harbors the second most somatic mutations reported in cancer (Forbes et al. 2015). Somatic mutations in *NRAS* are found in more than 15% of skin cancer and affect almost 10% of hematopoietic and lymphoid cancer and more than 6% of solid tumors in thyroid and meninges (COSMIC Database, Forbes et al. (2015)). Of the malignancies affecting hematopoietic and lymphoid tissues, *NRAS* mutations are found in approximately 20% of patients with juvenile myelomonocytic leukemia (JMML). This aggressive pediatric myelodysplastic syndrome is characterized by its early onset in childhood and usually severe progression (Flotho et al. 1999, Lauchle et al. 2006). Additionally, The Cancer Genome Atlas Research Network (2013) analyzed the genomes of 200 clinically annotated adult cases of *de novo* acute myeloid leukemia (AML, OMIM 601626) and identified recurrent mutations in the *NRAS* gene in 15 samples.

The congenital melanocytic nevi syndrome (CMNS, OMIM 137550) can be also caused by mutations in *NRAS*. Here, the somatic mutations are restricted to codon 61 of *NRAS* and are found in a mosaic fashion in the affected tissues, but not in blood samples of the patients, which excludes the possibility of germline mutations. The occurrence of mutations in members of the RAS-MAPK pathway in a somatic mosaic pattern raised term “mosaic Rasopathy” (Kinsler et al. 2013).

In 2010, heterozygous germline mutations in *NRAS* were identified as a rare cause of NS (Cirstea et al. 2010). A total number of 19 patients from 13 unrelated families have been reported previously (Cirstea et al. 2010, Digilio et al. 2011, Runtuwene et al. 2011, Denayer et al. 2012, Kraoua et al. 2012, Ekvall et al. 2015). Importantly, the reported *NRAS* mutations causing NS do not affect the oncogenic hotspots and appear to be functional hypomorphs compared to the cancer-associated somatic mutations (Cirstea et al. 2010, Runtuwene et al. 2011, Denayer et al. 2012). It was previously assumed that germline mutations in *NRAS* affecting the known oncogenic hotspots in codons 12, 13 and 61 are not compatible with life and might lead to embryonic lethality. We were able to present the first report to show that apparent non-mosaic germline mutations in *NRAS* affecting one of these hotspots for oncogenic variants may be compatible with life and lead to a clearly recognizable RASopathy phenotype (Altmüller et al. 2017a).

1.5. Molecular functions of SHP2

Phosphorylation of tyrosine residues of extracellular receptors as response to external stimuli or intracellular proteins is a major mechanism to control signal transduction and activity states of proteins as intracellular signal transducers. The tight control of phosphorylation and dephosphorylation events by protein tyrosine kinases and protein tyrosine phosphatases, respectively, represents an important mechanism in controlling intracellular signal transduction.

The Src homology2 (SH2) domain containing protein tyrosine phosphatase SHP2, encoded by *PTPN11*, is one of these signal transducers controlling the phosphorylation state by dephosphorylating intracellular interaction partners. Together with SHP1, it comprises the small family of SH2-containing non-receptor protein tyrosine phosphatases. SHP2 consists of two tandem SH2-domains (N-SH2 and C-SH2) located at the N-terminus followed by a protein tyrosine phosphatase (PTP) catalytic domain and a C-terminal tail with two tyrosine-phosphorylation sites and a proline-rich stretch (Figure 1.4A). The D'E-loop connecting two β sheets of the N-SH2 domain is able to insert into the PTP domain's catalytic site. This change in the conformation serves as intramolecular switch. Within the D'E-loop the amino acid D61 is located and is able to form hydrogen bonds with the amino acid C459 of the PTP domain, thereby inducing the conformational change and auto-inhibition of the protein resulting in the "OFF-state" of SHP2 (Figure 1.4B) (Barford and Neel 1998, Hof et al. 1998, Neel et al. 2003). The binding of phospho-tyrosine-containing activators like the GRB2-associated binding protein 1 (GAB1) to the SH2 domains weakens the intramolecular interaction between N-SH2 and PTP domain. A conformational switch makes the catalytic pocket available for its substrates and the phosphatase is in its functional "ON-state" (Figure 1.4C). The C-SH2 domain is not directly involved in ligand binding but regulates its specificity (Hof et al. 1998). The C-terminal tail of SHP2 can mediate the interaction with SH3 domain-containing proteins, although the precise role remains unclear. Via the two SH2-domains, SHP2 is able to bind selectively to phosphotyrosine residues and promote the association with cell surface receptors, cell adhesion molecules, and scaffolding molecules (Neel et al. 2003).

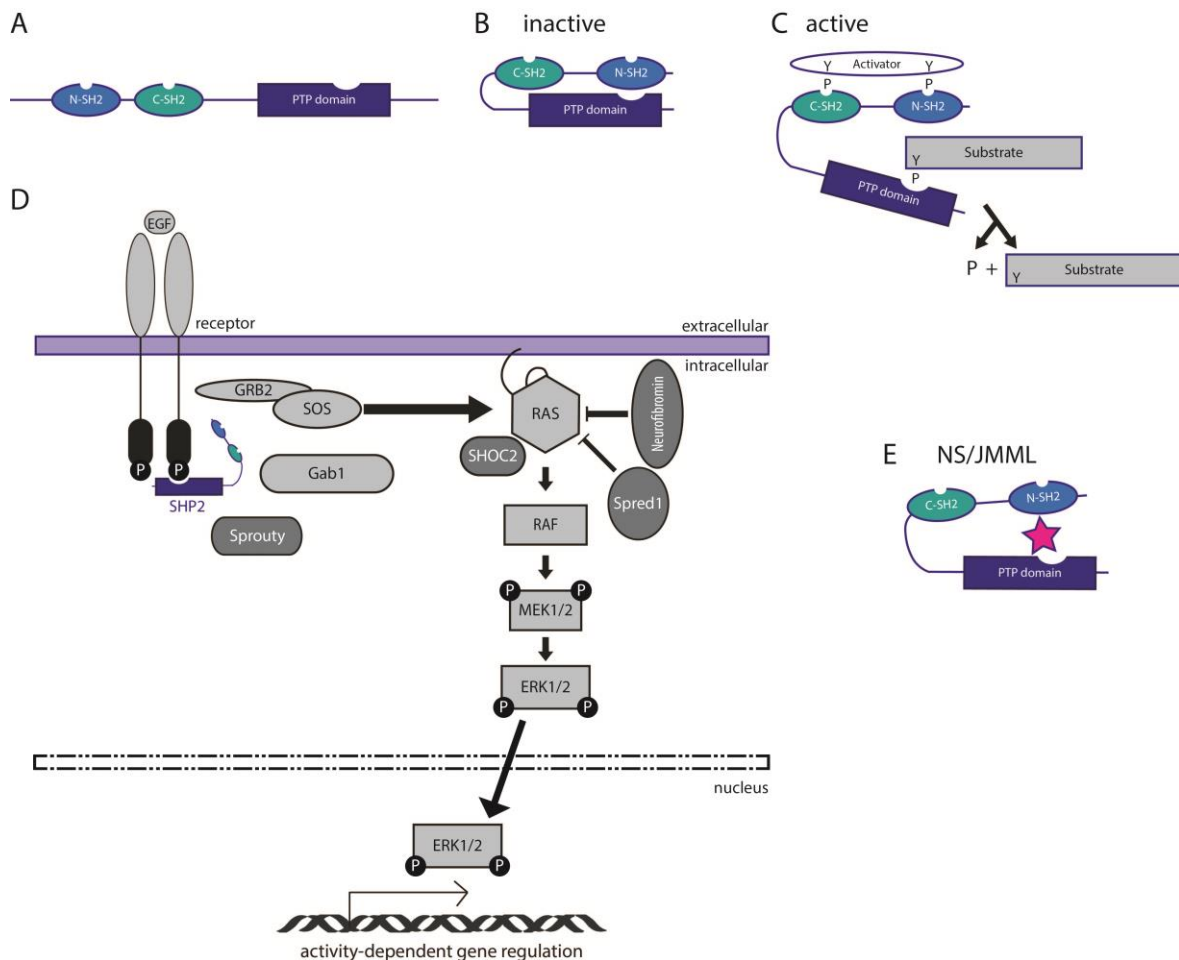


Figure 1.4: SHP2 structure and major components of the RAS-MAPK pathway. (A) SHP2 consists of two tandem SH2-domains, a PTP-domain and a C-terminal tail. **(B)** In the inactive state, the N-SH2 domain binds to the PTP-domain and renders the phosphatase in the closed conformation. **(C)** The proximity of a phosphorylated activator changes the conformation of SHP2 and opens it, making the catalytic cleft of the PTP domain available for substrates to be dephosphorylated. **(D)** Schematic representation of the major components of the RAS-MAPK signaling cascade. Molecules shown in light-grey have a positive modulatory role in signal transduction, while molecules displayed in dark-grey are involved in negative feedback mechanisms. **(E)** Mutations leading to NS or JMML predominantly affect the binding interface between the N-SH2 domain and the PTP domain leading to a constantly active state of the protein. This figure is based on Tajan et al. (2015).

SHP2 is one of the very few PTPs displaying a positive function in signal transduction: It promotes the activation of the RAS-MAPK signaling pathway and was shown to be necessary for maintained ERK activation. SHP2 is known to act upstream of RAS (Figure 1.4D). SHP2 can function as an adaptor protein and binds to phosphotyrosine residues of the GRB2-SOS complex, thereby promoting SHP2's association with tyrosine kinase receptors (Quilliam et al. 1995, Tartaglia and Gelb 2010). However, the precise mechanism of the activation of the RAS-MAPK signaling cascade is still not completely clear. Under which conditions SHP2 binds directly to the GRB2-SOS complex recruited to activated RTKs or whether a tyrosin-

phosphorylated substrate is needed is poorly understood (Tajan et al. 2015). However, SHP2 was recently shown to act on phosphorylated RAS. Phosphorylated RAS has a lower affinity for its effector RAF that in turn leads to a reduction in activated downstream RAS-MAPK signaling. SHP2 binds to Src-induced tyrosine-phosphorylated RAS and dephosphorylates it, promoting the binding of RAS to RAF and the subsequent activation of downstream RAS-MAPK signaling (Bunda et al. 2015). Other known substrates of SHP2 are mono- or dual-phosphorylated interaction partners. Examples are:

- Sprouty: Sprouty is phosphorylated at a conserved tyrosine residue in its amino-terminal domain in response to growth-factor stimulation. This phosphorylation site functions as a binding site for the SH2 domain of the adaptor molecule GRB2. It prevents the binding of GRB2 to SHP2. The recruitment of the GRB2-SOS complex to SHP2 is a necessary step in the activation of RAS and the sequestration of GRB2 by Sprouty is known to inhibit signaling events downstream of RAS. The dephosphorylation of Sprouty by Shp2 prevents the inhibitory action of Sprouty on RAS-MAPK signaling (Kim and Bar-Sagi 2004).
- PDGFR: SHP2 can dephosphorylate tyrosine kinase receptors like PDGFR on specific phospho-tyrosine residues. These phosphorylated residues mediate the recruitment of p120 RasGAP (a GTPase-activating protein), which triggers the release of GTP and subsequent RAS inactivation. The dephosphorylation of PDGFR by SHP2 results in the exclusion of RasGAP from signaling complexes and thereby supports RAS activation.
- SRC kinases: The SRC-dependent activation of RAS-MAPK signaling can be promoted by SHP2, which negatively regulates the recruitment of the kinase CSK (Tajan et al. 2015).

The human *PTPN11* gene consists of 15 coding exons with an open reading frame of 1779 bp. The resulting protein has 593 amino acids. Little is known about promoter or regulatory sequences, and transcriptional regulation (Grossmann et al. 2010). SHP2 is highly conserved between species. Corkscrew (*csw*) is the orthologue of SHP2 in *D. melanogaster* and *ptp-2* in *C. elegans* (Neel et al. 2003). The loss of SHP2 results in embryonic lethality and severe defects in gastrulation throughout different species including mice (Allard et al. 1996, Herbst et al. 1996, Gutch et al. 1998, Jopling et al. 2007, Bonetti et al. 2014, Tajan et al. 2015). SHP2 is ubiquitously expressed already in embryonic tissue and is involved in heart development and hematopoiesis

(Lauriol et al. 2015). Moreover, SHP2 plays a pivotal role in neurodevelopment determining neuronal progenitor fate decisions and patterning of cortex and cerebellum (Gauthier et al. 2007, Ke et al. 2007, Hagihara et al. 2009). SHP2 plays important roles in energy expenditure and energy homeostasis, insulin regulation and glucose metabolism (Allison and Myers 2014). Inducible Shp2 knockout mouse models further demonstrated an important function of SHP2 in bone, skeletal and cartilage development as well as muscle development (Kontaridis et al. 2004, Bauler et al. 2011, Kamiya et al. 2014). Based on specific disease-models, many functions of SHP2 during development and adulthood could be already linked to dysregulated cell signaling (Tajan et al. 2015).

1.6. *PTPN11* mutations and SHP2 dysregulation in human disease

RASopathy-associated mutations in *PTPN11* are almost exclusively missense changes that cluster in important functional domains. Biochemical and functional characterizations of disease-associated mutations support the view of perturbed SHP2 function by distinct mechanisms (Tartaglia et al. 2010). Typically, the mutations disrupt the binding interface of the N-SH2 and the PTP-domain, thereby destabilizing the binding network and preventing SHP2 to form its inactive closed conformation (Figure 1.4E). The protein in the constitutively open conformation results in an increased phosphatase activity. Mutated amino acids participate in hydrogen bond network. Substitutions on these positions can disrupt the N-SH2/PTP domain binding interface, as explained for the hydrogen bond of the amino acids D61 and C459, accounting for enhanced basal activity of the protein. Other known mutations alter the binding specificity or the flexibility of the N-SH2 domain (Keilhack et al. 2005). Due to the positive role of SHP2 in the RAS-MAPK signaling cascade it is well established that *PTPN11* GOF mutations lead to a hyperactivation of ERK1/2 in several cell types under basal state as well as upon stimulation by several agonists. However, the precise molecular mechanisms remain poorly understood (Araki et al. 2004, Fragale et al. 2004, Keilhack et al. 2005, Oishi et al. 2009, Bonetti et al. 2014, Lee et al. 2014).

Somatically acquired *PTPN11* mutations occur in hematological cancers and other malignancies. Most frequently mutated amino acid positions in cancer are E76, A72, D61, and G503 (COSMIC Database, Forbes et al. (2015)). The identification of GOF mutations in solid tumors and leukemia highlighted *PTPN11* as a new proto-oncogene. Mutations in *PTPN11* are particularly associated with juvenile myelomonocytic leukemia (JMML), a rare type of leukemia that may be associated with NS or occur as isolated sporadic neoplasia, and other forms of

leukemia. The D61Y substitution in *PTPN11* gene was identified as somatic mutation in patients with severe sporadic JMML (Tartaglia et al. 2003). Importantly, JMML can be also caused by activating mutations in *NRAS*, *KRAS* and loss of function of Neurofibromin, all known to have an activating function on RAS-MAPK signaling (Tajan et al. 2015).

In NS, amino acids in SHP2 most frequently substituted are N308, Y63, D61, Q79, and M504 (NSEuroNet database). NS-associated mutation cluster at the same domains as oncogenic mutations observed as somatic events in cancer, but individual amino acid substitutions are usually different between somatic and germline mutations in *PTPN11* probably related to a different degree of activity of the resulting mutant protein. Germline mutations observed in NS with JMML result in an intermediate activity of SHP2, which would explain the usually benign clinical course and spontaneous regression of the leukemia compared to the clinical course observed in isolated JMML. It is believed that NS-associated germline mutations have a tendency to cause milder GOF effects than somatic mutations found in cancer (Tartaglia et al. 2003, Keilhack et al. 2005, Niihori et al. 2005, Tartaglia et al. 2006). Moreover, germline mutations affecting amino acids D61 and T73 in NS patients are significantly associated with an increased risk of JMML (Strullu et al. 2014). An increase in ERK phosphorylation due to hyperactivation of the RAS-MAPK signaling cascade was shown for cell lines, neuronal and other tissues overexpressing NS- or JMML-associated mutants of *PTPN11* (Tartaglia et al. 2003, Araki et al. 2004, De Rocca Serra-Nedelec et al. 2012). The hyperactivity of RAS-MAPK signaling is thought to be causative for NS pathogenesis.

1.7. NS-associated animal models

Several animal models for NS and other RASopathies have already been established dependent on the research focus. Animal models of NS were shown to recapitulate several abnormalities seen in human RASopathies such as cardiac defects, skeletal and hematological anomalies (Table 1.1). However, only few animal models were used to investigate neurodevelopmental and neurocognitive aspects previously. One important limitation factor in the use of the animal models is the reduced viability and survival of animals with homozygous or constitutive mutations in the RAS-MAPK pathway. Conditional models and restricted expression of RASopathy-related mutations help to overcome the lethality and provide a suitable model for the investigation of the effect of a mutation in clearly defined tissues or organs. Several animal studies were already able to demonstrate that inhibition of ERK phosphorylation by the inhibition of its upstream kinase MEK is able to rescue fully or at least in part phenotypic

features in NS models, such as the cardiac defects, craniofacial malformations, and growth defects (Krenz et al. 2008, Araki et al. 2009, Nakamura et al. 2009, De Rocca Serra-Nedelec et al. 2012, Lee et al. 2014).

Recently, two mouse models with a constitutive knock-in of the NS-associated mutations Shp2^{D61G} and Shp2^{N308D}, respectively, were published. Both animal models showed learning deficits. Additionally, the Shp2^{D61G} model also displayed impairments in synaptic transmission, as well as increased ERK activation in the brain. In this model, the phenotype could be reversed by the application of MEK inhibitors decreasing the phosphorylation rate of ERK and normalizing synaptic function (Lee et al. 2014). Normally, it would be expected that the increased RAS-MAPK signaling would enhance the respective neuronal functions. However, the elevated signaling levels due to hyperactive RAS-MAPK signaling severely disturb the physiological properties. Thus, the impairments in neuronal functions reflect at least in part the complexity of this signaling cascade.

Results obtained from animal experiments offer the opportunity to perform a preclinical screen of possible pharmacological treatment strategies in a target-oriented manner. Prior to the initiation of clinical studies on patients with NS, it is inevitable to test the respective drugs in applicable dosage in animals. However, only a few drugs pass the preclinical screen. For example PD0325901 is a very potent and selective MEK inhibitor derived from benzhydroxamate esters, leading to the inhibition of ERK (Barrett et al. 2008). PD0325901 is already used in a clinical phase 2 study on patients with NF1 (<https://clinicaltrials.gov/show/NCT02096471>). Furthermore, it is tested in clinical phase 1 studies on patients with colorectal cancer and KRAS mutant non-small cell lung cancer (<https://clinicaltrials.gov/show/NCT02510001>; <https://clinicaltrials.gov/show/NCT02022982>).

However, animal models for NS provide not only the first step into clinical and pharmacological research but are also important to gain further understanding in pathophysiological basic research. Table 1.1 provides an overview of the most relevant NS-associated animal models.

Table 1.1: Published studies using NS-associated animal models

Target tissue, cells or construct	Genetic background	Phenotype	Signaling defect	Reference
Const. Shp2 ^{D61G/+} Const. Shp2 ^{N308D/+}	129S6/SvEv C57Bl/6J	Brain phenotype: Impairments in spatial learning and LTP, increased baseline excitatory function, increased surface AMPA receptor expression. Rescue with MEK inhibitor SL327 and lovastatin	ERK \uparrow	Lee et al. (2014)
Const. Shp2 ^{D61G/+}	B6 x 129Sv hybrid	Homozygous lethal, heterozygotes show decreased viability, Global phenotype: craniofacial abnormalities, myeloproliferative disease, severe cardiac defects	Cell context-dependent pERK \uparrow 3 fold higher PTP activity	Araki et al. (2004)
Cond. Shp2 ^{D61Y/+ *} Const. Shp2 ^{D61G/+} Const. Shp2 ^{N308D/+}	129S4/SvJae X C57BL/6, 129S6/SvEv, or C57BL/6	Cardiac defects and enhanced ERK activation, partial rescue by U0126	pERK \uparrow	Araki et al. (2009)
Const. Shp2 ^{D61G/+}	n.s.	Global phenotype: Postnatal growth retardation in length and weight associated with reduced IGF-1 serum levels, partial rescue of IGF-1 levels and growth deficits with MEK inhibitor U0126	IGF1 \downarrow , pERK \uparrow , no influence on JAK/STAT5 or PI3K/Akt	De Rocca Serra-Nedelec et al. (2012)
Const. Sos1 ^{E846K}	C57BL/6J x 129S1/SvImJ	Homozygous lethal, Global phenotype: Growth delay, distinctive facial dysmorphia, hematologic abnormalities, and cardiac defects, amelioration of phenotype by prenatal administration of MEK inhibitor PD0325901	ERK \uparrow Rac \uparrow Stat3 \uparrow	Chen et al. (2010)
Const. Raf1 ^{L613V/+}	129S6 x C57BL/6	Global phenotype: Short stature, craniofacial dysmorphia, hematologic abnormalities, splenomegaly, and cardiac defects, Rescue by postnatal MEK inhibition with PD0325901	MEK \uparrow ERK \uparrow	Wu et al. (2011)
Const. Kras ^{V14I}	129S2/Sv or C57BL/6J	Homozygous lethal, Global phenotype: Growth delay, craniofacial dysmorphia, cardiac defects, hematologic abnormalities, severe MPD, Increase of survival rate by MEK inhibitor PD0325901	ERK \uparrow only in the heart	Hernandez-Porras et al. (2014)
Inducible csw ^{A72S} , I. csw ^{E76K} , I. csw ^{N287D} (N308D)	<i>D. melanogaster</i>	Ubiquitous expression is lethal, ectopic wing veins	ERK \uparrow , Interaction with Notch, DPP and JAK/STAT	Oishi et al. (2006)
Inducible csw ^{D61Y} L, I. csw ^{A72S} , I. csw ^{T731} B, I. csw ^{E76K} L, I. csw ^{J282V} , I. csw ^{N287D} (N308D)	<i>D. melanogaster</i>	Brain phenotype: Impairments in long-term memory, Rescue with phosphatase inhibitor NSC-87877	Sustained ERK \uparrow	Pagani et al. (2009)

*same model as in our study. B: mutation is associated with leukemia and NS. Cond.: conditional. Const.: constitutive. I.: Inducible. L: leukemia-associated mutation.

1.8. Function of the RAS-MAPK pathway in neurons

Neurons are terminally differentiated cells and do not divide anymore. Proteins of the RAS-MAPK pathway, mainly responsible for cell proliferation and differentiation, are however highly expressed in neurons. The RAS-MAPK pathway in neurons mediates multiple forms of neuronal plasticity underlying memory formation and learning in animals and humans (Sweatt 2004). The precise regulation of the RAS-MAPK pathway in a cell type-specific manner is critical for normal neuronal function (Ryu and Lee 2016). Recently, the dysregulation of RAS-MAPK signaling was suggested to be the cause for impaired learning as well as defects in hippocampal synaptic transmission and plasticity in mice carrying the hyperactive *Shp2^{D61G}* mutation that is frequently found in NS patients (Lee et al. 2014).

Synaptic plasticity is the ability of the neuronal synapses to adapt to enduring changes in its signaling strength and is crucial for information processing in the brain. Long-term potentiation (LTP) is the long-lasting strengthening of synaptic responses following increased firing rates. The increase in synaptic strength can be caused either by a higher amount of neurotransmitters released from the presynaptic bouton, or by a higher sensitivity of the postsynaptic cell due to an increase in receptor density at the postsynaptic cell surface. Long-term depression (LTD) is the continuous weakening of synaptic transmission and strength due to decreased neurotransmitter release or decreased postsynaptic receptor density. Together, LTP and LTD interact and represent important cellular mechanisms of learning and memory. Experiments showing that MEK inhibitors prevent LTP clearly support a role for ERK involvement in learning and memory and ERK activation is necessary for the induction of LTP (English and Sweatt 1997, Atkins et al. 1998). ERK1 and 2 are activated in response to excitatory signaling in neurons, mediated by the most abundant neurotransmitter glutamate. However, the routes of neuronal ERK activation are particularly diverse, which is reviewed in Thomas and Huganir (2004) and depicted in Figure 1.5.

The requirement for RAS-MAPK signaling in synaptic plasticity and learning is evolutionarily conserved (Ye and Carew 2010). The activation of the RAS-MAPK pathway is tightly controlled in the postsynaptic spine near the postsynaptic density (PSD), which functions not only as a structural scaffold but also specifically couples the activation of neurotransmitter receptors to downstream signaling pathways at the synaptic site (Husi et al. 2000, Scannevin and Huganir 2000, Hardingham et al. 2001, Thomas and Huganir 2004, Sheng and Kim 2011). Classically, the neuronal RAS-MAPK pathway is thought to be activated mainly through receptor tyrosine kinases in response to neurotrophins, such as brain derived neurotrophic factor (BDNF). In addition, calcium influx through N-methyl-D-aspartate (NMDA) receptors or voltage-gated calcium channels in response to glutamate or membrane depolarization also activates the RAS-MAPK pathway in

postsynaptic neurons. Various regulators, such as RasGEFs and RasGAPs, mediate the neurotrophin- and glutamate-mediated activation of RAS. However, the precise route of RAS-MAPK activation is still not clear.

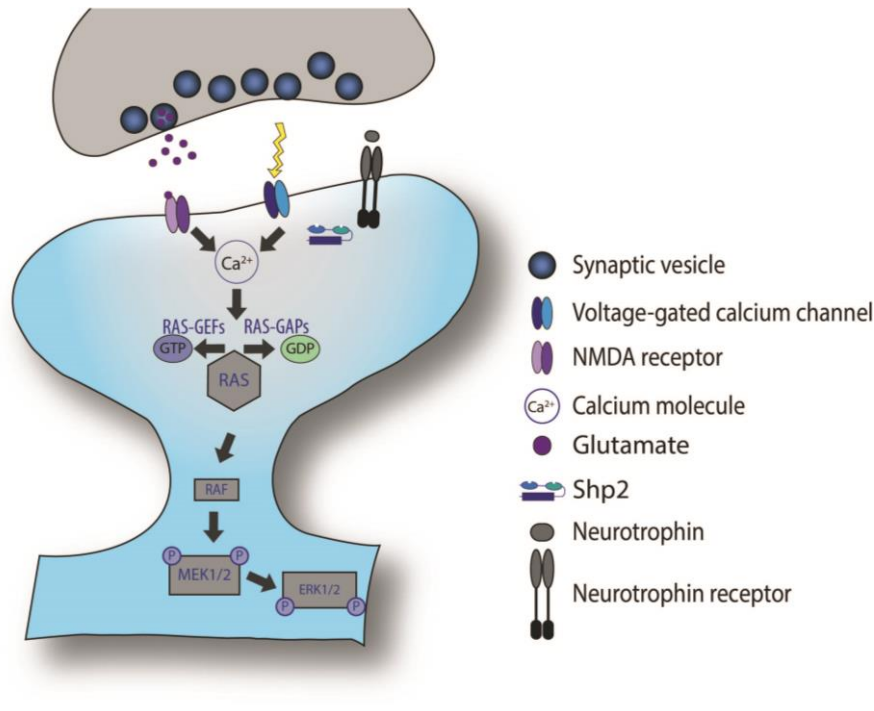


Figure 1.5: Neuronal routes to ERK activation. The RAS-MAPK signaling cascade can be activated in response to neurotrophin signaling. Calcium influx through either NMDA receptors or voltage-gated calcium channels can also trigger the increase in GTP-bound RAS and thus, activate also lead to the activation of ERK. However, it is not entirely clear, how the influx of calcium leads to the activation of RAS-MAPK signaling in neurons.

In neurons, RAS-MAPK signaling controls the trafficking of postsynaptic glutamate receptors, which is crucial for the activity-induced enhancement of neurotransmission during LTP (Patterson et al. 2010). Moreover, phosphorylated ERK1/2 can translocate from dendrites to the nucleus and mediate neuronal activity-induced reprogramming of gene expression, which is crucial for the persistent usage-dependent neuronal plasticity (Wiegert and Bading 2011). Furthermore, the activation of synaptic NMDA receptors is coupled to the activation of ERK and cAMP-responsive element binding protein (CREB) via RAS-MAPK signaling and has a neuroprotective effect. In contrast, the activation of extrasynaptic NMDA receptors leads to CREB-shut off and promotes cell death (Hardingham and Bading 2010). The activity-dependent activation of ERK prolongs the transcriptionally active state of CREB as a selective way to convey signals in a stimulus- and amplitude-dependent manner from the cell surface to the nucleus (Hardingham et al. 2001, Wu et

al. 2001a). However, it is still not entirely clear, how the complex regulation of calcium influx activates RAS-MAPK signaling and the subsequent activation of gene expression. Furthermore, it is currently unknown whether and how the neuronal RAS-MAPK signaling cascade is affected by NS-associated mutations in *PTPN11*.

Additionally, the activation of MAPK signaling and ERK phosphorylation was shown to be important for the control of dendritic shape, spine and filopodia formation, implementing the RAS-MAPK signaling cascade also in structural plasticity (English and Sweatt 1997, Wu et al. 2001b, Zhou et al. 2015). Moreover, SHP2 was shown to be involved in the regulation of neurite outgrowth (Rosario et al. 2007).

1.9. Synaptic vesicle pools

In hippocampal neurons, neurotransmitter-containing synaptic vesicles (SVs) are organized into functional pools. The readily releasable pool (RRP) is docked to the presynaptic active zone and primed for neurotransmitter release. It constitutes about 5% of the SVs. The Recycling Pool (RP) of SVs can be released upon persistent stimulation and corresponds to further 10-20% of SVs. The resting pool of SVs (RtP), which is refractory to release in response to both, electrical stimulation and short high potassium application, comprises the 85% of the total SVs. Currently, the function of this pool is not entirely clear, but it might serve as a reserve for the plasticity-induced recruitment of vesicles into the RP leading to synaptic strengthening. The RRP and RP together comprise the total recycling pool (TRP) of SVs (see Figure 3.7.1 in the results section). Importantly, SV pools are involved in numerous presynaptic mechanisms regulating synaptic strength and plasticity (Rizzoli and Betz 2005, Alabi and Tsien 2012). SV Pools are suggested to undergo three stages of development: First SVs accumulate and build up a recycling pool allowing a moderate synaptic release rate. Second, a transitory state emerges, in which the RRP gradually arises with SVs docked to the active zone and enables a fast release. Finally the increase in the number of recycling SVs leads to the formation of the RtP (Mozhayeva et al. 2002).

It has been described that RAS-MAPK signaling is implicated in the control of SV distribution and recycling, as well as the establishment of functional synaptic connections and presynaptic short-term plasticity. The presynaptic phosphoprotein Synapsin1 is involved in the modulation of neurotransmitter release at presynaptic terminals by tethering SVs to the actin cytoskeleton. Synapsin1 has four known ERK phosphorylation sites on Serine 62, 67, 549 and 551 (Jovanovic et al. 1996, Matsubara et al. 1996). If Synapsin1 is phosphorylated SVs are released from the binding to the actin cytoskeleton, which is also known as “synapsin dispersion”. It is suggested that MAPK-

dependent phosphorylation of Synapsin1 actively contributes to the activity-dependent modulation of SV cycling, distribution, and neurotransmitter release. Furthermore, the domain D of Synapsin1a interacts with SH3-domain containing proteins like Grb2, PI3K and c-Src (Cesca et al. 2010). However, the precise contribution of RAS-MAPK signaling to the regulation of SVs remains elusive.

1.10. Glutamate receptors

Glutamate is the most abundant neurotransmitter in the brain mediating excitatory neurotransmission. It is released from presynaptic terminals and activates glutamate receptors at the postsynapse. Ionotropic receptors are ligand-gated ion channels that lead to the depolarization of the postsynaptic cell via influx of cations. There are three subtypes of ionotropic glutamate receptors: α -amino-3-hydroxy-5-methyl-4-isoxazolepropionic acid (AMPA), kainate, and N-methyl-D-aspartate (NMDA) receptors, which are all implicated in neurotransmission and the regulation of synaptic plasticity. Their activation leads to the influx of Na^+ and/or Ca^{2+} , resulting in the depolarization of the postsynaptic neuron. Both AMPA and NMDA types of glutamate receptors are essential for the expression of LTP and LTD (Traynelis et al. 2010).

1.10.1. AMPA receptors

AMPA receptors are ionotropic transmembrane receptors that mediate fast synaptic transmission in response to the binding of glutamate. They are composed of four different subunits, namely GluA1 to GluA4. Together these subunits form homo- or heteromeric receptors. AMPA receptors in the hippocampus are mainly composed of GluA1/GluA2 or GluA2/GluA3 subunits. Importantly, the subunit composition determines the properties of the receptor (Luscher and Malenka 2012). The GluA2 subunit governs the permeability to calcium, sodium, and potassium. The channel is impermeable to calcium if a GluA2 subunit is present. GluA2-lacking AMPARs in contrast are permeable to calcium, sodium and potassium (Liu and Cull-Candy 2000). The interaction with scaffolding proteins is determined by the C-terminal sequence of the single subunits, which differs most between the single subunits. All GluA subunits have a PDZ binding domain in their C-terminal tail, allowing the binding to various interaction partners (Shi et al. 2001). Additionally, the channel localization, conductance, and open probability can be regulated by phosphorylation (Traynelis et al. 2010).

Already under unstimulated conditions, AMPA receptors show a relatively high turnover with 10 to 20% being internalized within 10 minutes. GluA2/GluA3 receptors have a constant recycling rate between intracellular and surface receptors, which is independent of activity and mediated by the short C-terminal tail of the receptor subunit. GluA1/GluA2 receptors remain rather cytoplasmic due to the anchoring function of the long C-terminal tail of GluA1 and remain dormant (Passafaro et al. 2001, Sheng and Lee 2001, Shi et al. 2001). However, the high mobility and recycling rate of AMPA receptors allows for the rapid changes in synaptic efficacy during LTP and LTD. GluA1 receptors belong to the main targets of synaptic plasticity. The surface level of GluA1 receptors can be influenced by synaptic activity (Sheng and Lee 2001). Their activity-dependent exocytosis requires the stimulation of NMDA receptors and the calcium/calmodulin-dependent protein kinase II (CaMKII), as well as RAS-MAPK signaling and ERK activation (Zhu et al. 2002, Patterson et al. 2010). Strong depolarization and calcium influx through NMDA receptors is known to trigger LTP, thus activating CaMKII and leading to the phosphorylation and subsequent exocytosis of AMPA receptors. As a consequence of LTP induction, more GluA1 receptors are inserted into the spine surface leading to the strengthening of synaptic transmission. In contrast, only a modest depolarization and calcium influx through NMDA receptors is achieved during weak activity of presynaptic neurons that preferentially activates phosphatases dephosphorylating AMPA receptors and promotes their endocytosis. This process subsequently leads to LTD (Luscher and Malenka 2012). The endocytosis of AMPA receptors can be also mediated by the activation of NMDA receptors, which happens in a Rap- and p38-dependent manner (Zhu et al. 2002).

The delivery and retrieval of AMPA receptors as mechanisms underlying long-lasting plasticity is further supported by the observation of “silent synapses”. This phenomenon describes the fact that a subset of glutamatergic synapses in the CNS lack AMPA receptor-mediated currents. However, these synapses contain functional NMDA receptors permeable to calcium. The activation of NMDA receptors by neuronal activity leads to the activation and “unsilencing” of the respective synaptic contact, leading to a potentiated synaptic transmission, either due to activation by phosphorylation of AMPAs already present at the surface or due to the insertion of new AMPA receptors (Sheng and Lee 2001, Kerchner and Nicoll 2008).

1.10.2. NMDA receptors

The NMDA receptor is a specific type of ionotropic glutamate receptor that has remarkable properties distinguishing them from other types of ligand-gated ion channels. This will be explained

in this paragraph. NMDA receptors are found on the pre- and postsynapse, where they can be found synaptically, as well as peri- and extrasynaptically (Shipton and Paulsen 2014). NMDA receptors are hetero-tetramers that consist of two GluN1 subunits and additional two GluN2 (A-D) or GluN3 (A-B) subunits. The two predominant isoforms in the adult brain, especially in the hippocampus, are GluN2A and GluN2B subunits. Either GluN1/GluN2A or GluN1/GluN2B, or tri-heteromers consisting of GluN1/GluN2A/GluN2B subunits build up a tetrameric complex and determine the properties of the receptor. Each subunit has four major domains, providing different binding or interaction sites for various extracellular and intracellular modulators. Of note, the permeation and gating properties of the receptor are also regulated by the subunit composition of the receptor (Luscher and Malenka 2012, Paoletti et al. 2013). Interestingly, the subunit composition of NMDA receptors undergoes a developmental switch. The GluN2B subunit is already highly expressed during embryonic stages and is maintained in the first postnatal week and later on restricted to the forebrain in the adult brain. In the first two postnatal weeks, a major change in the GluN2 subunit composition takes place. The GluN2A expression starts postnatal and rises steadily into adulthood. This subunit exchange is an evolutionary conserved process in the time window of synapse maturation and leads to the acceleration in the kinetics of the receptors. However, the molecular mechanism responsible for the GluN2B-to-GluN2A developmental switch is still not fully understood but is thought to be driven by neuronal activity. Importantly, even in the adult brain the NMDA receptor subunit composition is still plastic and can change rapidly (Paoletti et al. 2013).

One of the unique properties of the NMDA receptor is that the opening and closing of the ion channel are primarily ligand-gated by the binding of glutamate and its co-agonist glycine or serine. Glutamate binds to the GluN2 subunit, whereas glycine (or serine) binds to the GluN1 subunit. However, the current flow through the ion channel is additionally voltage dependent. At negative membrane potentials, NMDA receptors are inactive and the pore is blocked by magnesium ions, rendering the channel impermeable for all other ions. Upon depolarization of the cell membrane magnesium ions are ejected, allowing a voltage-dependent flow of sodium and calcium into the cell and potassium out of the cell. In this way, NMDA receptors act as coincidence detectors for the activation and depolarization of both, the pre and postsynaptic cell (Paoletti et al. 2013). The coincident depolarization and glutamate binding enables a maximum calcium influx and subsequently leads to the activation of intracellular signaling cascades altering synaptic efficacy (Luscher and Malenka 2012). However, this unique activation mechanism causes the unusually slow kinetics of the NMDA receptor, compared to the fast-acting AMPA receptors (Paoletti et al. 2013).

The GluN2 subunit is the major determinant of the NMDA receptor channels properties and kinetics. GluN2A receptors have a higher open probability and faster deactivation kinetics than GluN2B receptors. GluN2B receptors are mobile and recycle more frequently than GluN2A receptors, allowing the fine-tuned regulation of receptor number and subunit composition in an activity-dependent manner. Additionally, GluN2B receptors have a higher calcium permeability leading to a stronger calcium influx than GluN2A receptors (Paoletti et al. 2013). Importantly, GluN2A and GluN2B receptors differ in their association of the cytoplasmic C-terminus with intracellular signaling molecules. The most prominent signaling molecule linked to the NMDA receptor is CaMKII, which is highly abundant at synapses. CaMKII interacts more strongly with the C-terminal domain of GluN2B subunits than with the one of GluN2A. Because of the crucial role of CaMKII in LTP induction, the GluN2B–CaMKII interaction has major implications for synaptic plasticity (Barria and Malinow 2005). The interaction of GluN2B–CaMKII is necessary for the phosphorylation of GluA1 receptors on S831, leading to their membrane insertion and increasing synaptic strength, thereby supporting the important role of this interaction in LTP (Halt et al. 2012). The RAS-guanine-nucleotide-releasing factor 1 (RasGRF1) is another preferential binding partners of the C-terminal domain of GluN2B. The interaction of GluN2B and RasGRF1 is implicated in a positive modulatory role in ERK activation. RasGRF1 is a calcium/calmodulin-dependent RasGEF stimulating the conversion of the GDP to GTP and subsequent activation of RAS. RasGRF1 bound to GluN2B at the postsynaptic density is necessary for the activation of ERK and CREB (Krapivinsky et al. 2003, Tian et al. 2004). This implements GluN2B-mediated signaling in the activation of the RAS-MAPK pathway and the subsequent activation of its downstream targets ERK and CREB, both necessary for neuronal survival and plasticity (Paoletti et al. 2013).

2. Material and Methods

The chemicals used in this work were purchased from the companies as indicated. The quality of the reagents was of analytical grade.

2.1. Analysis of the *NRAS* mutations in a cohort of RASopathy patients

2.1.1. Subjects and phenotyping

Patients were clinically assessed by experienced clinical geneticists. All patients described here had molecular confirmation in a diagnostic setting, except for the clinically affected family member 5-3, who declined genetic testing. Standardized patient data was collected via the NSEuroNet database (www.nseuro.net) and entered by the referring clinician. This database uses a comprehensive online questionnaire to facilitate the collection and improve the standardization of clinical information.

Clinical data and samples for genetic testing were obtained from all individuals with informed consent of the patients' parents/legal guardians or the patients themselves, and all studies were performed in accordance with the Declaration of Helsinki and the national legal regulations. Specific written permission was obtained for the use clinical photographs for publication in this project.

2.1.2. Molecular analysis

NRAS mutations were identified by routine genetic testing of the known RASopathy genes using Sanger sequencing as well as whole exome sequencing (WES; Patients 10-1, 10-2, 11, and 12) of DNA extracted from venous blood samples, except for case 2, which was diagnosed prenatally on DNA extracted from chorionic villus samples. Where available, DNA samples from parents and additional affected family members were investigated for the mutation discovered in the index case in order to demonstrate the *de novo* occurrence of the mutation or co-segregation with the RASopathy phenotype (see Supplementary Table 6.1). In selected cases, DNA samples from various tissue sources were examined in addition to leukocyte DNA to prove that the mutation was not a clonal event in haematopoietic cells. These sources included buccal cells and fingernails in patient 1, urine, and saliva in patient 8, fingernails in patient 12, and fibroblasts in patient 13.

In our lab, DNA was isolated from leukocytes and other material if available by standard procedures. Exon 2 and 3 and exon–intron boundaries of the *NRAS* gene (GenBank:

NM_002524.4) were amplified from genomic DNA and sequenced using standard procedures in Sanger Sequencing. Reagents and volumes for standard PCR and the sequencing reaction are listed in Table 2.1 and 2.2.

Primer sequences: **Exon 2, fwd:** tccttcatttggtgcctac; **rev:** tgggtaaagatgatccgaca, 507 bp

Exon 3, fwd: caaaccagataggcagaaatgg; **rev:** ggtaacctcattccccataaag, 286 bp

Table 2.1: PCR master mix

Chemicals	1x Master Mix (µl)
H ₂ O	7.6
dNTPs	2
RxnBuffer (10x)	2
MgCl ₂ (50 mmol)	0.2
DMSO (5%)	1
Betaine (5 M)	4
Primer (2.5 pmol)	1
Taq Polymerase	0.1
DNA	0.7

The lab-internal standard-PCR conditions are designed as touchdown PCR program:

94 °C, 3 min initial denaturation, 94 °C (denaturation) for 30 sec; 65-55 °C (annealing) for 10 sec and 72 °C (elongation) for 45 sec for 33 cycles followed by 72 °C (final elongation) for 10 min.

Table 2.2: Sequencing master mix.

Chemicals	1x Master Mix (µl)
H ₂ O	2.7
Primer (2.5 pmol)	0.6
Big Dye Mix	0.2
Sequencing Buffer (5x)	1
PCR product	0.5

After PCR amplification and sequencing reaction, PCR products were purified using Agencourt AMPure magnetic beads (Applied Biosystems) in an automated workstation. Amplicons were directly sequenced using the ABI BigDye Terminator Sequencing Kit v3.1 (Applied Biosystems)

and an automated capillary sequencer (ABI 3500; Applied Biosystems). All other required chemicals were purchased from Applied Biosystems, too. Sequence electropherograms were analyzed using the Sequence Pilot software SeqPatient (JSI medical systems). PCR and subsequent sequencing was performed by experienced technicians in the diagnostics laboratory of the Institute for Human Genetics, Medical Faculty and University Hospital Magdeburg.

2.2. *Shp2*^{D61Y} animals

2.2.1. Breeding

For this study, the conditional mouse model *Shp2*^{D61Y} (B6.129S6-*Ptpn11*tm1Toa/Mmjax), originally published by Chan and colleagues in 2009 (Chan et al. 2009) was obtained from Dr. Benjamin G. Neel, Princess Margaret Cancer Centre Toronto, Canada, and kept under C57BL/6J background. This mouse model harbors a strong activating point mutation in exon 3 of *Ptpn11*, which is rendered inactive by flanking lox-STOP-lox cassettes. This mutation is an oncogenic mutation that was not found in the germline of patients with NS yet. Homozygous animals have no functional *Ptpn11* allele due to the flanking lox-STOP-lox cassettes. They are not viable and die already during midgestation. Heterozygous animals have only one functional allele of *Ptpn11* due to flanking STOP cassettes on the second allele but show no obvious phenotype and are undistinguishable from WT littermates. Importantly, global expression of the heterozygous mutant *Ptpn11*^{D61Y} using a universal Cre-driver strain leads to embryonic lethality, too (Chan et al. 2009). To induce the mutation for our experiments, heterozygous *Shp2*^{D61Y} animals were bred to homozygous *Emx1*^{IRESCre} animals (B6.129S2-*Emx1*tm1(cre)Krl/J) (Gorski et al. 2002), which we obtained from Jackson Laboratories. These animals harbor an IRES-Cre recombinase coding sequence in the 3' untranslated region of the *Emx1* gene, enabling the generation of a bicistronic messenger RNAs encoding for both, the *Emx1* and Cre proteins of the *Emx1* promotor using the Internal Ribosome Entry Site (IRES). Cre expression then starts from embryonic day 10.5 and is restricted to areas of the forebrain and ventral pallium. Mice homozygous for Cre are phenotypically undistinguishable from WT littermates. Heterozygous Cre expression is already sufficient for proper excision of lox-STOP-lox cassettes. For easy breeding and genotyping reasons, animals were crossed using parent animals homozygous for *Emx1*^{IRESCre} and heterozygous *Shp2*^{D61Y} animals, yielding offspring all heterozygous for *Emx1*^{IRESCre} and either heterozygous for *Shp2*^{D61Y} expression or *Shp2*^{WT}. The resulting F1 generation, which was used for experiments, is further on called *Shp2*^{D61Y} (*Shp2*^{WT/D61Y} and *Emx1*^{WT/IRESCre}) and Control (*Shp2*^{WT/WT} and *Emx1*^{WT/IRESCre}; or CTRL in Figure 3.4A), respectively. All experiments were carried out in

accordance with the European Communities Council Directive (2010/63/EU) and approved by the local animal care committees of Sachsen-Anhalt, Regierungspräsidium Halle, Sachsen-Anhalt/Germany (reference number AZ: 42502/2-988IfN and 42502-2-1295UniMD).

2.2.2. Genotyping

Mice were genotyped either as newborn pups (P0) that were used for experiments or by standard genotyping procedure at the age of three weeks after weaning. Prior to genotyping animals were labelled and biopsies of 1-5 mm tail tip from animals were cut with sterile scissors. DNA from tail cuts was isolated using Proteinase K digestion in tail cut buffer and 10 mg/ml Proteinase K (purchased from Sigma, see Table 2.6). Digestion was incubated for 30 min for P0 animals and overnight for adult animals slowly shaking at 55 °C using the Thermomixer (Eppendorf), followed by 10 min heat inactivation at 95 °C.

Genotyping for the $Emx1^{IRESCre}$ allele was performed using standard PCR protocol and primers as provided by Jackson laboratories. One Taq DNA Polymerase purchased from New England BioLabs (NEB) was used and PCR performed on the Mastercycler Nexus GSX1 from eppendorf. A detailed description of primer sequences, master mix, PCR programs, and solutions can be found below (Table 2.3, 2.4, 2.5, and 2.6, respectively).

Table 2.3: Primers and PCR product sizes used for genotyping

Mouse strain	Primer fwd	Primer rev	PCR product size
$Emx1^{IRESCre}$ (WT)	AAGGTGTGGTCCCAGAATCG	CTCTCCACCAGAAGGCTGAG	378 bp
$Emx1^{IRESCre}$ (KI)	GCGGTCTGGCAGTAAAACTATC	GTGAAACAGCATTGCTGCACTT	102 bp
$Shp2^{D61Y}$	TGGAGCTGTTACCCACATCA	GCACAGTTCAGCGGGTACTT	171 bp

Table 2.4: PCR Master Mix calculated for one reaction mix

Chemicals	1x Master Mix (µl)
H ₂ O	14.375
NEB reaction buffer (5x)	5
primer 1 (10 pmol)	0.5
primer 2 (10 pmol)	0.5
dNTPs (10 mM)	0.5
NEB OneTaq polymerase	0.125

Table 2.5: PCR program for genotyping EMX1^{IRESCre} mice

Process	EMX1 ^{IRESCre}		
	Temperature (°C)	Time	Cycles
Initial denaturation	94	3 min	1
Denaturation	94	30 sec	35 x
Annealing	62.3	45 sec	
Elongation	68	45 sec	
Final elongation	68	5 min	1
Cooling	10	end	1

Per sample 21 µl master mix and 4 µl of DNA are used. After PCR completion, samples are mixed with Orange loading dye and gel electrophoretically separated on 1% TAE agarose gel. Agarose gel contains GelRed Nucleic Acid Gel Stain purchased from Biotium. FastRuler Low Range DNA Ladder (ThermoFisher Scientific) was used to identify correct PCR product sizes.

Table 2.6: Solutions for Proteinase K digestion and agarose gel electrophoresis

Solution	Composition
Tailcut buffer	10 mM Tris/HCl, 100 mM NaCl, pH 8.0
Proteinase K stock	10 mg/ml in 10 mM Tris/HCl, 100 mM NaCl, pH 8.0
6 x DNA sample buffer	0,5 M EDTA, pH 7.5; 1 M TrisHCl pH7.6, glycerol, 150 mg OrangeG, 30 mg Xylene, dH2O
Agarose (Bio&SELL / BIOZYM)	
50 x TAE buffer	4.84 g Tris, 114.2 ml Acetic acid, 37.3 g EDTA

For genotyping Shp2^{D61Y}, High Resolution Melting and Gene scanning application on the LightCycler480 from Roche Diagnostics was used. This method detects sequence variations in the amplified DNA due to distinct patterns in melting point and melting curve shape. DNA is amplified by real-time PCR in the presence of a proprietary dye binding exclusively double stranded DNA. Amplification can therefore be traced in real time. Afterwards, melting curves are generated by monitoring the decrease in fluorescence intensity during the melting phase. Melting analysis of fluorescence data was performed subsequently in three basic steps: normalization, temperature-shifting, and difference plotting. This is followed by the analysis using the automated grouping function provided by the Gene Scanning software module (www.lightcycler.com; Figure 2.1). LightCycler480 High Resolution Melting Master purchased from Roche Diagnostics was used as reaction mix according to manufacturer's recommendations. The detailed PCR program and Melting Curve settings can be found in Table 2.7, primers are shown in Table 2.3.

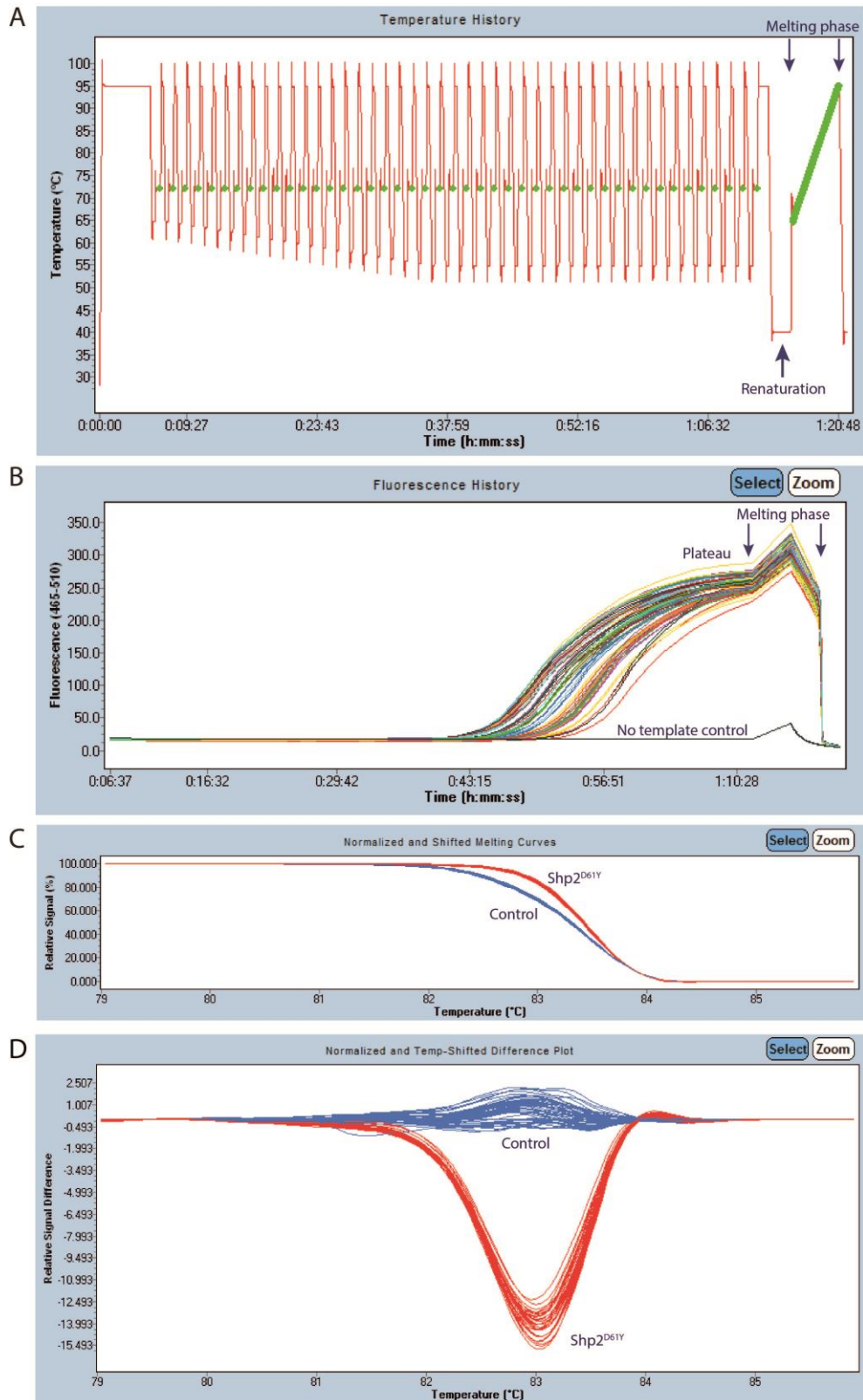


Figure 2.1: Workflow of High Resolution Melting Curve processing and analysis. (A) Temperature profile of the touch-down PCR program including fluorescence intensity measurements indicated as green dots. The PCR is followed by a short renaturation phase as indicated by the arrow to recover all PCR products with incorporated dye. During the melting phase the temperature increases from 65°C to 95°C and the fluorescence intensity is measured continuously. **(B)** Fluorescence profile of the amplifying PCR products over time. The more PCR products are amplified the higher the fluorescence intensity measured during the elongation phase. A plateau in fluorescence intensity is reached at the end of the PCR. The peak and drop in fluorescence intensity

represent the melting phase as indicated by the arrows. The sample without increase in fluorescence intensity represents the no template control. **(C)** Normalized fluorescence intensity profiles of all samples are plotted against temperature during melting phase. Two groups are already evident and represent the two genotypes analyzed. **(D)** Relative signal Difference of the normalized fluorescence profiles is plotted against temperature. The analysis clearly shows two groups of samples. Internal controls are used to identify control (blue) and Shp2^{D61Y} (red) animals.

In the software provided by Roche, the PCR program and subset of wells used on the 96well plate are selected and samples labeled. After run completion, raw data are normalized and temperature-shifted to internal standards and defined settings. Calculation using internal genotype standards enables the differentiation of control and Shp2^{D61Y} animals. Plotting the relative signal difference shows a separation into two groups (Figure 2.1C, D) and identifies the corresponding genotypes.

Table 2.7: Touch down PCR program for genotyping Shp2^{D61Y}

Process		Temperature (°C)	Time	Ramp Rate (°C/sec)	Acquisition
Amplification	Pre-incubation	95	5 min	4.4	None
	Denaturation	95	10 sec	4.4	None
	Annealing	65-55; 0.5 °C step size	15 sec	2.2	None
	Elongation	72	25 sec	4.4	Single
High Resolution Melting		95	1 min	4.4	None
		40	2 min	2.2	None
		65	1 sec	4.4	None
		65-95	/	0.02	Continuous 25°C
Cooling		40	30 sec	2.2	None

2.2.3. Breeding statistics

Breeding statistics were obtained using the PyRAT Python Based Relational Animal Tracking (Scionics Computer Innovation) and analyzed in MS Excel.

2.2.4. SHP2-specific Protein Tyrosine Phosphatase Activity assay

For the measurement of SHP2-specific protein tyrosine phosphatase activity in forebrain, 8 weeks old control and Shp2^{D61Y} mice were used. Animals were decapitated and forebrain was dissected. The assay was performed as by the manufacturer's protocol. Briefly, postnuclear S1 supernatant from forebrain homogenate was prepared and subsequently used to measure the activity of SHP2 in cell lysates. The cell lysate was incubated with SHP2-specific antibodies coupled to agarose beads for 3 h shaking at 4 °C. After two different washing steps, specific phosphorylated substrate was

added to precipitated SHP2 bound to agarose beads and incubated for additional 30 min at 37 °C. Then, molybdic acid and malachite green were added (Figure 2.2).

A



B

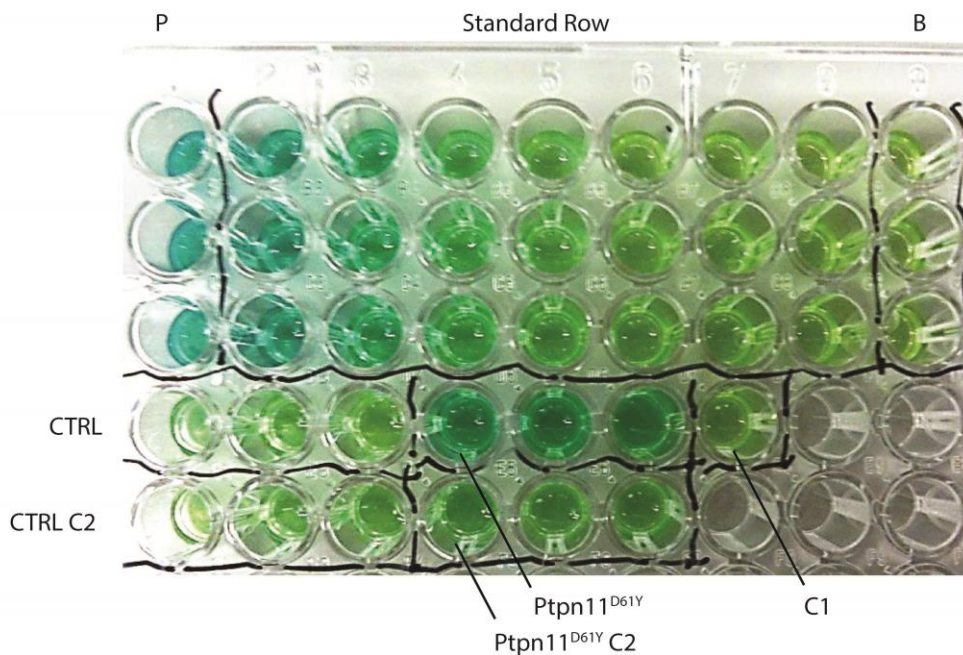


Figure 2.2: Workflow of SHP2-specific Protein Tyrosine Phosphatase activity assay. (A) Typical workflow as recommended from the manufacturer’s protocol. **(B)** 96well plate containing the completed PTPase activity assay and representative colorimetric change. Note the turquoise-blue color in Shp2^{D61Y} and green in control samples. P: Positive control containing high phosphate concentration (10 mM). Standard row (1.56 μM – 100 μM) is used to identify the magnitude of PTPase activity. B: Blank. C1: Control with only agarose beads. CTRL: sample from control animal. CTRL C2: sample from control animal supplemented with sodium orthovanadate as an inhibitor of PTPase activity.

Controls are C1, using only agarose beads without cell lysate, C2 using cell lysate mixed with agarose beads and 1 mM sodium orthovanadate (NaN₃) as an inhibitor of protein tyrosine phosphatases.

The standard row used defined concentrations ranging from 1.56 μM to 100 μM of free phosphate including positive and negative control (P [10 mM] and B [0 mM] in Figure 2.2). Colorimetric results were measured at 620 nm wavelength on FLUOstar Omega plate reader by BMG Labtech. The more free phosphate is available for malachite green-molybdate binding reaction the more the color shifts to from green to blue. All components were purchased as a kit DuoSet IC DYC2809 from R&D Systems Inc. and solutions prepared according to manufacturer's protocols. The assay is based on the malachite green-molybdate binding reaction and is a sensitive method to detect free phosphate.

2.2.5. Antibodies and chemicals

The following antibodies and chemicals were used: **mouse antibodies** against Bassoon (mAb7f, IHC: 1:1000; Assay Designs), β -III-tubulin (Western blot: 1:1000; Sigma-Aldrich), GluA2 (ICC 1:500; Chemicon/Merck Millipore), panGluA Oyster 550-labeled (ICC: 1:500; Synaptic Systems), Homer1 (ICC: 1:500; Synaptic Systems), MAP2 (1:1000; Sigma-Aldrich), and pERK (Western blot: 1:1000 Sigma-Aldrich), Tau1 (1:1000; Millipore), **rabbit antibodies** against phosphorylated ERK (ICC 1:200; Cell Signaling), ERK (Western blot: 1:500; Cell Signaling), GFP (ICC 1:1000; Invitrogen), GluN1 (ICC: 1:500, alomone labs) GluN2A (ICC: 1:200; alomone labs), GluN2B (ICC: 1:500; alomone labs), Homer1 (ICC: 1:500; Synaptic Systems), Synaptotagmin1 Oyster 550-labeled (ICC: 1:100; Synaptic Systems), VGAT (ICC and IHC: 1:500; Synaptic Systems), VGLUT1 (IHC 1:1000; Synaptic Systems), **guinea pig** antibodies against Bassoon (ICC 1:500; Synaptic Systems), GAD65 (ICC 1:500; Synaptic Systems), GluA1 (ICC 1:100; alomone labs), and MAP2 (ICC 1:1000; Synaptic Systems).

The following **secondary antibodies** raised in goat were used: Alexa 488- (ICC: 1:2000; IHC: 1:500) and 680- (Western blot 1:20000) coupled secondary antibodies from Invitrogen, Cy3- (ICC: 1:2000; IHC: 1:500), Cy5- (ICC: 1:2000) coupled antibodies from Jackson ImmunoResearch Laboratories, and CF770- (Western blot 1:20000) coupled secondary antibody from Biotium.

4',6-Diamidin-2-phenylindol (DAPI) for the staining of nuclei (1 $\mu\text{g}/\text{ml}$) was obtained from Sigma-Aldrich.

For the treatments of acute hippocampal slices and dissociated hippocampal cultures, the following **pharmaceuticals** were used: D-(-)-2-amino-5-phosphonopentanoic acid (APV, 40 μM ; Tocris), 6-cyano-7-nitroquinoxaline-2,3-dione disodium (CNQX, 100 μM ; Tocris), 4-aminopyridine (4AP,

2.5 mM; Sigma-Aldrich), bicuculline (Bic, 50 μ M; Sigma-Aldrich) Brain-derived neurotrophic factor (BDNF, 100 ng/ml; PEPROTECH).

2.2.6. Primary hippocampal culture

Dissociated hippocampal cultures from newborn (P0-P1) mice were prepared based on the protocols for Banker cultures (Kaech and Banker 2006) that were adapted to our lab (Davydova et al. 2014). Primary neurons cells were cultured in 5% CO₂ at 37 °C and a humidity of 95%. All supplemented cell culture media were filtrated using sterile filtration bottles with a pore size of 0.22 μ m and kept at 4 °C until usage. Media and reagents are listed in Table 2.8. All media were preheated to 37 °C before addition to cells. Cells were plated in densities of either 10000 cells for 5 DIV old neurons, 20000 cells per coverslip for 14 DIV cells for low density cultures, or 30000 cells per coverslip for 14 DIV cells for high density cultures.

2.2.6.1. Preparation of glass coverslips

Glass coverslips (\varnothing 18 mm, VWR) for dissociated cell culture were placed into 50 ml tubes with 65% HNO₃ (Carl Roth) and incubated on a small rotation incubator overnight. Next day, pH was neutralized by washing with cell culture water (Millipore water in sterile flasks). Coverslips were then boiled three times in cell culture water using a microwave oven with exchanging the water in between. Then, clean coverslips were separately dried on precision wipes and baked for 4 h at 200 °C for sterilization.

Prior to culture preparation coverslips were transferred into \varnothing 10 cm petri dishes and three dots per coverslip were attached with paraffin heated to 150 °C. Then, coverslips were coated with 100 μ l of poly-L-lysine working solution of 500 mg/ml per coverslip and incubated overnight in the cell culture incubator. On the next day, poly-L-lysine was removed and cell culture water was added to each plate. Before usage of the coverslips for neuronal cultures, they were washed three times with cell culture water and dried completely prior to plating of the cells.

2.2.6.2. Glial cells

For glial feeder layers C57BL/6 pups (P0-P2) were decapitated and brain hemispheres were dissected, washed twice with HBSS⁻ (Gibco), and incubated in 4.5 ml HBSS⁻ with 0.5 ml 10x

Trypsin (Gibco) for 20 min at 37 °C. Hemispheres are washed with HBSS⁻ twice and medium was exchanged for 1 ml DMEM (10% FCS), followed by trituration of the hemispheres using a glass Pasteur pipette to obtain a homogeneous cell solution. This cell suspension is then filled up to a volume of 10 ml with DMEM (10% FCS) and transferred to 75 cm² cell culture flask. Cells were cultured for 5 to 7 days and every second day cells were washed with HBSS⁻ to remove cell debris and supplemented with fresh DMEM (10% FCS). After reaching confluence, glia cells are split 1:4 and cultured for further 5-7 days until cells reach confluence. Then glia cells are trypsinized and the cell suspension transferred to 50 ml tubes. Cells are pelleted by centrifugation for 5 min at 1000 x g and resuspended in DMEM (10% FCS) containing 10% DMSO. Slow freezing of the cells was performed using Mr. Frosty Cryo freezing container (Nalgene) with isopropanol at -80 °C. On the next day, aliquots were transferred to -150 °C and stored until usage.

For plating of glia cells prior to culture preparation 2-4 frozen glial cell tubes are quickly thawed at 37 °C and transferred into 100 ml of prewarmed DMEM (10% FCS) and plated on Ø 6 cm plates with a final volume of 5 ml each. Cells are cultured for 2-5 days until ready to be used. The cells are the used as glial feeder layer.

2.2.6.3. Dissociated mouse hippocampal neurons

Mouse hippocampal cultures were prepared from genotyped P0 (in exceptional case from P1) mouse pups (for genotyping see section 2.2). Animals were decapitated, hippocampi were dissected, meninges removed, and collected in HBSS⁻. 10x trypsin was added and incubated for 15 min at 37 °C. Hippocampi were washed once with HBSS⁻ and the medium was replaced by 1 ml plating media (DMEM + 10% FCS + 1% P/S + 0.5% glutamine). Trituration of the tissue was performed using Pasteur pipets with big and small diameters. Cells were counted using Trypan blue (Gibco) in Neubauer hemocytometer. After counting the cells, the cell suspension was diluted to 300000 cells/ml for experiments done with cells of an age of 14 and 21 DIV, 350000 cells/ml for pHlourine experiments performed with cells of an age of 17-18 DIV, and 100000 cells/ml for the morphological characterization with cells of an age of 5 DIV. 100 µl of cell suspension were plated on each washed and dried coverslips and incubated for 1 h in the cell culture incubator. In the meantime, media of petri dishes with glial feeder layer was exchanged to neuronal media containing Neurobasal A supplemented with 2% B27, 1% P/S, and 2 mM Glutamax (Gibco). Then, 4-5 coverslips were turned into each plate with neurons and paraffin dots facing down. One day and three days after plating 2 µl AraC (100 x, Sigma) diluted in 100 µl neuronal media were added per

plate to inhibit glial cell proliferation. The cells were fed each week by replacing 1 ml of old media with fresh one.

2.2.7. Immunocytochemistry

For quantitative assessments, all coverslips compared in one experiment were processed in parallel using identical antibodies, solutions, and other reagents.

Cells were fixed in 4% paraformaldehyde (PFA) in phosphate buffered saline (PBS) for 4 min, washed three times in PBS, permeabilized with 0.2% Triton X-100 (Carl Roth) in PBS for 10 min, washed again with PBS and blocked in blocking buffer (see Table 2.9) for one hour. Paraffin dots were removed and coverslips were transferred to a wet chamber. Primary antibodies diluted in the blocking buffer were applied overnight at 4 °C. Cells were washed with PBS and incubated with an appropriate secondary antibody diluted in the blocking solution for 1.5 h at RT. Coverslips were subsequently stained with DAPI diluted in PBS or washed in PBS, rinsed in water and mounted using Mowiol. Mounted coverslips were stored at 4 °C until usage.

2.2.7.1. Synaptotagmin1 uptake

To determine the relative amount of synaptic vesicles (SVs) undergoing transmitter release under physiological conditions (representing the ready releasable pool of SVs) and hyperpolarized conditions (total recycling pool of SVs) we used an Oyster 550-labeled Synaptotagmin1 antibody (Syt1, Synaptic Systems) recognizing its luminal, intra-vesicular domain (see Figure 3.7.1). Neurons aged 14 DIV were washed twice with Tyrodes buffer and then incubated with Syt1 antibody diluted in either the same physiological Tyrodes buffer for 20 min or for 4 min in Tyrodes buffer containing 50 mM KCl to hyperpolarize the cell membranes. Then, neurons were washed again twice with physiological Tyrodes buffer to remove unbound antibodies, fixed with 4% PFA, permeabilized and stained with antibodies against Bassoon and Homer1 to label excitatory synapses.

2.2.7.2. ERK activation and deactivation

To investigate activity-dependent changes of the RAS-MAPK cascade 14 DIV old neurons were treated for the indicated time points with either 2.5 mM 4AP and 50 μM Bic or 100 ng/μl BDNF

to induce network activity or 100 μ M APV and 40 μ M CNQX for 30 min to block the glutamate receptor-mediated network activity. DMSO and dH₂O were added as vehicle to controls. Neurons were fixed with 4% PFA, and stained with antibodies against MAP2, phosphoERK, and GAD65, and counterstained with DAPI.

2.2.7.3. CtBP1 nuclear export

For the investigation of nuclear CtBP1 export 14 DIV old neurons were treated with 2.5 mM 4AP and 50 μ M Bic for 2 hours, fixed with 4% PFA, permeabilized and stained with antibodies against MAP2, CtBP1, and GAD65. Nuclei were stained with DAPI.

2.2.7.4. Staining of glutamate receptors

For the surface staining of glutamate receptors coverslips with 14 DIV old neurons were washed twice with physiological Tyrodes buffer and incubated with antibodies recognizing the extracellular domain of GluA1, GluA2, panGluA, GluN1, GluN2A, or GluN2B receptors, respectively, for 30 min at 37 °C in the incubator. Then cells were fixed, permeabilized and stained with antibodies against Homer1 and Bassoon to label excitatory synapses.

Table 2.8: Buffers and solutions used for cell cultures

Media and reagents	Ingredients (Company)
DMEM full	10% FCS (Gibco) 1% Penicillin/Streptomycin 100x (Gibco), 2 mM L-Glutamine 100x (Gibco) in DMEM (Gibco)
Neuronal media	2% B27 (Gibco), 2 mM Glutamax (Gibco), 1 mM Sodium pyruvate (Gibco), Penicillin/Streptomycin 100x (Gibco) in NeurobasalA (Gibco)
Distilled Water	Millipore
HBSS--	Gibco
AraC 1.5 mM	Calbiochem
10x Trypsin	Gibco
1x Trypsin	10% 10x Trypsin (Gibco); DMEM (10% FCS)
Paraffin	Paraplast embedding medium (Fischer)
Freezing medium	DMEM full, 10% DMSO
Poly-L-lysine	100 mg/l poly-L-lysine (Sigma) in 100 mM boric acid, pH 8.5, sterile filtered

Table 2.9: Buffers for immunocytochemistry

Buffer	Composition
4 % PFA	4% PFA in PBS, pH 7.4
Blocking buffer	2% glycine, 2% BSA, 0.2% gelatin, 50 mM NH ₄ Cl in 1x PBS
1x PBS	2.7 mM KCl, 1.5 mM KH ₂ PO ₄ , 137 mM NaCl, 8 mM Na ₂ HPO ₄ , pH 7,4
Mowiol (for 96 ml)	9.6 g Mowiol, 24 ml H ₂ O, 24 g Glycerol → 2 h stirring, 48 ml 0.2 M Tris pH 8.5 → 10 min 50 °C, 2.5 g DABCO
Tyrodes buffer (physiological)	119 mM NaCl, 2.5 mM KCl, 25 mM HEPES pH 7.4, 30 mM glucose, 2 mM MgCl ₂ , 2 mM CaCl ₂
Tyrodes buffer (high KCl)	119 mM NaCl, 50 mM KCl, 25 mM HEPES pH 7.4, 30 mM glucose, 2 mM MgCl ₂ , 2 mM CaCl ₂

2.2.8. BDNF pl+plI-EGFP and Synpto-pHlourin lentiviruses

2.2.8.1. Production of lentiviral particles

For the production of lentiviral particles in HEK293T cells (ATTC) the following three plasmids were transfected using the calcium phosphate transfection method: FUGW-based transfer (as backbone), psPAX2 (12260, Addgene) for packaging and pVSVG (8454, Addgene) pseudotyping vectors (Lois et al. 2002). HEK293T cells were grown in DMEM (10% FCS) until 50-70% confluency in 75 cm² cell culture flasks. For the transfection of a single flask, 500 µl of 0.5 M CaCl₂ (Solution A) were mixed with 18 µg DNA in a molar ratio of FUGW:psPAX2:pVSVG as 2:1:1. For the Synpto-pHlourin lentivirus in total 20 µg DNA in a molar ratio of 4:2:1 was used. Then, 500 µl of 140 mM of Solution B (NaCl, 50 mM HEPES, and 1.5 mM Na₂PO₄, pH 7.05) were added, incubated for 1 min, and applied to the cells in culture. Six to eight hours after transfection, the media was exchanged to neuronal media. HEK293T cells were grown for 48 h and the supernatant containing viral particles is collected and centrifuged for 15 min, 2000 rpm to pellet cell debris. Supernatant is aliquoted and stored at -80 °C until use, or used immediately. For the infection of primary hippocampal neurons, the viral supernatant was diluted in neuronal media and applied over night at 4 DIV. Neurons were cultured as indicated.

2.2.8.2. BDNF pl+plI-EGFP reporter construct

The lentiviral construct harboring the promoter regions I and II of BDNF used for the BDNF promoter assay was subcloned previously by Dr. Daniela Ivanova into FUGW backbone vector (schematic construct see Figure 3.10.). The original construct was obtained from the lab of Masaaki Tsuda in Toyama, Japan and published by Hara et al. (2009).

Cells were grown until 14 DIV and treated for 30 min with 2.5 mM 4AP and 50 μ M Bicuculline and fixed for 4 min with 4% PFA. Immunostaining was done as described above using antibodies against GFP and MAP2, and DAPI as nuclear marker.

2.2.8.3. Synapto-pHlourin

The Synapto-pHlourin (SypHy) construct was subcloned by Dr. Daniela Ivanova into FUGW backbone vector and original construct was obtained from the lab of Thomas Oertner in Basel, Switzerland, published by Rose et al. (2013). SypHy is a fusion protein with GFP coupled to the luminal domain of the SV protein Synaptophysin. The fluorescence of the pHlourin reporter is quenched at rest with the acidic pH inside SVs (pH 5.5) and starts fluorescence after membrane fusion and subsequent exposure to the neutral extracellular pH (pH 7.4) (Rose et al. 2013). The fluorescence is then quenched again after endocytosis and reacidification.

This experiment was performed by Dr. Carolina Montenegro. Live imaging of cells expressing the SypHy construct was performed with 16-18 DIV dissociated hippocampal cultures from Shp2^{D61Y} and control animals. Coverslips were placed in an imaging chamber (Warner Instruments) that was equipped with a pair of parallel platinum electrodes 10 mm apart for electrical stimulation. Live imaging was performed at RT (25 °C) in extracellular solution (119 mM NaCl, 2.5 mM KCl, 25 mM HEPES pH 7.4, 30 mM glucose, 2 mM MgCl₂, 2 mM CaCl₂, 10 μ M CNQX (Tocris), and 50 μ M APV) on an inverted microscope (Observer D1, Zeiss) equipped with an EMCCD camera (Evolve 512, Photometrics) controlled by MetaMorph Imaging (MDS Analytical Technologies) and VisiView (Visitron Systems GmbH) using 63x objective and EGFP ET filter set (exciter 470/40, emitter 520/50, dichronic 495 LP) and Cy3 ET filter set (exciter 545/25, emitter 605/70, dichronic 565 LP). By checking the RFP expression in the red channel infected neurons were selected for analysis.

The alkaline trapping method was used for quantification of the recycling pool of vesicles. Here, the stimulation of SypHy-expressing neurons was performed in the presence of 1 μ M Bafilomycin A1 (Calbiochem) as a specific inhibitor of the vesicular proton pump V-type ATPase. In the presence of Bafilomycin in the extracellular solution, the vesicles that undergo exocytosis are not quenched but remain fluorescent after endocytosis and fail to reacidify. The unquenched vesicles do not contribute to the rise of fluorescence upon triggering of another round of release. In this way, the net exocytosis can be estimated. The readily releasable pool (RRP) was released by delivering 40 APs at 20 Hz using S48 stimulator (Grass Technologies) for 30 sec. To reveal the

total recycling pool (TRP) 900 APs at 20 Hz were delivered, following a break of 120 seconds in the recording after the first train of stimuli. The relative sizes of RRP and TRP were determined as fractions of the total SynHy-expressing pool measured after addition of 60 mM NH₄Cl pulse.

Synaptic puncta that respond to stimulation were identified by subtracting the first frame of the baseline before stimulation from the 20 frames directly after onset of the stimulus. In detail, the following formula was used: $\Delta F = (F - F_0) / (F_{\max} - F_0)$, whereas F_0 is the average from 20 frames before stimulus, F is the GFP fluorescence intensity divided by the mean IF of RFP fluorescent puncta. F_{\max} is the fluorescence after the addition of ammonium. Mean IF intensities were measured in ROIs centered over each responding synapse using Time Series Analyzer V2.0 plugin in ImageJ software. RRP and TRP were quantified using mean values of 110 values corresponding to 15 sec to 25 sec and 45 sec to 55 sec after the first stimulus, respectively (see example trace in Figure 3.7.1E). Data traces were determined after background subtraction and correction for bleaching was done. Only neurons that showed more than a 20% increase in fluorescence on average after treatment with ammonia were used. The protocol is adapted from published procedures by Burrone and colleagues (Burrone et al. 2006). Cells used in this experiment were provided by me. All further procedures were performed by Dr. Carolina Montenegro.

2.2.9. Immunohistochemistry

This experiment was done by Anil Annamneedi in the frame of his PhD thesis since he was familiar with the technique that requires a special education and permission to perfuse animals. Mice were anesthetized with isoflurane and transcardially perfused with PBS for 20 minutes, then with 4% PFA for another 20 minutes. Animals were decapitated and brains were carefully dissected. Post fixation of the brains was done with 4% PFA overnight, followed by 0.5 M sucrose in PBS and 1 M sucrose in PBS. Brains were frozen using Isopentane and liquid nitrogen and stored at -80 °C until analyzed. 30-40 µm thick sagittal sections were cut on a Leica CM3050S cryostat, collected free floating, and washed with PBS (10-15 min) followed by blocking with 10% NGS, 0.3% Triton X-100 in PBS for 1 hour at room temperature. Primary antibodies were anti-Bassoon and anti-VGLUT or anti-VGAT diluted in blocking solution and incubated overnight at 4° C. Then sections were washed in PBS and blocked again with 0.4% BSA/0.3% Triton X-100 in PBS for 60 min followed by overnight incubation with secondary antibodies diluted in blocking solution. Sections were washed three times with PBS and mounted on glass slides and covered with coverslips using fluoromount g DAPI (Southern biotech). Genotyped animals were provided by me. The subsequent acquisition and processing of images was done by me.

2.2.10. Image analysis

Images of stainings were acquired on a Zeiss Axio Imager A2 microscope with Cool Snap EZ camera (Visitron Systems) controlled by VisiView (Visitron Systems GmbH) software. In general, single coverslips were acquired using camera settings identically applied to all samples quantified in one experiment. Unspecific background was removed by measuring small regions in acquired images that clearly contained no specific staining in all pictures of the same channel. The average of the maximum IF intensity was calculated and this value was subtracted from all pictures of the same channel in ImageJ software (NIH, <http://rsb.info.nih.gov/ij/>).

Overview pictures of single sagittal brain sections were obtained using a 2.5x objective. All blocks of single sagittal section were rearranged using Adobe InDesign CS3. Brightness and contrast levels of the presented images were minimally adjusted using either ImageJ software or Adobe Photoshop CS3.

For morphological analysis images were taken with high exposure using a 10x objective, converted to 8bit binary images, processed in Adobe Photoshop CS3, and analyzed using the Sholl analysis Plugin in ImageJ software. Longest outgrowing dendrite was measured with the same software.

For the quantification of surface and total staining of glutamate receptors acquired using a 63x objective, Bassoon and Homer1 stainings served as synaptic markers and stainings were analyzed in proximal dendritic segments 10-30 μm away from the soma. Synaptic puncta were defined semi-automatically by setting rectangular regions of interest (ROI) with dimensions of about 0.8 x 0.8 μm around local intensity maxima in the channel with staining for Bassoon. In ROIs positive for staining of Homer1 and glutamate receptor subunit corresponding antibody mean IF intensities were measured using OpenView software (written by N.E. Ziv (Tsuriel et al. 2006)).

To quantify the number of excitatory and inhibitory synapses Bassoon puncta were matched with either Homer1 or VGAT staining. The number of active synapses is determined by matching Bassoon puncta with Homer1 and Synaptotagmin1-labeled puncta in neurons hyperpolarized with 50 mM KCl in Tyrodes Buffer. The relative ratio of SVs in the ready releasable pool and in the total recycling pool using Syt1 live staining was determined in the same way with antibodies against Bassoon and Homer1 to label excitatory synapses. Intensities were measured using OpenView software.

For the quantification of phosphorylated ERK or BDNF pI+pII-EGFP reporter construct fluorescence in the nucleus, ROIs were defined using DAPI as a mask. Integrated density was

measured using ImageJ software. Only cells that were negative for the staining of GAD65 were used for this analysis.

2.2.11. Statistical Analysis

All results are shown as mean \pm standard error of the mean (SEM) from two or three independent experiments and plotted using Prism 5 software (GraphPad Software, Inc.). Values were normalized to the mean of control values unless indicated differently. Statistical analysis was performed using One-way ANOVA, Dunnett's test, one-sample t-test or student's t-test. Only p-values <0.05 were considered as statistically significant.

3. Results

3.1. Clinical and molecular spectrum of *NRAS* mutations

After the first publication of germline mutations in *NRAS* as a cause of NS (Cirstea et al. 2010), we identified four individuals with *NRAS* mutations in our local cohort. Along with 15 additional cases from international collaborators, we were able to describe the largest cohort in “Genotype and phenotype spectrum of *NRAS* germline variants” (Altmuller et al. 2017a).

3.1.1. Spectrum of *NRAS* mutations

In this study, we identified 19 affected individuals from a total of 13 unrelated families with mutations in *NRAS*. In summary, we identified nine different heterozygous *NRAS* mutations. Importantly, all changes affected highly conserved residues as depicted in Figure 3.1. In four cases, the respective *NRAS* mutation was inherited from affected parents and co-segregated with the phenotype. Moreover, we identified nine sporadic cases, in which we were able to prove the *de novo* occurrence of the mutation by testing parental DNA, if available. Notably, the amino acid substitutions p.I24N, p.T50I and p.G60E in *NRAS* that we found to segregate in the four families, had already been documented in NS previously (Cirstea et al. 2010, Runtuwene et al. 2011). We found six novel changes affecting the residues p.G12R/D/S/V, p.E37dup and p.T58I. These mutations occurred exclusively in sporadic cases and were not described as germline mutations in NS yet. *De novo* occurrence was demonstrated for the missense changes predicting the amino acid substitutions p.G12R, p.G12D, p.G12S and p.G12V. The germline nature of the mutations resulting in the p.G12R, p.G12D, p.G12S and p.T58I changes was further supported by their occurrence in a heterozygous pattern in non-hematopoietic tissues. Regarding the p.E37dup mutation, the father was unavailable for testing, and in the case of p.T58I the father was found to have a mosaicism for the mutation in his peripheral blood leukocytes (see Figure 3.2 for the sequence electropherograms).

3.1.2. Clinical presentation of patients with *NRAS* mutations

We identified heterozygous *NRAS* mutations in nine males and ten females with a range from three months to 50 years and a median age of 7.1 years. Fifteen patients of our cohort had a clinical diagnosis of NS. However, in two patients, the proposed diagnosis based on clinical assessment was CFCS. Moreover, a very young patient at the age of one year was initially suspected to have

CS. One case was diagnosed prenatally because of a large hygroma colli during early pregnancy. The clinical data are summarized in Table 3.1.

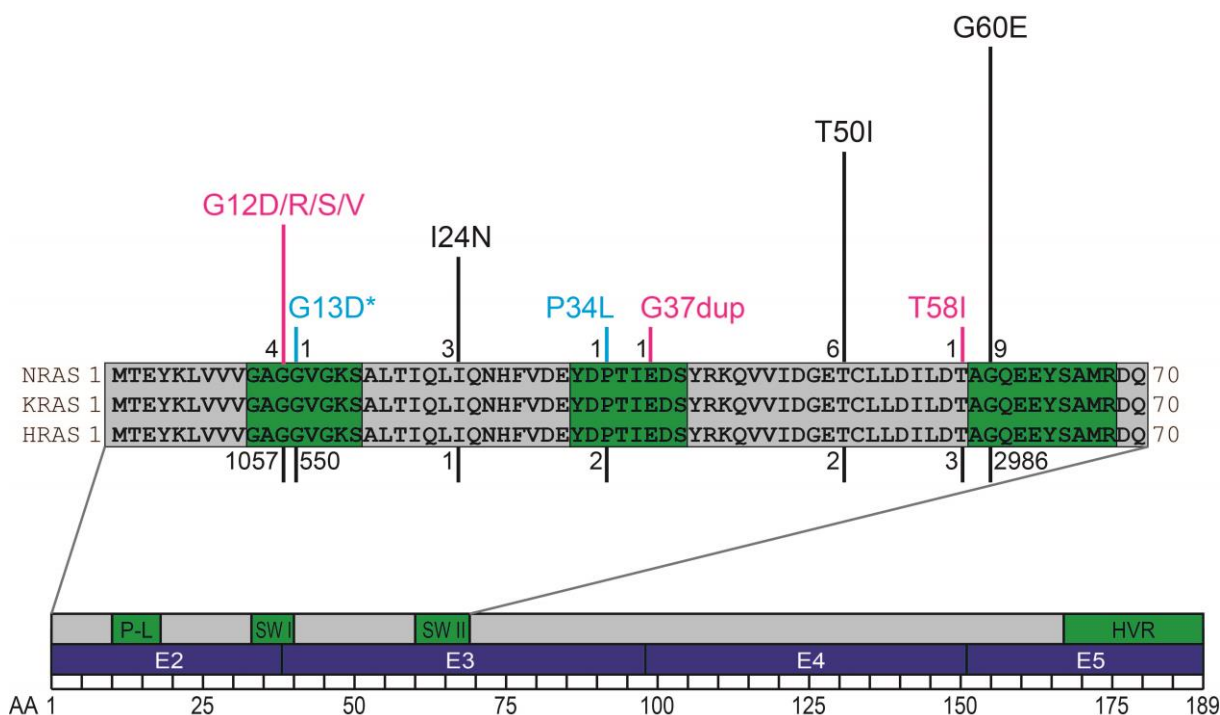


Figure 3.1: NRAS mutational spectrum and protein domain structure. Upper panel: The sequences of amino acids 1-70 of three RAS proteins are aligned. RASopathy-associated and germline mutations in *NRAS* are represented above the sequence alignment. Length of bars and numerals at their basis indicate the numbers of unrelated observations for each mutation. Novel mutations identified in this study are printed in magenta. Black color indicate mutations described previously, which were also identified in our cohort. Cyan blue color indicates mutations previously reported to cause NS but not found in our cohort. *Notably, the reported case with the G13D mutation had a diagnosis of JMML. Mild NS-like features were only noted retrospectively. Black bars and numerals below the alignment represent the numbers of somatic mutations associated with cancer at the respective position (according to COSMIC, Forbes et al. (2015)). **Lower panel:** Domain structure of NRAS. Numbers represent amino acids, blue boxes: coding exons, green boxes: functional domains, P-L = P-Loop, SW I = Switch I region, SW II = Switch II region, HVR = Hypervariable region. This figure is adopted from Altmüller et al. (2017a).

All individuals with heterozygous *NRAS* mutations presented with craniofacial features typical or suggestive for a RASopathy. Additionally, we found the typical appearance with short and broad or webbed neck in 94%, and ocular ptosis in 82% of the cases. Motor delay and intellectual or learning disabilities were present in 43% and 46% of the patients of our cohort respectively. Fifty-nine percent of the patients in our cohort had cardiac anomalies: hypertrophic cardiomyopathy (HCM) was most common in 33%, whereas septal defects and pulmonary stenosis (PST) were reported only in 12% and 6% of our cohort, respectively. Short stature was recorded in only four out of 15 cases (27%). Patient 7 showed a severe global developmental delay, but other learning disabilities reported in our cohort were mild. For most of patients (69%), prenatal abnormalities were reported with polyhydramnios occurring in 46% of the cases, and nuchal edema and fetal

chylothorax/hydrops in 15 and 23% of the cases, respectively. Cryptorchidism was reported in 63% of affected males. One patient had a confirmed coagulopathy (von Willebrand disease, patient 8), but bleeding diathesis was reported in only three out of 15 individuals. Two individuals were found to have neoplasias: one patient had a brain tumor of unclear etiology (patient 12), which is shown in Supplementary Figure 6.1 and another patient had a JMML-like myeloproliferative disorder (patient 13). Selected patients with novel mutations and/or unusual phenotypic features are presented in more detail in the following.

Patient 1 (p.G12S) presented with typical physical signs of NS: facial anomalies (Figure 3.3), left ventricular hypertrophy, atrial and ventricular septal defects that was corrected by surgery, a persistent ductus arteriosus, and short stature. She exhibited marked muscular hypotonia in infancy. Her development was mildly delayed; she was able to walk freely with 2.3 years and spoke 2-3 word sentences at the age of 2.5 years. Her language skills at last evaluation at the age of 5.5 years were classified as normal for age. Intellectual development was also tested normal for age, but deficits were noted in spatial performance and attention. She had regular follow-up in the pediatric hemato-oncology during infancy, and had no signs of myeloproliferative disorder. The heterozygous *NRAS* mutation was found in leukocyte DNA, confirmed in DNA from buccal mucosal epithelial cells and finger nail keratinocytes, and was absent in the parents (Figure 3.2).

Patient 2 (p.G12V) was a fetus with a suspected RASopathy based on the finding of a very large cystic nuchal hygroma (14.3 mm) at twelve weeks of gestation. Progressive hydrops fetalis developed, eventually leading to intrauterine death at 22 weeks of gestation. No autopsy data were available but hydropic appearance of the fetus was reported. No heart defect could be detected. Fetal karyotyping was performed on a chorionic villus sample and resulted in a normal male karyotype. The heterozygous *NRAS* mutation was demonstrated in DNA from cultured chorionic villus fibroblasts. Parents were negative for the mutation.

Patient 5-2 (p.G60E) is an affected child of a three-generation family with obvious features of NS in her father and grandfather. She died on the first day of life from severe hydrops. Post-mortem MRI revealed bilateral pleural effusions, a small pericardial effusion and left ventricular hypertrophy.

Patient 7 (p.E37dup) came to medical attention because of developmental issues and an atrial septal defect. She had a prenatal history of fetal nuchal edema, polyhydramnios, an intracerebral arachnoid cyst, and bilateral hydronephrosis detected by antenatal ultrasound. Subcutaneous edema was noted at birth. She required gavage feeding due to severe failure to thrive. In addition, she developed epilepsy and a sleep disorder. She had renal and urogenital abnormalities and recurrent

urinary tract infections. An MRI in the newborn period revealed thinning of the cortex with white matter changes, consistent with hypoxic ischemic encephalopathy. At the age of 2 years and 5 months her stature was below third centile (-2.69 SD) and she had a short webbed neck, shield chest, wide-spaced nipples, while facial anomalies were less typical (Figure 3.3). She was suspected to have CFCS because of her severe developmental delay, hypotonia and ectodermal abnormalities. She continued to demonstrate head lag at age 4 years old and unsupported sitting was not possible. Other features included microcephaly (43 cm at 2 years and 5 months (-3.27 SD)), ocular abnormalities including nystagmus and strabismus, hearing deficits and hemangioma. The *NRAS* mutation was detected in leukocyte DNA. Additionally, she was identified to harbor a 1.24 Mb gain from chromosome 22q11.23 detected by array CGH analysis (arr[GRCh38]22q11.23(23408742_24595702)x3). This duplication was considered to have an impact on phenotypic complexity and modification of the RASopathy phenotype, specifically the severity of neurodevelopmental issues. Neither genetic abnormality was detected in the mother, but the father was unavailable for testing. Because of the complex phenotype and its probable modification by the 22q11.23 duplication and hypoxic ischemic encephalopathy, this patient was excluded from the aggregate clinical tables and statistics.

Patient 8 (p.T58I) presented with suggestive facial features of NS, ocular ptosis, strabismus, and pectus excavatum, but without cardiac anomalies and short stature. She displayed muscular hypotonia and mild motor delay. The *NRAS* germline origin of the mutation was supported by its identification in DNA from urine, saliva, and peripheral blood. The patient's father was found to have a mosaicism for the mutation in his peripheral blood (Figure 3.2).

Patient 11 (p.T50I) presented with typical facial features of a RASopathy, and mitral valve prolapse. At age 11, her height was in the low normal range (-1.47 SD). The suspected clinical diagnosis was CFCS because of typical facial features with substantial supraorbital hypoplasia and prominent ectodermal findings (curly hair, sparse eyebrows, keratosis pilaris, facial keratosis and multiple nevi), while her motor and intellectual development was only mildly delayed (IQ 65). Her perinatal history was characterized by multiple complications that may have contributed to her developmental problems. She had perinatal asphyxia (Apgar scores 2/5/7) and required mechanical ventilation for 17 days. In addition, she developed sepsis and portal vein thrombosis after umbilical vein catheter. She was discharged from the hospital at 45 days of life. Brain MRI at four months of age revealed a non-obstructive hydrocephalus requiring ventriculoperitoneal shunting at six months. The *NRAS* mutation was demonstrated in leukocyte DNA.

Patient 12 (p.G12R) had a RASopathy-typical facial phenotype, short webbed neck, macrocephaly and HCM. She was born at 36 weeks of gestation after a pregnancy complicated by polyhydramnios. Birth weight was increased at 4.145 g. The postnatal period was complicated by prolonged hyperinsulinemic hypoglycemia, severe feeding difficulties including oral aversion and respiratory difficulties due to upper airway collapse. She was treated with a percutaneous gastrostomy and a tracheostomy with continuous positive airway pressure ventilation. A brain MRI at 8 months of age revealed an expansive lesion of 0.8x0.7x0.6 cm in the hypothalamus proposed to represent a hamartoma or lipoma (Supplementary Figure 6.1), but neither surgery nor biopsy have been performed, so far. Her EEG was normal, and she has been followed by a clinical neurologist. Her motor development was delayed (unsupported sitting at age 10 months), but no detailed assessment of her development is available due to her young age (1 year at last follow-up). She had sparse, thin hair, full lips, deep palmar and plantar creases, several small nevi and one café-au-lait spot. Based on the clinical findings, CS was suggested, but no *HRAS* mutation was found. The heterozygous *NRAS* mutation was detected by WES. It was confirmed in DNA obtained from fingernail keratinocytes by Sanger sequencing, and was not found in DNA samples from both parents.

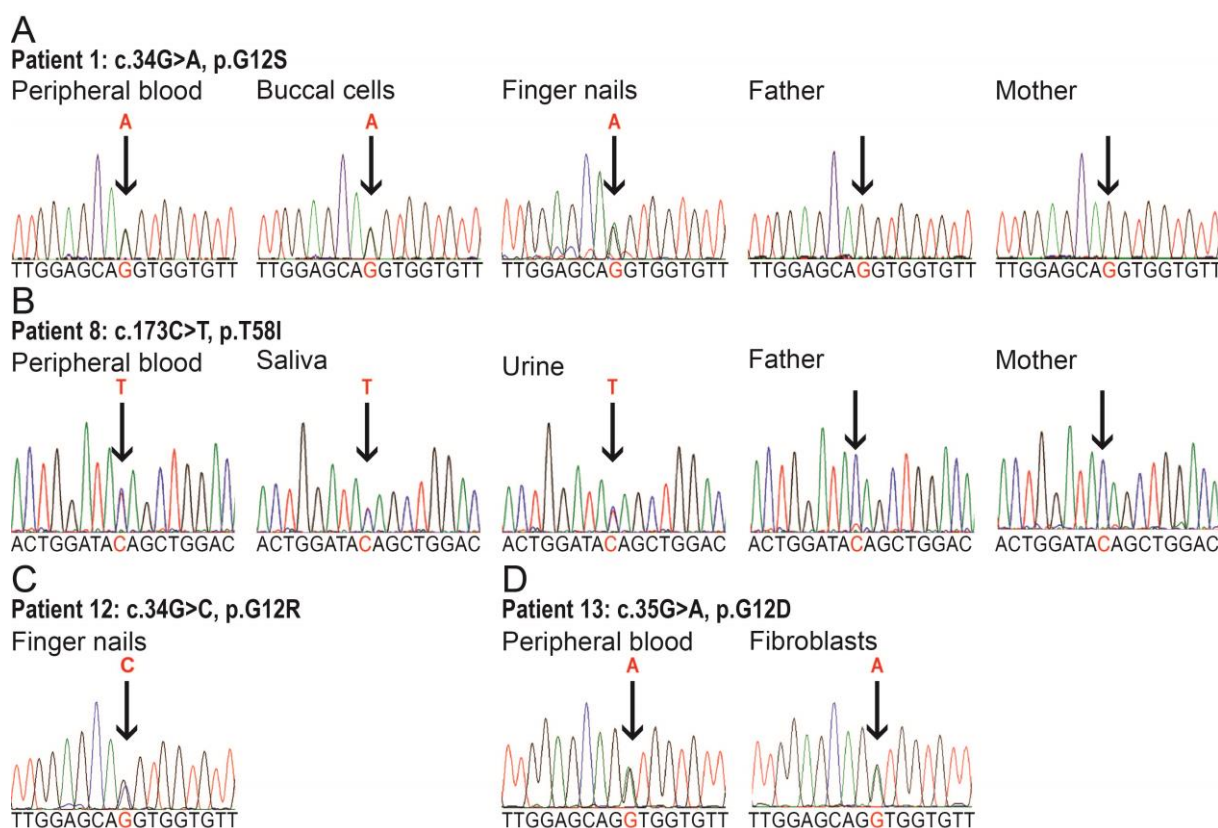


Figure 3.2: Sequence electropherograms demonstrating *de novo* occurrence of the mutation and supporting its germline origin in patient 1, patient 8, patient 12, and patient 13. For better comparison only forward sequences are shown. Arrows indicate the position of the mutation. **(A)** From Patient 1 DNA specimens from peripheral blood and buccal cells were analyzed. The c.34G>A substitution (p.G12S) was found

in a heterozygous non-mosaic distribution in both samples. Parents were negative for the mutation. **(B)** Electropherograms of patient 8 in DNA samples from peripheral blood, saliva and urine demonstrating the germline origin of the c.173C>T mutation (p.T58I). Sequencing of parental DNA revealed the father to have a low-level mosaicism for the mutation in his peripheral leukocytes. The mutation was absent in the mother. **(C)** In patient 12 the c.34G>C change (p.G12R) was identified in a heterozygous non-mosaic distribution in leukocyte DNA using next generation sequencing (not shown). DNA extracted from fingernails was analyzed to confirm the germline origin of the mutation. **(D)** From Patient 13 DNA specimens from peripheral blood and fibroblasts were analyzed. The c.35G>A substitution (p.G12D) was found in a heterozygous non-mosaic distribution in both samples. Parents were negative for the mutation (data not shown). This figure is adopted from Altmüller et al. (2017a).

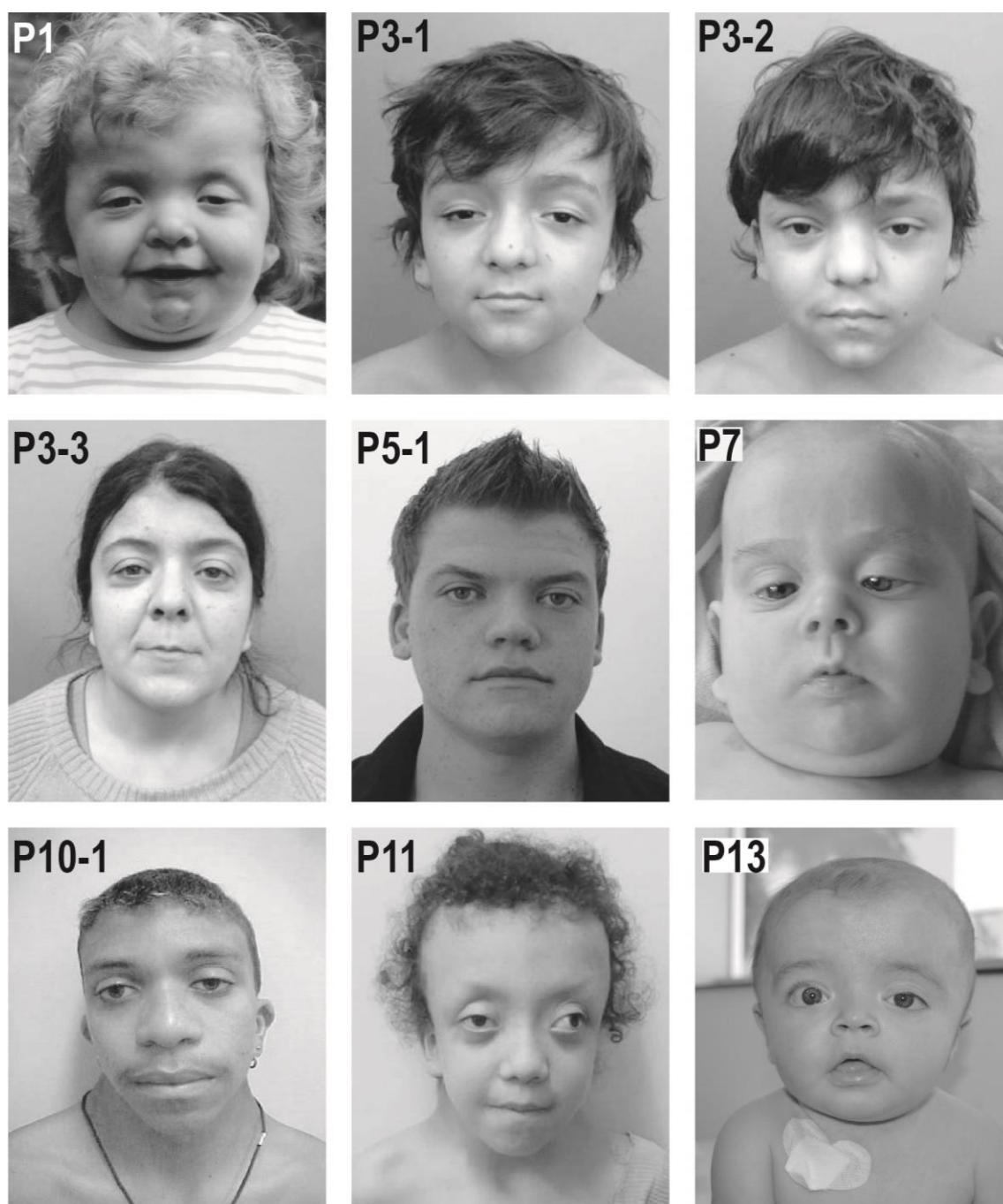


Figure 3.3: Clinical photographs documenting the craniofacial phenotype of patients with heterozygous *NRAS* mutations. The patients' ID numbers (according to Table 3.1) are given in the upper left

corner of each photograph. Written consent was obtained from the patient or his/her legal guardian for publication of the images. P1: G12S, 4 years old; P3-1, P3-2, P3-3: I24N, familial observation with affected family members shown at age 10, 13, and 36 years, respectively; P5-1: G60E, 17 years old; P7:E37dup, 6 month old; P10-1: G60E, 18 years old; P11: T50I, 11 years old; P13: G12D, 1 year old. This figure is adopted from (Altmuller et al. 2017a).

Patient 13 (p.G12D) is a male born after an uneventful pregnancy except for mild fetal pyelocalyceal dilatation (7 mm) of the left kidney detected on ultrasound scans. Birth weight at term was 4.060 g, body length 51 cm, and head circumference 37.5 cm. He had no feeding problems and no lymphatic anomalies. A few café-au-lait spots were noted on neonatal examination, and he was therefore followed up because of a suspected diagnosis of neurofibromatosis. At the age of three months, a blood cell count showed leukocytosis with 3% blast cells on a peripheral blood smear, mild anemia, and thrombocytopenia. On examination, he showed four café-au-lait spots over 0.5 cm diameter and three melanocytic nevi on lower limbs and buttocks, macrocephaly with suggestive facial features of NS (Figure 3.3), short neck but no thorax deformities, hepatosplenomegaly (4 and 3 cm, respectively), normal male genitalia with descended testes, and normal hands and feet. Bone marrow biopsy showed findings consistent with a myeloproliferative disorder. A brain MRI showed subdural fluid accumulations but no brain structural anomalies. Cardiological examination and echocardiography were normal. The heterozygous *NRAS* mutation was identified in leukocyte DNA and later confirmed in DNA extracted from skin fibroblasts, but was absent in both parents. Although he met clinical and analytical/cytological criteria for the diagnosis of JMML, in view of the stability of the blood cell counts and absence of complications, it was decided not to start treatment and follow him up closely. Until the age of 11 months, this child has remained stable hematologically, without proliferative phenomena or infectious complications. He was not short in stature, and his motor development was still within the normal range. A detailed developmental assessment was not possible yet due to his young age.

Table 3.1 Clinical features of patients with *NRAS* mutations.

Patient ID	1	2	3-1	3-2	3-3	4-1	4-2	5-1	5-2	5-3	6	7	8	9	10-1	10-2	11	12	13
Age at last follow-up	5y	IUFD at 22+3 weeks	13y8mo	10y3mo	36y	6y8mo	42y	21y	1 day	50	2y5mo	2y5mo	7y1mo	2y1mo	18y4mo	8y11mo	11y3mo	1y0mo	1y0mo
Gender	f	m	m	m	f	f	f	m	f	m	f	f	f	m	m	m	f	f	m
Genotype	p.G12	p.G12V	p.I24A	p.I24A	p.I24A	p.T50I	p.T50I	p.G60E	p.G60E	untested	p.G60E	p.E37dup	p.T58I	p.T50I	p.G60E	p.G60E	p.T50I	p.G12A	p.G12A
Segregation	<i>de novo</i>	<i>de novo</i>	Mat. Inherit.	Mat. Inherit.	?	Mat. Inherit.	likely <i>de novo</i>	Likely pat. Inherit.	Likely pat. Inherit.	Possibly mat. Inherit.	<i>de novo</i>	father untested, mother no mutation	Mosaicism in father	parents not tested	?	Pat. Inherit.	?	<i>de novo</i>	<i>de novo</i>
Mutation confirmed in non-hematopoietic tissue	finger nails, buccal cells												saliva, urine					finger nails	skin fibroblasts
Phenotype	NS	ND	NS	NS	NS	NS	NS	NS	NS	NS	NS	CFCS	NS	NS	NS	NS	CFCS	CS	NS
Prenatal findings	-	NE, HF	PH	-	ND	PH, HD	ND	PH, PST	PE, FA	ND	NE, PE, mild VM, congenital chylothorax	NE, PH, intracerebral arachnoid cyst, bilateral hydro-nephrosis	ND	ND	-	PH	-	PH	PH, mild pyelo-calycal dilatation left kidney
Feeding difficulties	+	ND	-	-	ND	-	ND	ND	-	ND	+	+	-	+	-	-	-	+	-
Heart defects/anomalies	VSD, ASD, HCM, PDA	ND	HCM	HCM	HCM	HCM	-	PST, VSD	HCM	-	-	ASD	-	AVS	-	-	MVP	PDA, HCM	-
Lymphedema	-	ND	-	-	-	-	-	-	nLE	-	nLE, nCT	nLE	-	-	-	-	-	-	-
Height SDS	-2.91	ND	-2.60	-1.91	-1.41	0.13	ND	0.32 (at 12y)	ND	-1.81	-2.44	-2.69	0.17	-1.43	-3.60	-1.35	-1.47	-0.80	1.03
Developmental delay	MD	ND	ID(m)	MD, ID(m)	ID(m)	-	-	ID(m)	ND	-	-	MD, ID(s)	MD	-	-	-	MD, ID(m)	MD	-
Cryptorchidism	NA	ND	+	+	NA	NA	NA	+	NA	+	NA	NA	NA	+	-	-	NA	NA	-
Hair and skin	CH	ND	WH, MN	WH	CH, MN, HA	SH, CH, SE, KP	-	ML	ND	ML	-	SH, HA	KP	KP, HA	MN	-	KP, MN	SH, MN	MN, CalS
Skeletal	SN	ND	SN	SN	SN	TH, SN	SN	TH, SN	ND	TH, SN	-	TH, SN	TH, SN	SN	SN	SN	SN	TH, SN	SN
Bleeding diathesis	-	ND	+	+	-	-	-	-	ND	-	-	-	VW	-	-	-	-	-	ND
Ocular abnormalities	PT	ND	PT	PT, RE	PT	PT	PT	PT	ND	PT	PT	RE, ST, optic nerve pallor, gaze deviation	PT, RE	ST	PT, RE	-	PT, RE, ST	PT	PT
Additional									died on 1st day of life from severe hydrops; post mortem MRI: left ventricular hypertrophy		mildly dilated ventricles and extra-axial spaces	1.24 Mb gain from 22q11.23; hydro-nephrosis with duplex collecting system			Right clubfoot	Bilateral clubfoot	Hydrocephalus; perinatal complications with asphyxia, sepsis, and portal vein thrombosis	upper airway obstruction requiring tracheostomy; hyper-insulinemic hypoglycaemia; hypothalamic tumor	minor renal anomalies, JMML, external hydrocephalus

NRAS mutations are described in the one-letter code according to the isoform NP_002515.1; +: present; -: absent; ASD: atrial septal defect; AVS: atrial valve stenosis; CalS: Café au lait spots; CFCS: Cardio-Facio-Cutaneous syndrome; CH: curly hair; CS: Costello syndrome; f: female; FA: foetal ascites; HA: haemangioma; HCM: hypertrophic cardiomyopathy; HD: prenatal heart defect; HF: hydrops fetalis; ID(m): intellectual disability (mild); ID(s): intellectual disability (severe); IUFD: intrauterine foetal death; KP: keratosis pilaris; m: male; mo: month(s); mat. inherit: maternally inherited; MD: motor delay; ML: multiple lentiginos; MN: multiple nevi; MVP: mitral valve prolapse; NA: not applicable; nCT: neonatal chylothorax; ND: no data; NE: foetal nuchal oedema; nLE: neonatal lymphatic oedema; NS: Noonan syndrome; pat. inherit: paternally inherited; PDA: persistent ductus arteriosus; PE: fetal pleural effusions; PH: polyhydramnios; PST: pulmonary stenosis; PT: ocular ptosis; RE: refractive error; SE: sparse eyebrows; SH: sparse hair; SN: short neck/webbed neck; ST: strabismus; TH: thorax anomaly; VM: ventriculomegaly; VSD: ventricular septal defect; VW: von Willebrand syndrome; WH: wooly hair; y: year(s). This table is adopted from Altmuller et al. (2017a).

3.2. Characterization of Shp2^{D61Y} animals

3.2.1. Generation of Shp2^{D61Y} mouse strain

To obtain viable animals expressing overactive Shp2^{D61Y} selectively in brain, we crossed heterozygous conditional Shp2^{floxedD61Y/WT} animals (Chan et al. 2009) with animals homozygous for Emx1^{IRESCre} allele (Figure 3.4A). The endogenous Emx1 promoter drives expression of cre recombinase from embryonic day 10.5 onwards selectively in excitatory neurons and astrocytes of the forebrain and ventral pallidum in mice carrying the *Emx1*^{IRESCre} allele (Gorski et al. 2002). Our breeding scheme was designed to yield offspring that are all heterozygous for Emx1^{IRESCre} allele, while 50% are wildtype for the *Ptpn11* locus (Shp2^{WT/WT}; from here on referred to as **control** or **CTRL**) and 50% are heterozygous for the mutation (Shp2^{floxedD61Y/WT}; referred to as **Shp2^{D61Y}** further on). The average breeding couple had five litters with a mean litter size of six pups. Data are calculated from approximately 200 litters of 40 breeding couples. The analysis of 348 male offspring confirmed an equal ratio of animals surviving by the age of 5 weeks (49% control vs. 51% Shp2^{D61Y}). Female offspring were not weaned and genotyped but their occurrence at birth quantified as the male/female ratio in Figure 3.4B was equal to their male littermates. Thus, the spatially and temporally restricted expression in Shp2^{D61Y} obviously circumvented embryonic lethality reported earlier for its constitutive expression (Chan et al. 2009). The expression of a functionally activated gene product was proven by measuring the protein tyrosine phosphatase (PTP) activity of Shp2 using a specific colorimetric assay. Therefore, forebrain lysates were prepared from eight weeks old control and Shp2^{D61Y} animals. Using this lysate, we measured an almost three-fold increase in the SHP2-specific PTPase activity in Shp2^{D61Y} samples compared to controls (288±4% PTPase activity of control, n=3 experiments with 1 mouse per genotype; *p≤0.05; one-sample t-test; Figure 3.4C). This finding is in line with previous publications (Chan et al. 2009). In sagittal brain slices stained with antibodies against the presynaptic marker Bassoon, the inhibitory marker VGAT, the excitatory marker VGLUT, and DAPI we did not observe any gross morphological defects in the brain structure comparing control and Shp2^{D61Y} animals (Figure 3.4D). Brain slices and subsequent staining was performed by Anil Annamneedi.

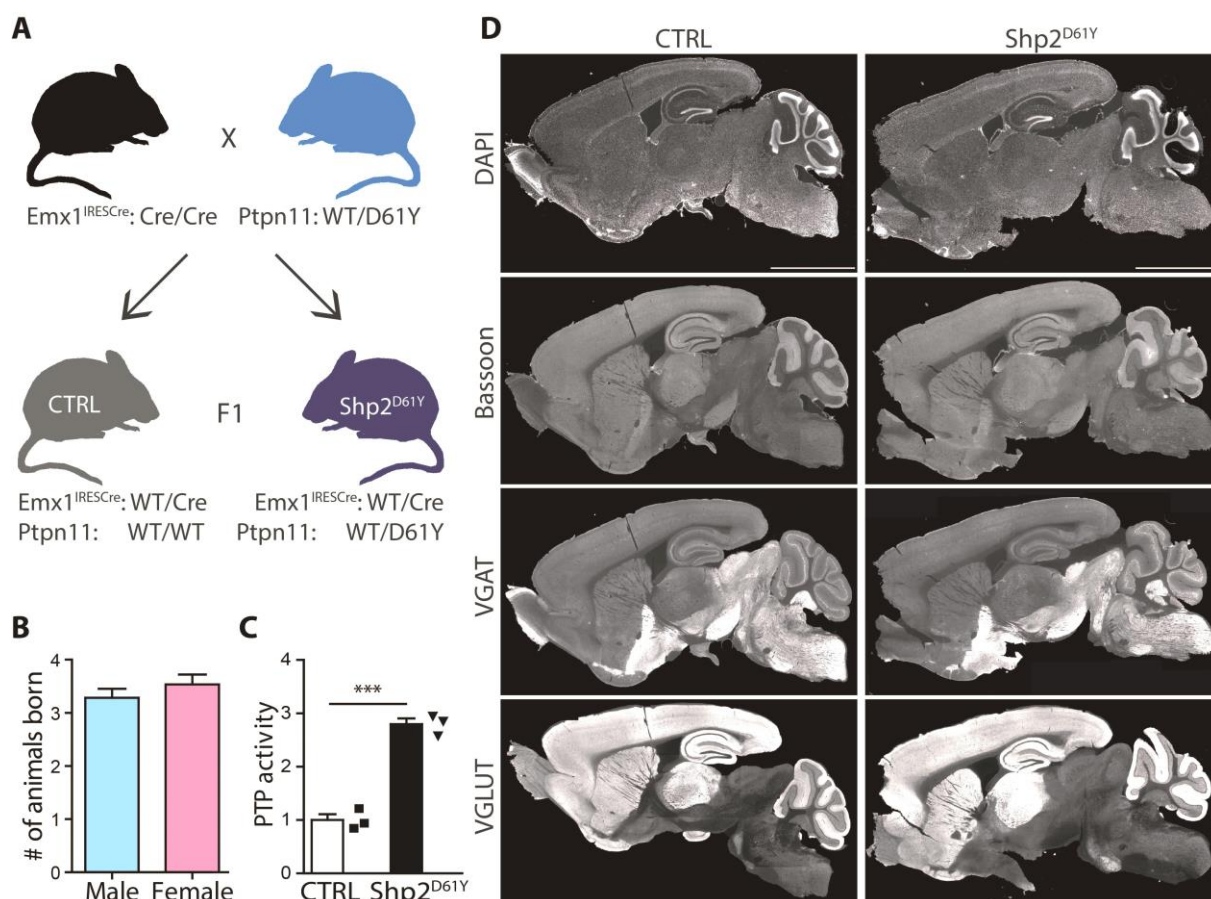


Figure 3.4: Establishment of the mouse strain $Shp2^{D61Y}$. (A) Breeding scheme. Animals homozygous for the knock-in allele $Emx1^{IRESCre}$ (Cre/Cre, black) and animals heterozygous for the KI allele in $Ptpn11$ (WT/D61Y, light blue) were used as parent animals. Resulting offspring are all heterozygous for the $Emx1^{IRESCre}$ knock-in allele expression ($Emx1^{IRESCre/WT}$) and either wildtype (WT/WT, grey), further on referred to as Control (CTRL), or heterozygous for $Ptpn11$ transgene expression (WT/D61Y, dark blue), now called $Shp2^{D61Y}$. (B) Sex ratio of progeny from breeding couples described in (A) is not affected by the transgene expression. (C) $Shp2$ -specific PTPase activity was 3-fold higher in $Shp2^{D61Y}$ forebrain homogenate as compared to controls. Data are shown as normalized mean \pm SEM and analyzed using one sample t-test, * $p < 0.05$. Dots indicate the values of three $Shp2^{D61Y}$ animals. (D) The overall brain morphology is not affected in $Shp2^{D61Y}$ animals. Sagittal sections of brains from control and $Shp2^{D61Y}$ mice were stained with antibodies against Bsn, VGAT, and VGLUT and with DAPI. Scale bar: 3.5 mm. Slices were prepared and stained by Anil Annamneedi. This figure is adapted from Altmuller et al. (2017b).

3.2.2. Morphometric analyses of $Shp2^{D61Y}$ neurons

Since there is evidence that $Shp2$ is required for neuronal outgrowth (Rosario, Franke et al. 2007), we analyzed the axon length and the dendritic arborization of hippocampal neurons derived from $Shp2^{D61Y}$ newborns and their control littermates. Dendrites and axons were visualized by immunostaining with antibodies against MAP2 and Tau1 in neurons cultured for 5 days *in vitro* (DIV; Figure 3.5A). The complexity of dendritic arborization was assessed by counting the number of intersections on the array of concentric circles centered over the cell body (Figure 3.5B) and plotting the number of intersection as a function of distance from the soma (Sholl analysis; Figure

3.5D). No significant differences were found in this analysis using the area under the curve as a statistical readout (control vs. Shp2^{D61Y}, 427.5 ± 13 vs. 404.5 ± 13 , $n=137$ vs. 134 cells from 3 experiments, $p \geq 0.05$; student's t-test, Figure 3.5D). The length of the longest outgrowing neurite did also not differ between the genotypes (Control vs. Shp2^{D61Y}, 249 ± 9 vs. 243 ± 11 μm , $n=187$ vs. 188 cells from 3 experiments, $p \geq 0.05$; student's t-test, Figure 3.5D). This indicates that the Shp2^{D61Y} mutation does not lead to profound changes in the neuronal morphology in our model, which is consistent with the unchanged gross brain morphology in these mice (Figure 3.4D).

Next, we tested whether the neuronal expression of Shp2^{D61Y} affects synaptogenesis. The number of excitatory synapses was characterized by the co-localization of the presynaptic marker Bassoon with the postsynaptic marker of excitatory synapses Homer1. Inhibitory synapses were identified using antibodies directed against the vesicular GABA transporter (VGAT) and Bassoon. Both, inhibitory and excitatory synapses were quantified on 20 μm long segments of proximal dendrites of 14 DIV old neurons. Neither the number of excitatory nor the number of inhibitory synapses differed between neurons from control and Shp2^{D61Y} (Figure 3.5E-H; control vs. Shp2^{D61Y}; excitatory: 46 ± 2 vs. 48 ± 2 puncta, $n=183$ vs. 185 cells from 11 experiments; inhibitory: 17 ± 2 vs. 16 ± 1 puncta, $n=49$ vs. 47 cells from 3 experiments). Thus, the essential basis of a balanced excitatory-inhibitory synaptogenesis is unchanged.

In hippocampal neurons, a part of the existing synapses is silent and does not take part in synaptic transmission. This can be linked to either the lack of neurotransmitter release from presynaptic terminals or to low/no expression of α -amino-3-hydroxy-5-methyl-4-isoxazolepropionic acid receptors (AMPA receptors) at the surface of the postsynaptic element (Voronin and Cherubini 2004, Kerchner and Nicoll 2008). To test this hypothesis, we first visualized active presynapses undergoing neurotransmitter release in living neurons at the age of 14 DIV with an antibody against the luminal epitope of synaptotagmin1 (Syt1 AB) upon brief stimulation with 50 mM KCl. This antibody binds to its epitope when exposed to the synaptic cleft during synaptic vesicle fusion and is taken up during compensatory endocytosis (Kraszewski et al. 1995). The brief hyperpolarization facilitates the identification of active synapses. After fixation, neurons were co-stained with the synaptic markers Bassoon and Homer1 to identify excitatory synapses. We did not observe any differences in the density of active excitatory presynapses between the genotypes (Control vs. Shp2^{D61Y}, 13 ± 1 vs. 12 ± 1 puncta per 20 μm dendrite, $n=82$ vs. 61 cells from 5 experiments Figure 3.5G, H). Based on these data, we can exclude the lack of presynaptic neurotransmitter release and alterations in the abundance of functional synapses in Shp2^{D61Y} neurons.

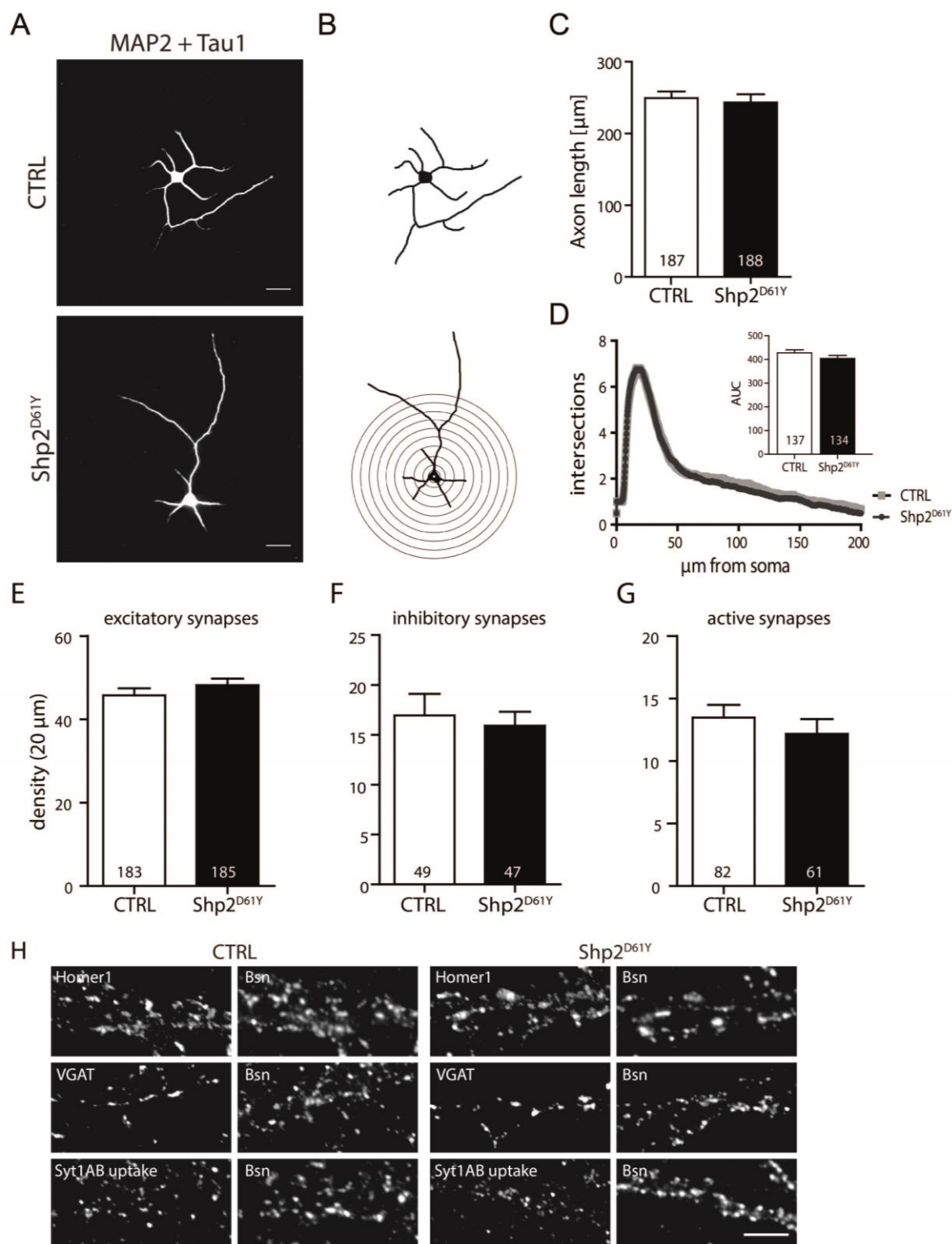


Figure 3.5: Morphological analysis of Shp2^{D61Y} neurons. (A) DIV5 neurons were stained with antibodies against the dendritic marker MAP2 and the axonal marker Tau1 for the assessment of dendritic arborization and axonal outgrowth. Scale bar: 50 μm . (B) Top: Example image of a neuron from (A) after binarization and placement of the array of concentric circles used for Sholl analysis. Bottom: Sholl analysis of DIV5 neurons is shown, where the number of ramifications is plotted against the distance from the soma. (C-D) The axonal length (C) and the area under the curve (AUC) in Sholl analysis (D) do not differ between control and Shp2^{D61Y} neurons. (E-H) Immunostaining of excitatory (positive for Homer1; E), inhibitory (positive for VGAT; F) and active (showing syt1AB uptake; G) synapses in DIV14 neurons from control and Shp2^{D61Y}. Data are presented as mean \pm SEM and analyzed using unpaired t-test. The numbers in columns indicate the number of cells analyzed. (H) Images show representative staining on 20 μm sections of proximal dendrites used for the

quantification of excitatory, inhibitory, and active synapses. Scale bar 5 μ m. This figure is adapted from Altmuller et al. (2017b).

3.2.3. Surface expression of glutamate receptors in Shp2^{D61Y} neurons

Ras signaling has been implicated in the regulation of the delivery of AMPARs to the postsynaptic plasma membrane (Zhu, Qin et al. 2002), which is a major determinant of the sensitivity of postsynapses to neurotransmitters. To monitor the surface expression level of AMPARs in synapses, living cells were stained with antibodies against the extracellular epitopes of AMPAR subunits. We used an antibody binding to the GluA isoforms 1-4 (panGluA) and antibodies specific to the extracellular epitopes of GluA1 and GluA2 (Figure 3.6A). There were no changes in the staining density of the antibodies recognizing panGluA and GluA1 subunits on the surface of control and Shp2^{D61Y} neurons (Figure 3.6B and Table 3.2). However, in Shp2^{D61Y} neurons the surface staining intensity of the GluA2 receptor subunit was slightly but significantly decreased ($86\pm 4\%$ of controls, $p < 0.05$, t-test; Figure 3.6B).

In a parallel experiment the total expression levels of synaptic AMPARs in 14 DIV hippocampal neurons was quantified, too. After fixation and permeabilization of the cells the total synaptic expression of AMPAR subunits was assessed as immunofluorescence intensity (IF) that colocalizes with synaptic markers. The staining with GluA1 antibodies showed a significant decrease in the IF in Shp2^{D61Y} neurons ($74\pm 5\%$ of expression in control, $p < 0.001$, t-test), but was unchanged for panGluA and GluA2 antibodies (Figure 3.6A, C). In addition, the number of synapses showing GluA1 staining was significantly decreased, too (48 ± 2 in control vs. 37 ± 2 in Shp2^{D61Y}, $p < 0.01$, t-test, for all numerical values see Table 3.2 and 3.3), which points to a lower total expression level of synaptic GluA1 in Shp2^{D61Y} neurons.

Synaptic trafficking and removal of GluN2-containing NMDA receptors is tightly regulated and controlled by multiple pathways including RAS-MAPK signaling (Barria and Malinow 2002, Chung et al. 2004). To investigate the effect of dysregulated RAS-MAPK signaling on NMDA receptor abundance in postsynapses of Shp2^{D61Y} neurons, we made use of antibodies binding specifically the extracellular epitopes of GluN1, GluN2A, and GluN2B receptors. We again quantified the surface abundance as well as the total level of NMDA receptors in synapses as IF that colocalizes with synaptic markers. We found that both, the total expression levels and the total number of stained synapses, were unchanged for GluN1, GluN2A, and GluN2B receptors. Regarding the surface staining we could detect significant alterations neither in the surface density nor IF intensity of GluN1 and GluN2A receptor subunits. However, the surface IF intensity of GluN2B receptors

was markedly reduced in Shp2^{D61Y} neurons ($72 \pm 5\%$ of controls, $p < 0.001$, t-test; Table 3.2, Figure 3.6A-C), although their surface density was not affected.

The calculation of the relative change in the surface/total ratio (Table 3.2) of the single receptor subunits confirmed the observed alterations in their synaptic expression. We find a relative decrease in the ratio of GluN2B receptor subunits on the surface as well as a relative increase in the level of GluA1 receptor subunits. The surface/total ratio of panGluA receptors staining also points to a relative increase in GluA receptor levels. In summary, these data reveal striking changes in the trafficking of AMPA and NMDAR in spines of Shp2^{D61Y} neurons.

Table 3.2: Synaptic expression of glutamate receptors

Receptor antibody	Surface staining			Total staining			Relative Change: Surface/Total
	Shp2 ^{D61Y} % of CTRL	Statistical Result	n (CTRL vs. Shp2 ^{D61Y})	Shp2 ^{D61Y} % of CTRL	Statistical Result	n (CTRL vs. Shp2 ^{D61Y})	
GluA1	95 ± 4	ns	26 vs. 24	74 ± 5	p<0.001	32 vs. 30	1,29
GluA2	86 ± 4	p<0.05	26 vs. 27	90 ± 5	ns	29 vs. 28	0,95
panGluA	116 ± 7	ns	31 vs. 30	91 ± 6	ns	45 vs. 41	1,28
GluN1	116 ± 10	ns	32 vs. 29	83 ± 13	ns	29 vs. 31	1,41
GluN2A	105 ± 6	ns	27 vs. 32	91 ± 4	ns	39 vs. 39	1,15
GluN2B	72 ± 5	p<0.001	41 vs. 42	95 ± 4	ns	48 vs. 44	0,76

This table is adopted from Altmüller et al. (2017b).

Table 3.3: Glutamate receptor density

Receptor antibody	Surface puncta			Total puncta		
	CTRL vs. Shp2 ^{D61Y} Mean ± SEM	Statistical Result	n (CTRL vs. Shp2 ^{D61Y})	CTRL vs. Shp2 ^{D61Y} Mean ± SEM	Statistical Result	n (CTRL vs. Shp2 ^{D61Y})
GluA1	9 ± 1 vs. 10 ± 1	ns	26 vs. 24	48 ± 2 vs. 37 ± 2	p<0.01	32 vs. 30
GluA2	11 ± 2 vs. 12 ± 2	ns	26 vs. 27	27 ± 3 vs. 20 ± 3	ns	29 vs. 28
panGluA	15 ± 1 vs. 17 ± 2	ns	31 vs. 30	17 ± 2 vs. 14 ± 2	ns	45 vs. 41
GluN1	46 ± 3 vs. 43 ± 3	ns	32 vs. 29	34 ± 3 vs. 30 ± 3	ns	29 vs. 31
GluN2A	36 ± 4 vs. 40 ± 3	ns	27 vs. 32	41 ± 2 vs. 42 ± 2	ns	39 vs. 39
GluN2B	29 ± 3 vs. 29 ± 4	ns	41 vs. 42	55 ± 3 vs. 52 ± 3	ns	48 vs. 44

This table is adopted from Altmüller et al. (2017b).

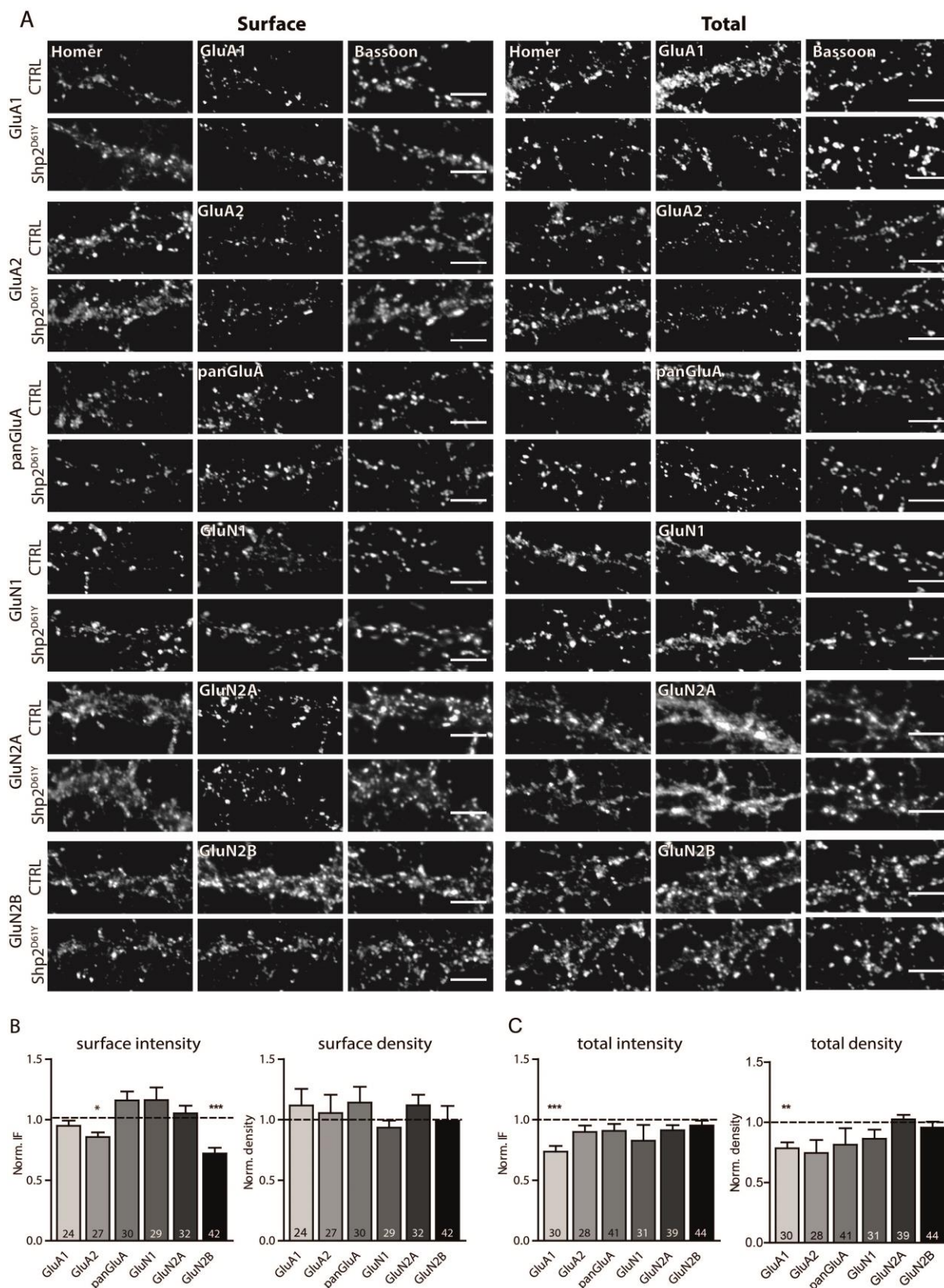


Figure 3.6: Synaptic expression level of glutamate receptors is affected in Shp2^{D61Y} neurons. (A) Representative examples of the staining of synaptic surface (left) and total (right) glutamate receptors containing GluA1, GluA2, panGluA, GluN1, GluN2A, or GluN2B subunits, respectively, in neurons from control and Shp2^{D61Y} animals. Excitatory synapses were stained for Homer and Bassoon. Scale bar: 5 μ m. **(B, C)** Synaptic IF intensity and density (puncta per 20 μ m of proximal dendrite) of surface **(B)** and total **(C)** staining for all tested receptor subunits are shown. Values are normalized to the respective value in control, represented by

the dashed line in the graphs. Note the reduced surface expression of GluA2 and GluN2B and the decrease of the overall expression of GluA1 in Shp2^{D61Y} neurons as compared to controls. All numerical values and statistics are listed in Table 3.2 and 3.3. Scale bar: 5 μ m. Data are presented as mean \pm SEM and analyzed using unpaired t-test (* $p \leq 0.05$, ** $p \leq 0.01$, *** $p \leq 0.001$). Numbers in columns indicate the number of cells analyzed. This figure is adapted from Altmüller et al. (2017b).

3.2.4. Reorganization of synaptic vesicle pools in Shp2^{D61Y} neurons

SV pools are involved in numerous presynaptic mechanisms regulating synaptic strength and plasticity (Alabi and Tsien 2012). Furthermore, hyperactive RAS was shown to modulate docking and release probability of SVs (Seeger et al. 2004, Kushner et al. 2005). To answer the question, whether synaptic vesicle pools are altered in Shp2^{D61Y} neurons, we first performed the Synaptotagmin1 antibody (Syt1 AB) uptake assay in 14 and 21 DIV old neurons. Using this assay, we can monitor the recycling rate of SV. This antibody is internalized into the lumen of synaptic vesicles after their exo- and endocytosis, and the amount of uptake closely reflects the level of vesicle recycling as a measurement of activity and release probability at individual synapses (Kraszewski et al. 1995) (see Figure 3.7.1A). The Syt1 AB uptake assay was performed either in physiological solutions for 20 min (displaying the network activity-driven release of SVs) or upon brief application of the physiological solution containing 50 mM KCl for 4 min leading to the depolarization-induced release of all SVs of the total recycling pool (TRP). In both conditions, cells were stained with antibodies against Homer1 and Bassoon to identify functional excitatory synapses after completion of the Syt1 AB uptake assay. Only excitatory synapses were analyzed as judged by the colocalization of the presynaptic marker Bassoon and the excitatory marker Homer1.

The quantification of the Syt1 AB uptake assay IF intensity under physiological conditions in 14 DIV old neurons showed a clear increase in IF intensity in Shp2^{D61Y} neurons, reflecting an increase in the basal recycling of SVs (Control vs. Shp2^{D61Y}, $100 \pm 5\%$ vs. $132 \pm 11\%$ IF, $n=70$ vs. 72 cells from 6 experiments, Figure 3.7.2A and B). However, hyperpolarization of the membrane with 50 mM KCl to evoke the release of vesicles from the TRP did not show any differences in 14 DIV Shp2^{D61Y} neurons (Control vs. Shp2^{D61Y}, $100 \pm 6\%$ vs. $101 \pm 10\%$ IF, $n=77$ vs. 64 cells from 6 experiments, Figure 3.7.2A and C). Furthermore, the number of active synapses in 14 DIV neurons was not changed as shown in Figure 3.5G. In contrast to the data obtained from 14 DIV neurons, the spontaneous activity-driven recycling of SVs in 21 DIV neurons did not show significant differences between the two genotypes (Control vs. Shp2^{D61Y}, $100 \pm 9\%$ vs. $96 \pm 12\%$ IF, $n=46$ vs. 46 cells from 4 experiments, Figure 3.7.2D and E). Strikingly, the KCl-induced release of SVs was significantly reduced in 21 DIV old Shp2^{D61Y} neurons, implying a significant downregulation of the RP size in Shp2^{D61Y} neurons as compared to control (Control vs. Shp2^{D61Y}, $100 \pm 9\%$ vs. $58 \pm 6\%$ IF, $n=43$ vs. 33 cells from 3 experiments, Figure 3.7.2D and F).

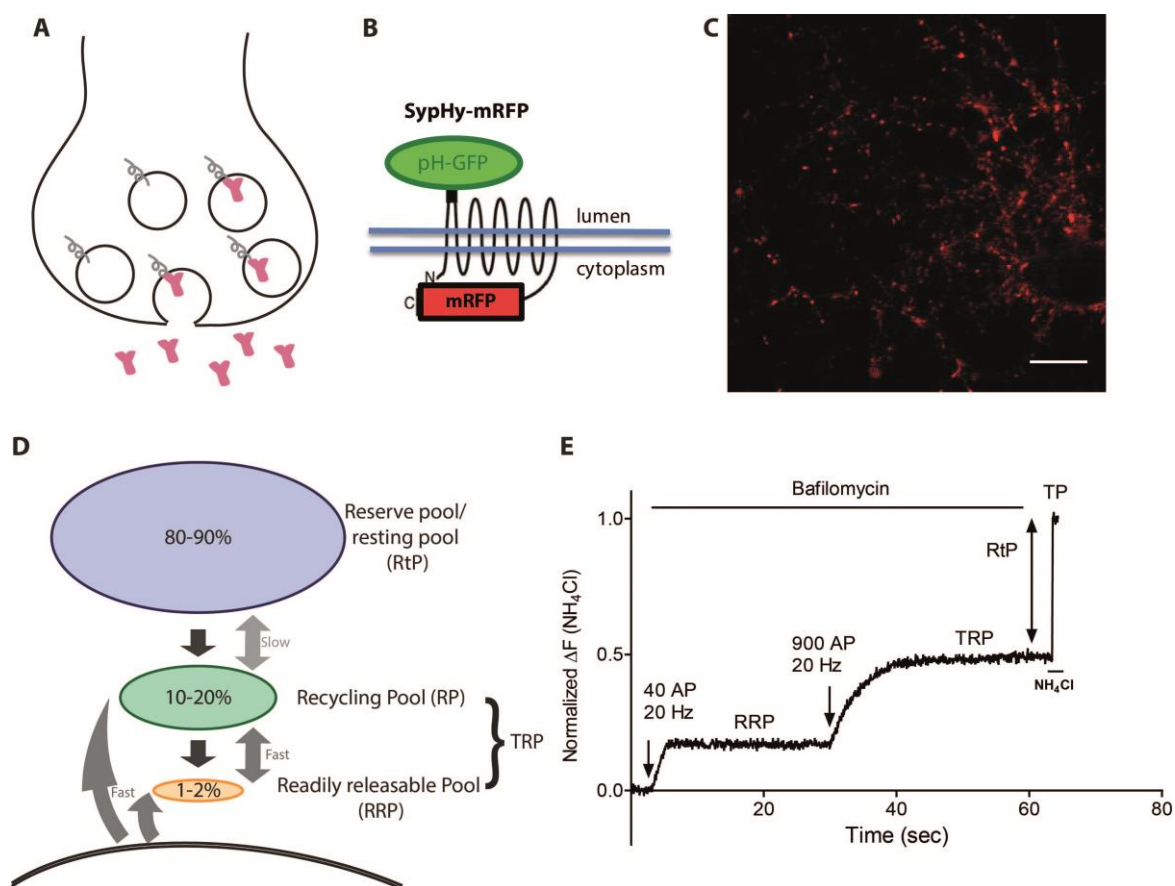


Figure 3.7.1: Methods for the analysis of synaptic vesicle pool sizes. **(A)** Principle of Syt1 AB uptake. During neurotransmitter release the inner luminal domain of Syt1 is available for the antibodies to bind. During vesicle recycling antibodies are incorporated into recycling vesicles and thus serve as an indirect readout for release probability. In this way the relative sizes of readily releasable pool (RRP) released under physiological conditions and total recycling pool (TRP), released upon stimulation with a 50 mM KCl pulse can be estimated. **(B)** Schematic construct of SypHy molecule. An mRFP tag is coupled to the cytoplasmic domain of synaptophysin and a GFP-coupled pH sensor is coupled to its luminal domain. Cells infected with SypHy-virus can be identified by red fluorescent Synaptophysin staining at synapses. Upon vesicle fusion and neutralization of surrounding pH GFP fluorescence is quenched and lights up during live imaging. **(C)** Representative image of a neuron infected with SypHy-virus used for live imaging. Scale bar: 20 μm **(D)** Pool sizes and exchange rates of SVs in hippocampal neurons. Dark grey arrows indicate endocytosis and light grey arrows indicate mixing between pools. Figure based on Rizzoli and Betz (2005) and Alabi and Tsien (2012). **(E)** Example trace of a typical recording of SypHy experiment showing the three stimuli using 40 APs, 900 APs and a final ammonium pulse to unmask all SypHy-expressing vesicles. The change in fluorescence (ΔF) is plotted as a function of time. AP: Action potential; TRP: Total Recycling Pool; SypHy: Synaptophysin coupled to pH-sensor. The image in C and the example trace shown in E were kindly provided by Dr. Carolina Montenegro.

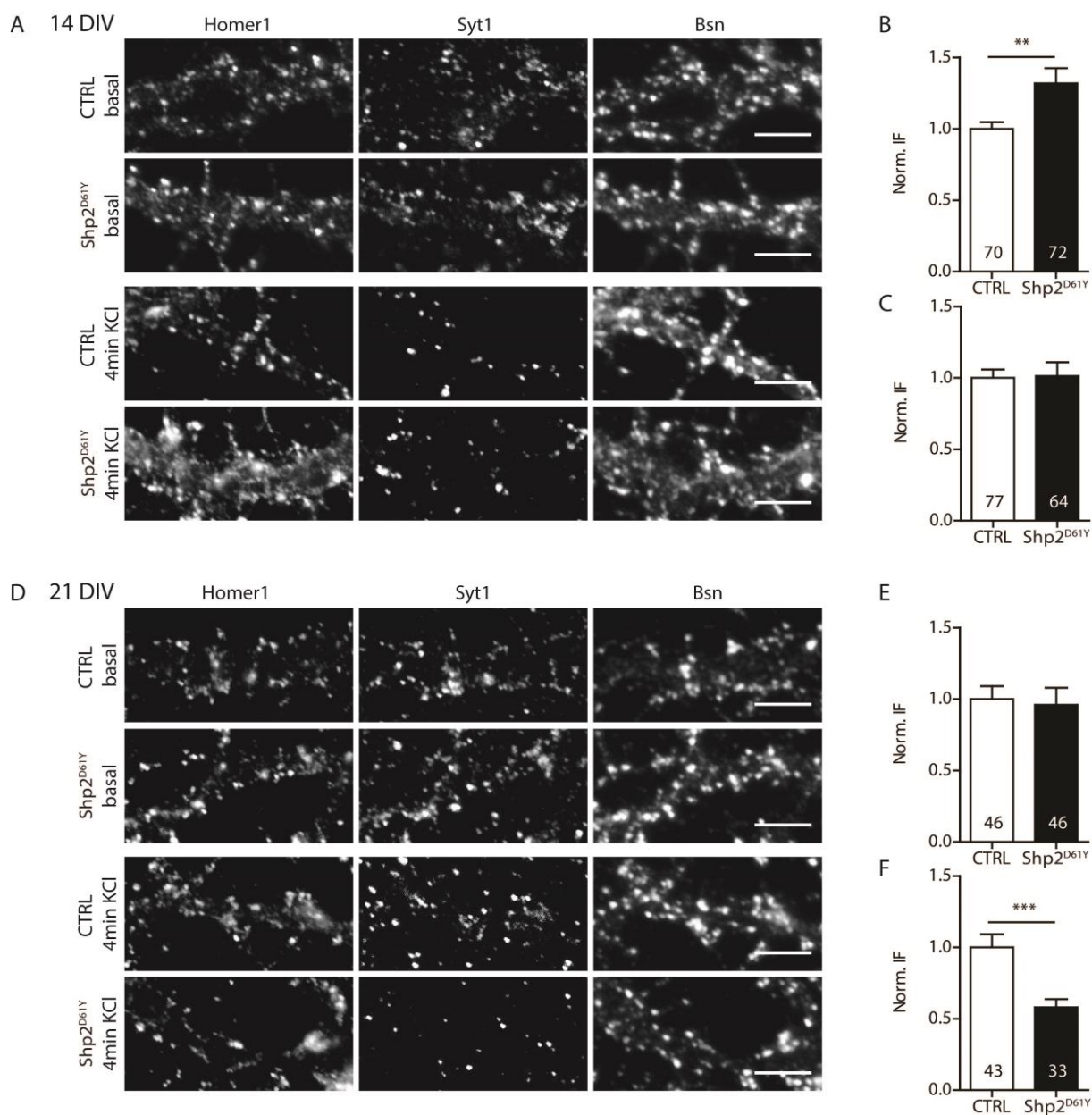
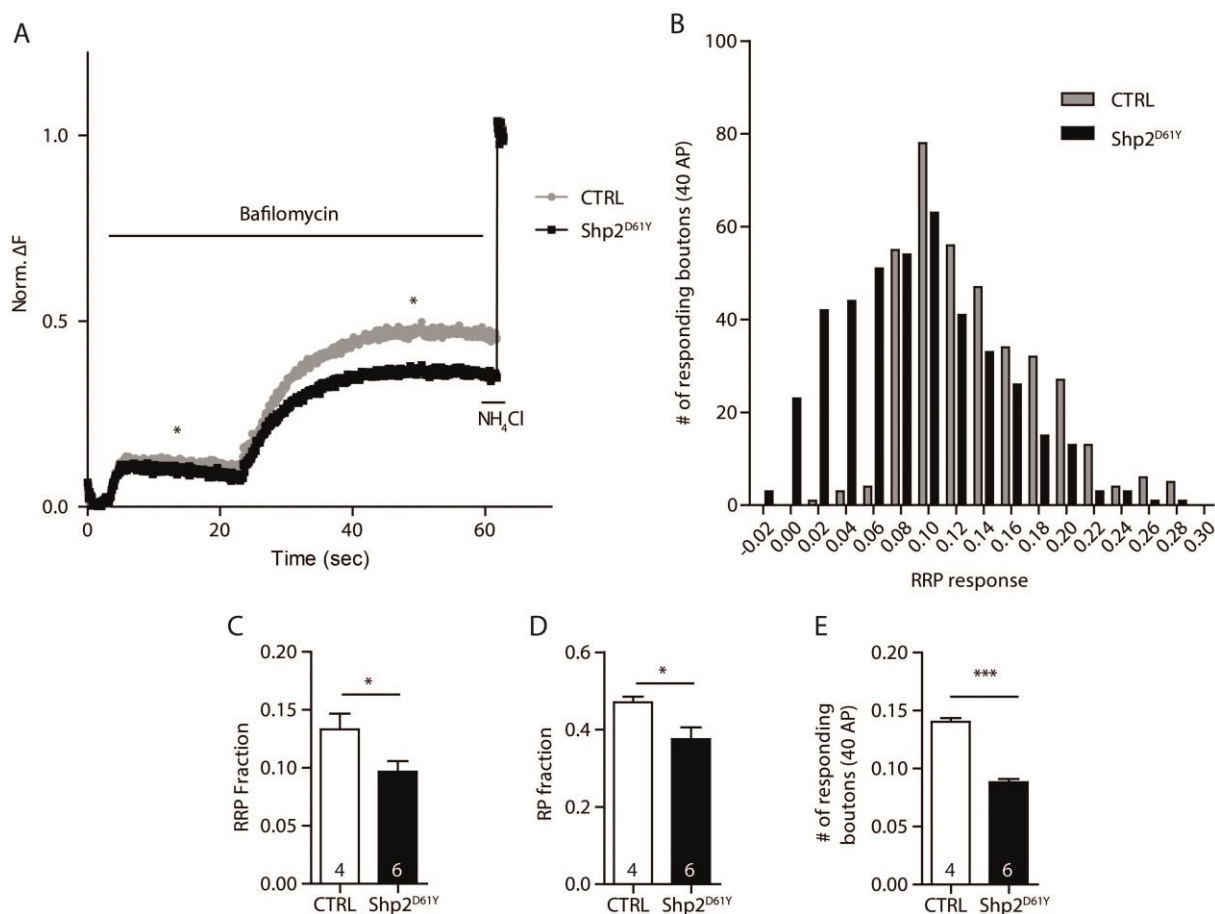


Figure 3.7.2: Changes in synaptic vesicle pool size in Shp2^{D61Y} neurons. (A and D) Representative images of 14 (**A**) and 21 (**D**) DIV old control and Shp2^{D61Y} neurons after Syt1 AB uptake assay under basal (physiological) and evoked conditions using 50 mM KCl for 4 min stained with antibodies against Homer1 and Bassoon. (**B**) Quantification of Syt1 IF under physiological conditions in 14 DIV old neurons. Shp2^{D61Y} neurons show a higher network activity-driven release of synaptic vesicles compared to control. (**C**) Quantification of Syt1 IF under evoked conditions using 50 mM KCl for 4 min in 14 DIV old neurons. There are no changes in the size of TRP between control and Shp2^{D61Y} neurons. (**E**) Quantification of Syt1 IF under physiological conditions in 21 DIV old neurons. Shp2^{D61Y} neurons are not altered in their basal vesicle recycling. (**F**) Quantification of Syt1 IF under evoked conditions using 50 mM KCl for 4 min in 21 DIV old neurons. There is a strong downregulation Syt1 IF in Shp2^{D61Y} neurons, indicating a smaller TRP in mutant neurons. Scale bar: 5 μ m. Data are presented as mean \pm SEM and analyzed using unpaired t-test (** $p \leq 0.01$, *** $p \leq 0.001$). Numbers in columns indicate the number of cells analyzed.



To verify the results from Syt1 AB uptake assay, we performed synapto-pHluorin (SyHy) experiments on 16 to 18 DIV control and Shp2^{D61Y} neurons. This experiment was done by Dr. Carolina Montenegro. As shown in Figure 3.7.3A, the change in fluorescence intensity after stimulation with 40 and 900 APs are smaller in Shp2^{D61Y} neurons compared to control. The delivery of 40 APs revealed that the RRP in Shp2^{D61Y} neurons was reduced by 27% on average ($73 \pm 10\%$ of control, $n=4$ vs. 6 cells from 2 experiments, Figure 3.7.3A and B). The RP size, revealed by the delivery of 900 APs, showed a reduction of 20% in Shp2^{D61Y} neurons ($80 \pm 3\%$ of control, Figure 3.7.3A, C). Thus, the analysis of vesicle pool size showed that 16 to 18 DIV old Shp2^{D61Y} neurons

have a significant reduction in the fraction of RRP and RP. Furthermore, the number of responding boutons upon stimulation with 40 APs was shifted in Shp2^{D61Y} neurons and decreased about 37% ($63 \pm 2\%$ of control, Figure 3.7.3D, E). The histogram of the peak of response upon stimulation with 40 APs implies that less SVs responded and the response itself was weaker (Figure 3.7.3D, E). This result is in line with the findings from Syt1 AB uptake assay in 21 DIV neurons. In summary, we demonstrate convincing evidence of a reduction of SV pool size and the subsequent reorganization of SV pools in Shp2^{D61Y} neurons.

3.2.5. Impairments of activity-induced phosphorylation of ERK in Shp2^{D61Y} neurons

To understand more about the underlying pathophysiology of the dysregulation of neuronal RAS-MAPK signaling due to the expression of Shp2^{D61Y} allele, we investigated a downstream target of this pathway. Therefore, we quantified the phosphorylation level of ERK in dissociated hippocampal cultures from control and Shp2^{D61Y} animals in basal conditions and after pharmacological stimulation of neuronal activity.

To investigate the translocation of pERK from neurites to the soma and its nuclear import in a time-dependent manner, we visualized the nuclear pERK level with an antibody specifically recognizing phosphorylated ERK1/2 upon stimulation of neuronal activity in 14 DIV old high-density hippocampal neurons (30000 cells per coverslip) from Shp2^{D61Y} animals and their control littermates by the application of 4AP and Bic. This treatment is known to enhance synaptic activity and induce activity-dependent gene transcription via calcium influx through NMDA receptors and voltage-gated calcium channels (Xiang et al. 2007, Vashishta et al. 2009). The cells were treated with 2.5 mM 4-AP and 50 μ M Bic (4AP/Bic) for 10 min, one, three, and 24 hours to increase network activity. The time course of changes in the nuclear abundance of pERK was investigated. Only excitatory neurons that specifically express overactive Shp2^{D61Y} in our animal model and therefore only neurons negative for staining against GAD65, a broad marker of inhibitory cells, were considered for this analysis. After ten min and one hour of 4AP/Bic stimulation, a strong increase in nuclear pERK level was evident in control neurons in high-density cultures. The nuclear pERK level returned to baseline after three hours and again increased after 24 hours of treatment in control cells (10 min: $166 \pm 8\%$; 1 h: $171 \pm 15\%$; 3 h: $122 \pm 9\%$; 24 h: $162 \pm 15\%$ of unstimulated control, t-test, Figure 3.8A, B). In contrast, already the basal level of nuclear pERK was strongly increased in Shp2^{D61Y} neurons. After ten min of 4AP/Bic treatment the nuclear pERK level in the mutant was still strongly increased, but decreased to control level after one and three hours. After

24 hours of treatment, the nuclear pERK level in the mutant rose again to a comparable extent as seen in the control (unstim.: $179\pm 14\%$; 10 min: $164\pm 12\%$; 1 h: $98\pm 9\%$; 3 h: $107\pm 7\%$; 24 h: $156\pm 11\%$ of unstimulated control, t-test, Figure 3.8A, B). These results suggest a biphasic activation of ERK with an early peak up to 1 hour and a second delayed peak after 24 hours of 4AP/Bic treatment in control neurons. A biphasic pattern of ERK activation is also seen in Shp2^{D61Y} neurons; however, time points and magnitude are altered (Figure 3.8B).

In a second approach of a time course experiment, we used the brain-derived neurotrophic factor (BDNF, 100 ng/ μ l, Figure 3.8C) as a stimulant for the same time points as before. BDNF can bind to TrkB receptors, which is known to be coupled to the activation of RAS-MAPK signaling (Leal et al. 2014). Moreover, Shp2 was shown to be important for the full activation of RAS-MAPK signaling (Easton et al. 2006). In our experiments, the stimulation of 14 DIV Shp2^{D61Y} and control neurons with BDNF led to a different pattern of pERK activation and nuclear translocation. All time points analyzed showed an increase in nuclear pERK level after BDNF treatment in control neurons (10 min: $180\pm 15\%$; 1 h: $172\pm 12\%$; 3 h: $161\pm 10\%$; 24 h: $177\pm 17\%$ of unstimulated control, t-test, Figure 3.8C, D). In Shp2^{D61Y} neurons the basal activity level was again increased. However, upon stimulation with BDNF we could not induce an activity-dependent additional increase in the phosphorylation of ERK in the mutant neurons (unstim.: $142\pm 10\%$; 10 min: $134\pm 13\%$; 1 h: $171\pm 12\%$; 3 h: $181\pm 18\%$; 24 h: $161\pm 16\%$ of unstimulated control, t-test, Figure 3.8C, D). This experiment was performed in collaboration with Santosh Pothula.

We further investigated the changes in neuronal activity upon 4AP/Bic treatment for 30 min in low density cultures (20000 cells/coverslip). Here, the basal level of nuclear pERK was not significantly changed comparing Shp2^{D61Y} to control neurons (Figure 3.9, nuclear pERK: $97\pm 5\%$ of control). The stimulation of neuronal activity led to significant increase in the nuclear pERK level in control neurons (Figure 3.9, nuclear pERK: $136\pm 8\%$ of control). Strikingly, this increase was fully absent in neurons from Shp2^{D61Y} (Figure 3.9, nuclear pERK: $102\pm 4\%$ of basal levels in Shp2^{D61Y}) further implying a pronounced dysregulation in neuronal activity-controlled ERK activation.

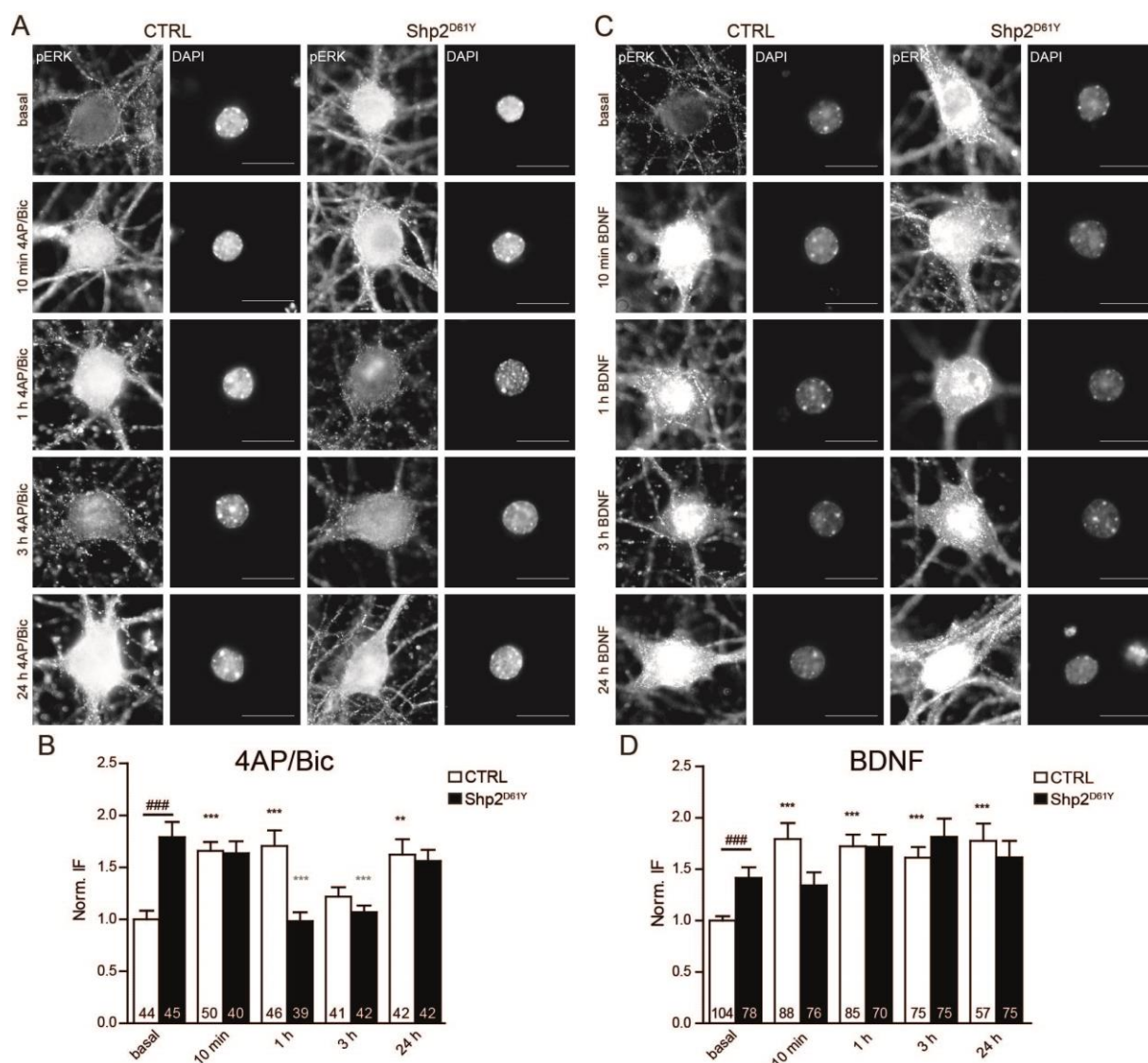


Figure 3.8: Time course of nuclear pERK accumulation induced by neuronal activity or BDNF is affected in Shp2^{D61Y} neurons. (A, C) Neurons of both genotypes are stained for pERK at different time points upon 4AP/Bic (A) or BDNF (C) application. DAPI staining was used as nuclear mask. Scale bar: 10 μ m. (B, D) Quantification of the nuclear pERK level as exemplified in the staining in A and C. The basal levels of nuclear pERK significantly differ between the genotypes (unpaired t-test, ### $p \leq 0.001$). The time course upon stimulation by both stimuli differed between Shp2^{D61Y} and control neurons. Data are shown as mean \pm SEM and numbers in columns of graphs indicate number of analyzed cells. The stimulation-induced changes were compared to basal pERK levels in each genotype and significance was assessed using one-way ANOVA and Dunnett's multiple comparison test (** $p \leq 0.01$ and *** $p \leq 0.001$). Data are shown as mean \pm SEM. Santosh Pothula and I performed this experiment together. This figure is adopted from Altmuller et al. (2017b).

Finally, control and Shp2^{D61Y} neurons from low density cultures with the inhibitors of glutamate receptors D(-)-2-amino-5-phosphonopentanoic acid (40 μ M, APV) and 6-cyano-7-nitroquinoxaline-2,3-dione disodium (100 μ M, CNQX) for 30 min to decrease the overall network activity. In contrast to the ineffective activity-induced activation and translocation of ERK into nucleus in the mutant, silencing of neuronal activity led to rapid decrease of nuclear pERK in both control and Shp2^{D61Y} neurons (Figure 3.9, Shp2^{D61Y}: $49 \pm 4\%$ and Shp2^{D61Y}: $44 \pm 2\%$ of baseline levels

in the respective genotype), suggesting that neuronal inactivity-induced dephosphorylation and nuclear export of pERK is unaffected in $\text{Shp2}^{\text{D61Y}}$ neurons.

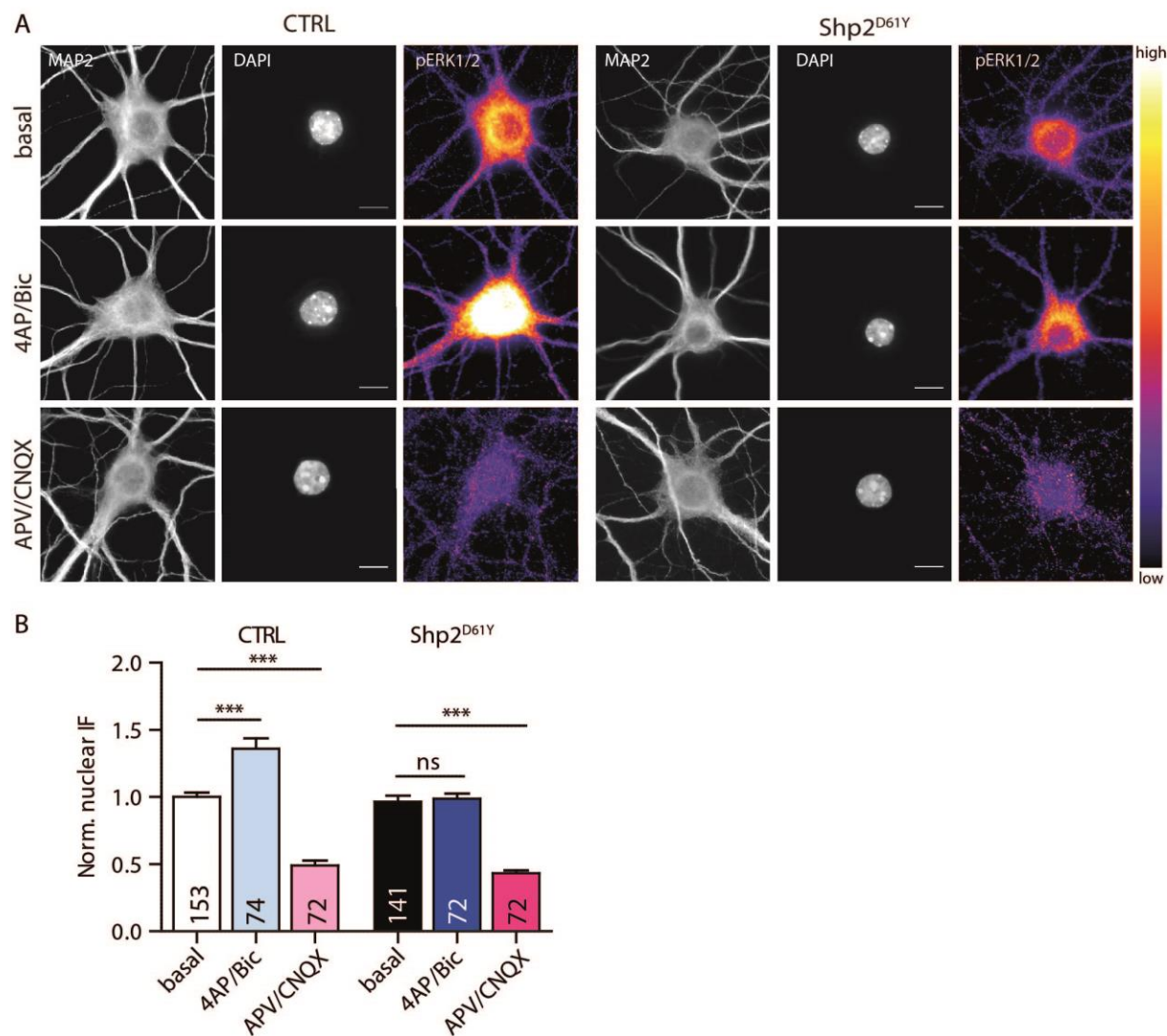


Figure 3.9: Activity-induced nuclear translocation of pERK is disturbed in $\text{Shp2}^{\text{D61Y}}$ neurons. (A) Representative pictures of 14 DIV old neurons in control situation, 30 min after stimulation of network neuronal activity using 2.5 mM 4AP and 50 μM Bic, and 30 min after silencing with 40 μM APV and 100 μM CNQX. Neurons are stained with antibodies against MAP2 as neuronal marker, pERK, and DAPI as a nuclear marker. Scale bar 10 μm . (B) Quantification of the nuclear IF of pERK in control and $\text{Shp2}^{\text{D61Y}}$ neurons upon stimulation (4AP/Bic) and silencing of NMDA receptor-mediated network activity (APV/CNQX). The stimulation protocol leads to a significant increase in the nuclear pERK level in control neurons, but fails to do so in $\text{Shp2}^{\text{D61Y}}$ neurons. APV-CNQX treatment shows comparable effects in control and $\text{Shp2}^{\text{D61Y}}$ neurons without major differences. Numbers in columns represent the number of cells analyzed. This figure is adopted from Altmüller et al. (2017b).

Moreover, we quantified the phosphorylation level of ERK in a second experimental approach using acute hippocampal slices from control and $\text{Shp2}^{\text{D61Y}}$ animals in basal conditions and after

pharmacological stimulation of neuronal activity with 4AP/Bic. The investigation of ERK phosphorylation in acute hippocampal slices was part of the work of Santosh Pothula. The experiment is described in detail in his thesis, as well as in Altmuller et al. (2017b).

3.2.6. Impairments of activity-induced gene regulation in Shp2^{D61Y} neurons

To further investigate the effect of the overactive Shp2^{D61Y} on the regulation of neuronal gene expression, the regulation of the BDNF promoter I and II containing the cAMP-response element (CRE)-binding protein (CREB) was investigated. CREB is an important downstream target of nuclear pERK and binds to CRE in the promoter region of BDNF (Wu et al. 2001a, Hardingham et al. 2002). Additionally, a role of the C-terminal Binding Protein 1 (CtBP1) was examined, which is a transcriptional co-repressor and is known to be involved in the activity-dependent reconfiguration of gene expression in neurons (Ivanova et al. 2015).

3.2.6.1. BDNF promoter activity is impaired in Shp2^{D61Y} neurons

To monitor pERK-induced gene expression, we expressed a BDNF promoter activity reporter, in which the BDNF promoters I and II drive the expression of EGFP (Figure 3.10A, B). The BDNF reporter construct was expressed in 14 DIV old low-density control and Shp2^{D61Y} neurons and we measured the nuclear EGFP fluorescence under basal conditions and 30 min after 4AP and Bic treatment. There were no significant differences in the expression of the reporter between genotypes in cultures with basal activity levels (Shp2^{D61Y}: 92±7% of control, Figure 3.10A and C). The increase in network activity by stimulation with 4AP/Bic led to an increase in the expression of the reporter construct in control cells (129±9% of untreated control, Figure 3.10A, C), but had no significant effect on the expression level of the reporter in Shp2^{D61Y} neurons (92±5% of untreated Shp2^{D61Y} Figure 3.10A, C). This result is in line with the defect in activity-induced activation of pERK seen in these cells.

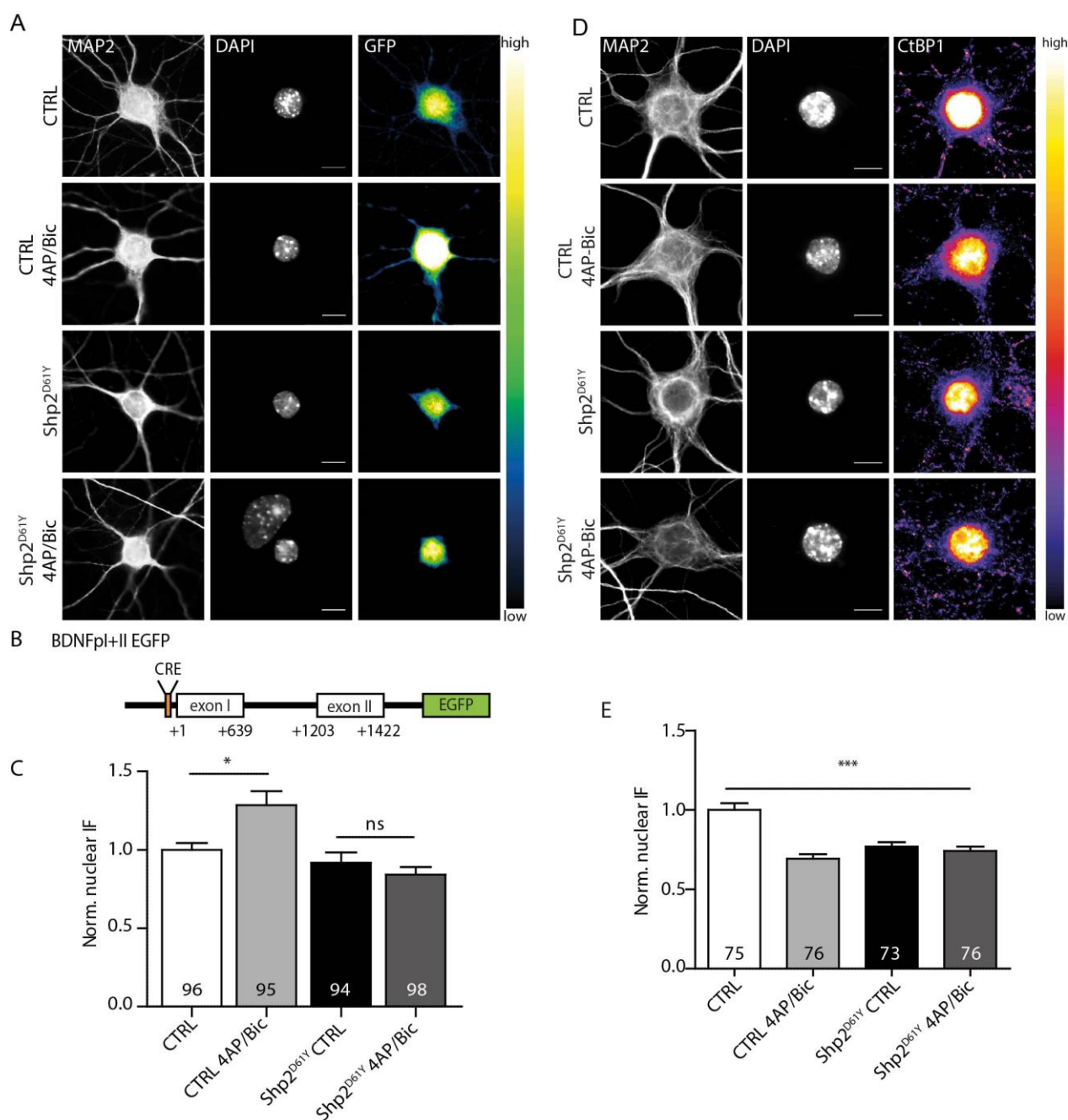


Figure 3.10: The activity-induced gene regulation is disturbed in 14 DIV Shp2^{D61Y} neurons. (A) Representative images of neurons in low-density cultures infected with the lentivirus containing the BDNFpI+II EGFP reporter in basal conditions and upon treatment with 4AP/Bic for 30 min. Neurons are stained with antibodies against GFP to enhance the intrinsic EGFP signal, MAP2 as a neuronal marker, and DAPI. **(B)** Schema of the activity reporter, in which the BDNF promoters I and II drive the expression of EGFP. The cAMP response element (CRE) is depicted. **(C)** Quantification of the GFP IF measured in the nuclei of control and Shp2^{D61Y} neurons. The reporter signal increased significantly upon stimulation in control but not in Shp2^{D61Y} neurons. **(D)** Representative images of neurons in low-density cultures in basal conditions and upon treatment with 4AP/Bic for 30 min. Neurons are stained with antibodies against MAP2 as a neuronal marker, CtBP1 and DAPI. **(E)** Quantification of the nuclear level of CtBP1 measured in nuclei of control and Shp2^{D61Y} neurons. Note that the induction of activity did not lead to a further export of the transcriptional co-repressor CtBP1 in Shp2^{D61Y} neurons. Data are shown as mean \pm SEM and analyzed using one-way ANOVA followed by Bonferroni's multiple comparison test (* $p \leq 0.05$) Scale bar: 10 μ m. Parts A-C of this figure are adapted from Altmüller et al. (2017b).

3.2.6.2. Disturbance of the activity-induced nuclear export of CtBP1 in Shp2^{D61Y} neurons

CtBP1 has a basal nuclear localization; upon activation of network-activity, CtBP1 is exported from the nucleus and the CtBP1-mediated transcriptional repression is released. The nuclear export of CtBP1 was assessed in low-density 14 DIV control and Shp2^{D61Y} neurons upon 4AP/Bic treatment for two hours. In control cells this treatment led to a significant export of CtBP1 from the nucleus ($69\pm 3\%$ of untreated control, Figure 3.10D, E). Interestingly, the nuclear level of CtBP1 in Shp2^{D61Y} neurons was already under basal conditions significantly depleted in comparison to control neurons (Shp2^{D61Y} basal: $77\pm 3\%$ of untreated control, Figure 3.10D, E). Importantly, the nuclear levels of CtBP1 upon activity-induction did not change and showed no further decrease ($104\pm 3\%$ of untreated Shp2^{D61Y}, Figure 3.10E). These results support our findings concerning the disturbance of functional gene regulation.

4. Discussion

In the first part of this thesis, a patient cohort of individuals with NS and confirmed mutation in *NRAS* is described. So far, clear genotype-phenotype correlations exist only for few of the known genes harboring NS-causing mutations, such as *PTPN11*. For mutations in *NRAS*, which is only a very rare cause of NS, a clear correlation was not possible yet. We performed the first classification of the phenotypic spectrum of RASopathy patients with *NRAS* mutations and revealed important aspects in the phenotypic and mutational spectrum. In addition, the previous assumption that mutations clustering in the oncogenic hotspots in *NRAS* affecting codons 12, 13 and 61 are not compatible with life if occurring in the germline is now refuted (Altmüller et al. 2017a). These findings will be discussed in the following chapter 4.1.

In the second part of my thesis, the molecular consequences of dysregulated RAS-MAPK signaling were investigated. Little is known about the role of Shp2 in synaptic plasticity, learning and memory and the current knowledge about molecular dysfunctions in the brain leading to the cognitive impairments in NS is limited. To address these aspects, we generated a new mouse model to study the molecular consequences of Shp2 hyperactivation (Altmüller et al. (2017b)). The cellular consequences of this mutation will be discussed in the following chapter 4.2.

4.1. Clinical and molecular spectrum of *NRAS* mutations

4.1.1. Spectrum of *NRAS* mutations

Our cohort consisted of 19 new patients with a RASopathy due to germline *NRAS* mutations. The size of this cohort is even larger than the total number of previously reported patients harboring germline mutations in *NRAS* (Cirstea et al. 2010, Digilio et al. 2011, Runtuwene et al. 2011, Denayer et al. 2012, Kraoua et al. 2012, Ekvall et al. 2015). We show *de novo* as well as familial occurrence of already known mutations resulting in the p.I24N, p.T50I, and p.G60E amino acid exchanges, confirming these codons to be hotspots for germline mutations in *NRAS*. Moreover, we found six novel mutations affecting the residues G12, E37, and T58 in *NRAS* to cause a RASopathy phenotype.

We hypothesize that the novel amino acid substitutions resulting in p.G12D/R/S/V, p.E37dup and p.T58I are indeed pathogenic. This assumption is supported by the following facts: All amino acid substitutions affect highly conserved residues of *NRAS*, and they are located at or near known hotspots for somatic or germline *NRAS* mutations, respectively. Importantly, all novel *NRAS*

mutations described here have previously been reported as pathogenic mutations in the other RAS genes *KRAS* and/or *HRAS*. Further, their activating effects have been reported in functional studies (Fasano et al. 1984, Ahmadian et al. 1999, Aoki et al. 2005, Schubbert et al. 2006, Cirstea et al. 2010, Gremer et al. 2010, Gremer et al. 2011, Wey et al. 2013, Altmuller et al. 2017a).

Most common somatic changes in cancer are missense changes in NRAS or other RAS proteins affecting G12 and result in impaired GTPase activity and GAP resistance, thereby leading to constitutive activation (Schubbert et al. 2006, Gremer et al. 2011, Wey et al. 2013). Although there are no reports about somatic or germline mutations affecting codon p.E37 in NRAS, the duplication p.E37dup in *HRAS* has already been reported in a case of CS (Gremer et al. 2010). In the same study, mutant *HRAS*^{E37dup} was shown to exhibit lower intrinsic GTPase activity, thus preferentially remaining in the active GTP-bound state. Moreover *HRAS*^{E37dup} showed complete resistance to GAP, but its impact on signal flux through the MAPK and PI3K-AKT cascades was found to be milder in comparison to *HRAS*^{G12V}, because it has reduced binding affinities for effector proteins (Gremer et al. 2010). Missense mutations resulting in p.T58I were reported six times in *KRAS* mainly associated with NS and eight times in *HRAS* as a cause of CS (www.nseuronet.com). Additionally, this mutation has occasionally been observed in RAS isoforms as a somatic mutation in various types of malignancy (COSMIC, Forbes et al. (2015)). The functional characterization of the *KRAS*^{T58I} mutant revealed a mild overactivating behavior of the GTPase and enhanced activation of downstream effectors (Schubbert et al. 2006, Gremer et al. 2011). In the frame of our joint publication, our collaborators performed the functional characterization of the *NRAS*^{T58I} mutant and demonstrated that this mutant has similar gain-of-function effects. The T58I substitution promoted a shift towards the constitutively activated GTP-bound conformation and enhanced ERK and AKT activation basally. Thus, the findings from the *KRAS*^{T58I} mutant were experimentally confirmed (Altmuller et al. 2017a). The four novel RASopathy-associated *NRAS* variants affecting Gly12 represent well-known oncogenic mutations that occur with a decreasing prevalence (p.G12D > p.G12S > p.G12V > p.G12R) as somatic changes in various tumors, particularly in hematopoietic and lymphoid malignancies (COSMIC database, Forbes et al. (2015)). Previous reports about *NRAS* germline mutations typically spared the classical oncogenic hotspots G12, G13, and Q61. This raised the assumption that oncogenic *NRAS* alterations in the germline might lead to embryonic lethality (Cirstea et al. 2010). We were therefore the first to report that apparent non-mosaic germline changes in *NRAS* affecting one of these hotspots for oncogenic mutations may be compatible with life and lead to a clearly recognizable RASopathy phenotype. Interestingly, the overlap of the germline mutation spectrum with oncogenic mutation hotspots is regularly observed for germline *HRAS* mutations leading to

CS but has very rarely been observed for germline *KRAS* mutations in CFCS (Nava et al. 2007). The occurrence of germline mutations on oncogenic hotspots has been correlated with a significant increase in tumor risk in CS (Gripp 2005). Consistently, one of the present subjects carrying a missense change at codon G12 had a tumor-like lesion in the hypothalamus but its precise nature was not delineated up to the time of the publication. Another patient had a JMML-like myeloproliferative disorder. Interestingly, JMML and JMML-like myeloproliferative disorders (MPDs) are associated with NS and somatic mutations in RASopathy genes, including also *NRAS* (Kratz et al. 2005, Niemeyer 2014, Strullu et al. 2014, Caye et al. 2015, Stieglitz et al. 2015). Moreover, we cannot exclude a myeloproliferative disease or other kind of neoplasia for the stillbirth with the mutation p.G12V (patient 2) due to lack of data.

In a previously published case report, the germline status of the *NRAS* mutation p.G13D in a patient with JMML is suggested (De Filippi et al. 2009). In this case, the mutation was found in buccal cells, hair bulbs, and fibroblasts, suggesting that the mutation was not restricted to hematopoietic tissue. Nevertheless, a mosaic status for the mutation cannot be excluded. Importantly, the infant affected by JMML was reported to have short stature and dysmorphic features reminiscent of NS. Notably, another patient affected by the autoimmune lymphoproliferative syndrome (ALPS) and without clinical signs of NS was erroneously reported to have a germline event solely based on the presence of the mutation in DNA from a buccal swab (Oliveira et al. 2007). During follow-up, the mutation was not retrieved in DNA samples from hair bulbs and a repeated buccal swab, thus disproving the germline status (personal communication J. B. Oliveira, February 2010). This is pointing to the difficulties in assessing the germline status of a mutation, which is one possible limitation of our data. Hematopoietic cells may migrate and reside in non-hematopoietic tissues including buccal mucosa and, more surprisingly, fingernails (Imanishi et al. 2007, Hiramoto et al. 2015). However, cultured fibroblasts that were tested in one of the patients from our cohort are devoid of contamination with hematopoietic cells (Kraoua et al. 2012, Caye et al. 2015, Stieglitz et al. 2015). Together with the clinical features observed in our patients, it is unlikely that *NRAS* mutations affecting G12 were acquired somatically or even mosaic.

Our findings suggest that clinically obvious RASopathy features constitute the major phenotype caused by activating *NRAS* mutations occurring in the germline, whereas hematological abnormalities do not invariably emerge even in the presence of mutations at oncogenic hotspots. Comparing the clinical symptoms recorded in our patients to previously reported cases with germline *NRAS* mutations, we generally found high congruency regarding the frequency of clinical findings in various organ systems. Taking together the clinical data from a total of 37 affected individuals (previously published cases and our newly reported cohort) allows us to further

delineate the RASopathy phenotype associated *NR4S* mutations (see Supplementary Table 6.1). Cardiac anomalies are present in approximately half of cases, but contrasting to what is generally observed in NS, PST is significantly less common (14%). HCM is the most common cardiac finding (28%) in our cohort, but has a slightly higher prevalence compared to the general NS population (Roberts et al. 2013). Septal defects also represent a relatively common cardiac anomaly in NS in general (Marino et al. 1999), which occurs in only 11% of the cases of our cohort. The typical craniofacial appearance is commonly seen and indistinguishable from NS of other etiologies. Short or webbed neck and ocular ptosis were highly prevalent among patients with *NR4S* mutations (84% and 61%, respectively). Short stature was present in 45% of patients, which is less prevalent than in NS in general. Motor delay is quite frequent (58%), while learning disabilities are observed in a similar frequency as in NS of other genetic etiologies (29%). Cryptorchidism in males and the occurrence of prenatal abnormalities, including polyhydramnios and nuchal edema, are also quite frequent (63%) and comparable to their general frequency in NS (Roberts et al. 2013).

While all previously reported patients had a clinical diagnosis of NS, three patients in this cohort were diagnosed as having CFCS or CS based on their clinical features. For patient 7 a working diagnosis of CFCS was initially made primarily based on her striking craniofacial features, profound hypotonia, significant developmental delay, and feeding issues. In addition to the *NR4S* mutation, she was found to have a 1.24 Mb duplication on chromosome 22q11.23. Similar 22q11.23 duplications have been found in individuals with variable clinical features, including muscular hypotonia, developmental delay, and seizures, with *de novo* occurrence but also inherited from apparently healthy parents (Coppinger et al. 2009, Chang et al. 2015). We cannot exclude the possibility that this copy number change contributed to the severity of the developmental phenotype and some atypical features described in this patient that led to the classification as CFCS. Similarly, patient 11, who carried the p.T50I change, was clinically classified as having CFCS because of significantly delayed motor development, mild intellectual disability (IQ of 65), and prominent ectodermal abnormalities (keratosis pilaris, multiple nevi, sparse eyebrows and curly, sparse hair). Of note, the same mutation had previously been reported in patients with a NS phenotype and no or only mild developmental problems (Cirstea et al. 2010, Denayer et al. 2012). We therefore think that the more prominent developmental issues in this patient are not primarily explained by this particular *NR4S* mutation. Patient 12 (p.G12R) showed severe perinatal complications typically seen in newborns with CS, including polyhydramnios, neonatal hyperinsulinemic hypoglycemia, severe feeding difficulties and respiratory problems. Furthermore, she had deep palmar and plantar creases and a tumor-like lesion of unknown etiology in the hypothalamus. Her motor development was delayed. This constellation prompted the diagnosis of CS, but the patient was very young at last follow-up and the phenotype may still change with age.

Considering the relatively severe expression of NS in patient 1 (p.G12S) and patient 13 (p.G12D), the CS-like neonatal presentation in patient 12 (p.G12R), and intrauterine death of patient 2 (p.G12V), it is tentative to speculate that this may be related to the more severe functional impact of these mutations at G12. Among these, the p.G12V mutation that was associated with intrauterine death in the present case series, is the most common oncogenic mutation at codon 12 in *NRAS* and demonstrated to represent the strongest effect on downstream signaling, while the others have somewhat weaker activating potential (Fasano et al. 1984, Ahmadian et al. 1999). Similarly, gradual differences in the phenotypic severity have also been proposed for different *HRAS* p.G12 mutations in CS (Lorenz et al. 2012). Regarding the clinical management, it has to be considered that *NRAS* mutations corresponding with CS-associated *HRAS* changes may also share a similar risk of malignancy as seen in CS. However, the number of patients is still limited and the observation period for the patients reported here was too short to draw definite conclusions about possible genotype-phenotype correlations.

4.1.2. Conclusion

In summary, this is the largest cohort to date of patients with germline *NRAS* mutations and their association with the typical clinical phenotype of RASopathies. It was shown that mutations affecting G12 might be compatible with life when occurring in the germline. This is comparable to the germline mutation spectrum previously documented in *HRAS* (Aoki et al. 2005), 2005), but different to the one in *KRAS* where RASopathy-associated germline mutations and somatic changes occurring in cancer do hardly overlap (Zenker et al. 2007). These findings emphasize the obvious RASopathy phenotype associated with activating germline *NRAS* mutations, thus challenging the germline status of oncogenic *NRAS* mutations in previous reports with hematological phenotypes. More data is required to ascertain the risk of malignancy in patients with oncogenic *NRAS* mutations in the germline.

Similar to what is seen in NS in general, patients with *NRAS* mutations may have mild developmental and cognitive impairments. Our cohort included a few patients with more severe developmental issues, but there is no robust correlation to specific mutations possible yet. This cohort was still too small to support the hypothesis that mutations with more severe functional consequences on RAS signaling, such as the presented G12 mutations, might also have more severe effects on brain functions. Nevertheless, the frequency of developmental issues in children with *NRAS*-related NS clearly indicates that *NRAS* also plays a role in the regulation of neuronal functions.

4.2. Characterization of the cognitive phenotype in Shp2^{D61Y} animals

4.2.1. Generation of the Shp2^{D61Y} mouse model

To decipher the underlying molecular mechanism of brain dysfunctions in RASopathies, a new mouse model was generated. In this model, the monoallelic expression of Shp2^{D61Y} in excitatory neurons occurs from an endogenous locus. This presumably results in the regulation of the expression of the mutant protein as it occurs in these cells in RASopathy patients. In this way, unphysiological perturbing effects caused by the overexpression of the protein can be circumvented. The amino acid D61 of SHP2 participates in a network of hydrogen bonds that regulates the switch between closed and open conformation of the protein. If perturbances occur in this network of hydrogen bonds, the conformation of SHP2 can be shifted towards a more active state (Keilhack et al. 2005). It was experimentally confirmed that the D61Y substitution in Shp2 leads to a strong increase of the basal PTP activity of Shp2 (Tartaglia et al. 2003, Keilhack et al. 2005, Chan et al. 2009). In previous studies, it was already demonstrated that the global expression of the D61Y mutation is lethal during embryonic stages in mice. Furthermore, in a mouse model with Shp2^{D61Y} expression restricted to liver and lymphocytes under the control of the MX1 promoter, the medium life span of the animals was reduced (Chan et al. 2009). The D61Y substitution in human SHP2 was shown to lead to an increased proliferation rate of hematopoietic cells and is a known cause of juvenile myelomonocytic leukemia (JMML) (Tartaglia et al. 2003). Thus, the *PTPN11*^{D61Y} allele has presumably oncogenic properties concerning its strength of overactivation. Consistently, this mutation has never been observed as a germline mutation in humans, while other germline missense changes at the same codon are compatible with life and lead to a NS phenotype. *PTPN11*^{D61G} has recurrently been found as a germline mutation in patients with relatively severe expression of NS (Tartaglia, Martinelli et al. 2006). Recently, also cognitive impairment was reported for mice constitutively expressing the Shp2^{D61G} mutant protein (Lee et al. 2014). The phosphatase activity of Shp2^{D61G} is of intermediate strength regarding the phosphatase activation compared to our mouse model (Keilhack et al. 2005). The global expression of Shp2^{D61G} leads to severe cardiac defects and perinatal and juvenile death of approximately 50% of the heterozygous progeny, malformations of organs, reduced length and weight, skull deformations and the development of myeloproliferative syndrome in mice (Araki et al. 2004, Araki et al. 2009). This systemic impairment can have a negative influence on the performance in e.g. behavioral tests. However, our mouse model with restricted expression of Shp2^{D61Y} in forebrain does not show increased neonatal lethality and the animals are viable without any severe systemic phenotype. We deliberately chose to use this particular mutant, because its stronger functional impacts promised that the recognition of significant abnormalities in the nervous system, where patients with NS

usually only have quite mild impairments, might be easier. As a confirmation of efficient expression of the mutant in this model, a threefold increase of the phosphatase activity was measured in forebrain lysate, which is in line with the previous publication (Chan et al. 2009). Since the Shp2^{D61Y} expression in this model is restricted to excitatory neurons and astroglia in the forebrain, it circumvents embryonic and juvenile lethality reported for the constitutive mutants (Araki, Chan et al. 2009, Chan, Kalaitzidis et al. 2009). Moreover, this design also allows studying the phenotype linked exclusively to the dysfunction of Shp2 in cortical brain circuits and excludes any influences of non-neuronal phenotypes.

4.2.2. Absence of morphological alterations in Shp2^{D61Y} neurons

SHP2 is known to play a role in neuronal outgrowth and is involved in neuronal branching in the cortical neurons (Rosario et al. 2007, Zhou et al. 2015). However, the detailed morphometric analysis using 5 DIV old cultured hippocampal neurons from our mouse model did not reveal any morphological alterations concerning axon length and dendritic morphology of outgrowing Shp2^{D61Y} neurons. Sagittal brain slices stained for excitatory and inhibitory markers did also not show major differences. In contrast, Shp2^{D61G} expression was shown to lead to an increase in the number of synapses expressing GluA1 receptors (Lee et al. 2014). In 14 DIV old Shp2^{D61Y} neurons the number of excitatory and inhibitory synapses was analyzed using immunocytochemical stainings showing the colocalization of the presynaptic marker Bassoon and the excitatory marker Homer1 or the vesicular GABA transporter VGAT. Neither the number of excitatory nor inhibitory synapses on 20 μm segments of proximal dendrites was changed. Besides this, the number of active synapses undergoing transmitter release and the number of synapses expressing GluA1 subunits of AMPA receptors on their postsynaptic surface was also not changed. Thus, we conclude that Shp2^{D61Y} neurons have no significant changes in synapse density. Importantly, the outgrowth and maturation of older neurons should be addressed in the future, since RAS hyperactivation was shown to cause increase in size and ramification of the dendritic arborization, as well as synaptic changes at the pre and postsynapse (Arendt et al. 2004, Seeger et al. 2004, Kushner et al. 2005). However, there are no reports about anomalies concerning the CNS morphology or neurons in patients with RASopathies, which supports our results.

4.2.3. Changes in the vesicle pool size in Shp2^{D61Y} neurons

The knowledge about the physiological function of RAS-MAPK signaling and its impacts on dysregulation in the presynaptic compartment is limited. However, indirect evidence exists that SHP2 might also be involved in the regulation of presynaptic function, since Shp2 KO animals display reduced paired pulse facilitation and post-tetanic potentiation in the hippocampus (Kusakari et al. 2015). Importantly, SV pools are a major subject of homeostatic adaptations (Alabi and Tsien 2012, Lazarevic et al. 2013). Our experiments revealed that the dysregulation of RAS-MAPK signaling by overactive Shp2^{D61Y} affects the vesicle pool sizes in presynaptic terminals. Further, our experiments in mature neurons upon either electrical stimulation using the pHlourin technique or chemical stimulation during live staining with specific Syt1 antibodies showed a comparable phenotype. Both approaches revealed a significant decrease in the amount of synaptic vesicles in the TRP. In 21 DIV neurons, the Syt1 AB uptake assay under physiological conditions revealed no alterations in the network activity-driven vesicle recycling, but showed a profound reduction in the TRP size upon membrane hyperpolarization using a brief pulse of 50 mM KCl. This finding is supported by the results from pHlourin experiments that show a decrease in both, the RRP and RP fraction of SVs. Regarding the higher recycling rate of SVs in 14 DIV mutant neurons we cannot exclude the effect of an overall higher excitability in these young neurons. The higher overall excitability might lead to the higher network activity-driven recycling of synaptic vesicles, which was assessed using the Syt1 AB uptake assay in our experiments. Importantly, for the Shp2^{D61G} mouse model an increased neurotransmission was already reported (Lee et al. 2014). Moreover, hyperactive RAS was also shown to increase the ERK-dependent phosphorylation of Synapsin I, thereby increasing the density of docked SVs as well as the frequency of miniature excitatory postsynaptic currents (mEPSCs) and paired-pulse facilitation (Kushner et al. 2005). In these two mouse models, the expression of the mutation occurred either acutely (Lee et al. 2014) or under the control of the CaMKII α promoter that has the highest expression level in adult stages (Bayer et al. 1999, Kushner et al. 2005). Consequently, the later onset of expression of the mutation can give less room for the adaptation of the neuronal network and compensatory mechanisms for the presumably increased network activity caused by the hyperactivating mutations. Thus, it is not unlikely that all three models share the phenotype of increased neurotransmission, but only in our model compensatory mechanism occur, which is supported by our data from the Syt1 AB uptake in 14 and 21 DIV Shp2^{D61Y} neurons. We hypothesize that the increase in the network activity without major changes seen in 14 DIV old Shp2^{D61Y} neurons might lead to compensatory homeostatic adaptations of the presynaptic strength, resulting in the lower TRP found in 21 DIV Shp2^{D61Y} neurons. This is further supported by the finding that the total amount of GluA1 receptors are also downregulated, which further suggests an increased network activity in Shp2^{D61Y}

cultures. The lower TRP could compensate for the increased network activity but this would also lead to differences in short term plasticity, which in turn might contribute to the impairments in transmission and plasticity. To verify this, electrophysiological experiments measuring the miniature excitatory postsynaptic potential (mEPSP) should be performed in future investigations. Moreover, the emergence of compensatory mechanisms is in line with the fading phenotype in older RASopathy patients, as children with developmental deficits show only mild or no cognitive deficits during adulthood.

The phosphorylation of Synapsin1 at its MAPK dependent sites 4 and 5 was shown to be linked to the stimulation of presynaptic AMPA receptors and the subsequent activation of RAS-MAPK signaling. Subsequently, the phosphorylation of Synapsin1 leads to its dispersion from the cytoskeleton and thereby increasing SV mobilization and neurotransmitter release (Schenk et al. 2005). The action potential-driven phosphorylation of Synapsin1 can also lead to synapsin dispersion from actin cytoskeleton (Chi et al. 2001). These studies provide a further hint for the implication of RAS-MAPK signaling in SV regulation, raising the question, how the phosphorylation of Synapsin 1 is affected by Shp2^{D61Y} expression. The ERK-dependent phosphorylation of Synapsin1 might have an influence on the size of synaptic vesicle pools and the availability of synaptic vesicles. Interestingly, using a KO mouse model it was shown that the loss of Shp2 leads to impairments in paired pulse facilitation and post-tetanic potentiation, arguing for an important presynaptic involvement of Shp2. Although an enhancing function of RAS-MAPK signaling on neurotransmitter release including synapsin involvement was shown (Jovanovic et al. 2000, Vara et al. 2009), detailed molecular events activating the RAS-MAPK signaling cascade in both, pre and postsynapse are still unclear. The phosphorylation status of Synapsin1 in Shp2^{D61Y} neurons represents another interesting target for future studies.

4.2.4. Alteration in the glutamate receptor abundancies in Shp2^{D61Y} neurons

LTP-inducing stimuli activate RAS-MAPK signaling leading to the phosphorylation of AMPA receptors, e.g. GluA1, and drive these receptors into synapses (Stornetta and Zhu 2011). The trafficking of NMDA and AMPA receptors plays an important role in neuronal plasticity (Malinow and Malenka 2002). Previously, the Shp2^{D61G} mouse model was reported to have a higher neurotransmission as well as a higher GluA1 receptor surface abundancy (Lee et al. 2014). It is well known that RAS mediates the activity-driven synaptic delivery of AMPA receptors (GluA1) in an ERK-dependent manner (Zhu et al. 2002). Although the surface expression level of GluA1

receptors was unchanged in Shp2^{D61Y} neurons, the distribution of glutamate receptor subtypes between their intra- and extracellular pools was shifted significantly. Our results indicated a diminished intracellular pool of GluA1 receptors. The smaller total level of GluA1 receptor subunits, but unchanged surface expression level implies that Shp2^{D61Y} neurons have a relatively higher surface level of GluA1 receptor subunits, suggesting a more efficient exocytosis of the receptor in Shp2^{D61Y} neurons. Discrepancies between the results from Lee and colleagues might be attributed to differences in the experimental procedure since in their experiments Shp2^{D61G} was introduced into neurons by acute viral-mediated overexpression. Our mouse model expresses the mutant allele from an endogenous locus during the entire development. This long-term overactivation of the RAS-MAPK signaling cascade might allow for homeostatic adaptations during the maturation, thereby decreasing the excessive glutamate receptor-mediated signaling by lowering the total expression level of GluA1 and the surface level of GluA2 receptors. Calcium influx through GluA2-lacking AMPA receptors was shown to drive the insertion of GluA2 receptors, thereby replacing GluA1 receptors. This change from calcium-permeable to calcium-impermeable AMPA receptors is known to stabilize LTP (Henley and Wilkinson 2013). However, exocytosis of GluA2 receptors is largely constitutive and approximately only 30% of GluA2 receptors are exocytosed in an activity-dependent manner (Araki et al. 2010). Interestingly, the C-terminal domain of GluA2 receptors can be phosphorylated by the Src family protein tyrosine kinases (PTK) Lyn. This phosphorylation on Y876 by the PTK Lyn is critical for the endocytosis of GluA2 and impairs the interaction of the PDZ-containing proteins GRIP1/2 (glutamate receptor-interacting protein1/2). However, this process is likely to explain rather the step of constitutive GluA2 receptor internalization since it is not dependent on calcium influx (Hayashi and Huganir 2004). In contrast, the activity-dependent endocytosis might be mediated by PICK1 (protein interacting with C kinase-1) that interacts with the PDZ domain of GluA2, thereby reducing its surface expression in a CaMKII- and protein kinase C-dependent manner (Terashima et al. 2004). Thus, we hypothesize that the lower surface abundance of GluA2 receptors might be influenced by the probably increased CaMKII activity due to hyperactive RAS-MAPK signaling in Shp2^{D61Y} neurons.

We also provided evidence for an altered ratio of surface to total GluA1 receptors indicating a relative increase in the surface level of GluA1 receptors. The insertion of AMPARs into synapses is driven by the interplay of activated RAS, ERK and CaMKII. Once activated, CaMKII becomes autophosphorylated at T286, rendering the kinase in an active conformation (Makhinson et al. 1999, Zhu et al. 2002). Thus, it would be of interest to investigate the CaMKII phosphorylation level in Shp2^{D61Y} neurons, too. Interestingly, SynGAP acts as a molecular “break” on RAS-MAPK

signaling and is critical for the induction of LTP. Neuronal cultures from SynGAP KO animals were found to have more synaptic AMPA receptor clusters, involving SynGAP in the trafficking of AMPA receptors, too (Kim et al. 2003, Kim et al. 2005). Accordingly, the observed alterations in glutamate receptor surface expression levels in our mouse model might contribute to impairments in LTP, as reported for the Shp2^{D61G} mutant and SynGAP mutant (Kim et al. 2003, Lee et al. 2014) and consequently lead to impairments in ERK activation and nuclear translocation, as described in this thesis.

It is well established that the RAS-dependent externalization of GluA1 at synapses is negatively regulated by calcium influx through GluN2B-containing receptors (Zhu et al. 2002). GluN2B receptors are mobile and recycle more frequently than GluN2A receptors, allowing the fine-tuned regulation of receptor number and subunit composition in an activity-dependent manner (Paoletti et al. 2013). We found a strong decrease in the surface expression of GluN2B receptors, while the total expression was unchanged, indicating a less efficient endo- and exocytosis of the GluN2B receptors. Additionally, the higher neurotransmission reported for the Shp2^{D61G} mutant (Lee et al. 2014) could also explain in part the observed decrease of GluN2B, as neurotransmission induces an increased endocytosis of synaptic GluN2B-receptors (Chung et al. 2004). Moreover, postsynaptic GluN2B and GluA1 receptors have a vital role in activity-dependent synaptic plasticity. For example, NMDA receptor-mediated calcium influx triggers the activation of CaMKII, which directly interacts with the GluN2B subunit and leads to a long lasting activation of ERK. This GluN2B/CaMKII interaction enhances synaptic activity by promoting the ERK-dependent delivery of GluA1 receptors to the surface (El Gaamouch et al. 2012). Although ERK is unlikely to phosphorylate AMPA receptors directly, other downstream kinases, such as p90 ribosomal S6 kinase (RSK) or mitogen- and stress-activated protein kinase (MSK), seem suitable for this (Stornetta and Zhu 2011). Additionally, the activation of synaptic GluN2A receptors is known to decrease the phosphorylation level of GluN2B receptors at Y1472 in a dose- and time-dependent manner (Ai et al. 2013). Thus, the increased GluA1 level we observed is in line with increased RAS activation. The presence of overactive Shp2^{D61Y} and the presumably diminished calcium influx through less available GluN2B receptors further support our hypothesis. Future studies should address whether and how calcium signaling and the recycling rate of GluA1 and GluN2B receptors are affected in Shp2^{D61Y} neurons. In the light of the dysregulated GluN2B levels in Shp2^{D61Y} neurons it would be interesting to see whether the phosphorylation level of GluN2B receptors is altered.

4.2.5. Disturbed activity-induced phosphorylation of ERK in Shp2^{D61Y} neurons

The phosphorylation of ERK in neurons is known to have multifaceted effects including the regulation of protein synthesis, changes in gene expression, modulation of ion channels, and the regulation of receptor insertion (Sweatt 2004). We could show that already under basal conditions the level of pERK is increased in Shp2^{D61Y} neurons (Altmüller et al. 2017b). This is consistent with the elevated phosphatase activity in cells expressing Shp2^{D61Y} as it was described previously and confirmed in our experiments (Keilhack et al. 2005). This result further supports the positive and activating role of Shp2 on RAS-MAPK signaling. Interestingly, the expression of the mutant Shp2^{D61G} led only to a modest increase of 20 to 30% of phosphorylated ERK in the hippocampus (Lee et al. 2014), which is in line with the intermediate strength of the phosphatase overactivation caused by Shp2^{D61G} (Keilhack et al. 2005), indicating a correlation of Shp2 activity and the level of ERK phosphorylation in the brain. Importantly, our data from ERK phosphorylation in time laps experiments showed that not only the magnitude but also the time course of ERK phosphorylation were strongly perturbed. The stimulation of neurotransmission or TrkB receptors led to the nuclear accumulation of phosphorylated ERK in a physiological manner in control cells. In contrast, upon stimulation with either BDNF or 4AP/Bic Shp2^{D61Y} neurons failed to increase their nuclear pERK level, which is most likely due to their already basally increased pERK level leading to a saturation of ERK activation. Additionally, we found a biphasic pattern of ERK activation in response to 4AP-Bic stimulation in the control, which is still present, but shifted in Shp2^{D61Y} neurons. Thus, our data also indicate a disturbed dynamic regulation of ERK activation in the Shp2^{D61Y} mouse model. A similar pattern of biphasic ERK activation was shown to be linked to contextual fear conditioning and memory consolidation. Importantly, the inhibition of the first phase of ERK activation did not prevent the second phase, suggesting independent molecular mechanisms underlying this phenomenon (Trifilieff et al. 2006, Trifilieff et al. 2007). Moreover, the treatment of neurons with ketamine in subanesthetic doses was also shown to induce a biphasic activation of pERK with an early and a delayed activation after three and 24 hours, respectively. The delayed activation suggests the existence of homeostatic mechanisms that act in a temporally shifted manner (Pothula et al., unpublished data). However, possible feedback loops and underlying molecular mechanisms of the biphasic pattern of ERK activation are still unknown.

We provide sufficient data supporting the profound dysregulation of ERK activation. It is known that only phosphorylated ERK can enter the nucleus and the transient nuclear translocation of ERK is needed for the regulation of gene expression (Brunet et al. 1999). However, the nuclear import of activated ERK is complex and there are evidences that the nuclear import of ERK in

Shp2^{D61Y} neurons is hampered. It is likely that we do not only have a dysregulation in the activation of ERK but also additionally have a perturbed nuclear translocation of ERK, which represents an interesting approach for future investigations.

4.2.6. Aberrant activity-dependent regulation of *BDNF* gene transcription and the transcriptional co-repressor CtBP1

The stimulation of synaptic activity and subsequent calcium influx lead to the activation of the RAS-MAPK signaling cascade and consequently to phosphorylation of ERK and CREB, both important for the activity-dependent induction of *BDNF* gene transcription (Flavell and Greenberg 2008). CREB acts as a transcriptional activator, binding to the CRE element upstream of the *BDNF* promoter 1 region (West et al. 2002, Hara et al. 2009). By monitoring the activity of the promoters I and II of *BDNF* upon induction of network activity we found a defect in the neuronal activity-induced activation of the *BDNF* promoter in Shp2^{D61Y} neurons. The hampered activity-induced activation of *BDNF* promoter I and II is in line with the impaired activation of ERK. CREB as a downstream target of ERK has a pivotal role in the regulation of gene transcription by recruiting other members of the transcription machinery. Therefore, CREB needs to be phosphorylated on S133 in an activity-dependent manner (West et al. 2002, Thomas and Huganir 2004). Our data strongly support the finding that the gene regulation is indeed impaired. Thus, the investigation of the phosphorylation status of CREB in Shp2^{D61Y} expressing neurons is important to identify other molecules involved in the molecular and cellular dysregulation causing NS.

Another activity-dependent regulator of gene expression is CtBP1. The transcriptional co-repressor CtBP1 is involved in the activity-driven reconfiguration of gene expression in neurons. Sustained neuronal activity leads to the dissociation from the transcriptional repressor complex and active nuclear export of CtBP1. Recently, CtBP1 was found to play a role in the activity-dependent gene transcription of immediate early genes, such as *BDNF* (Ivanova et al. 2015). In line with the elevated phosphorylation level of ERK, we find an already basally decreased nuclear level of CtBP1 in Shp2^{D61Y} neurons, which might argue for an elevated network activity in Shp2^{D61Y} neurons. Importantly, our data from the Syt1 AB uptake further support this finding. In 14 DIV Shp2^{D61Y} neurons, we found an increase in network activity-driven recycling of SVs. However, this might be only an indirect effect of the increased RAS-MAPK signaling in Shp2^{D61Y} neurons since a direct regulation of CtBP1 by the RAS-MAPK signaling cascade is not known and is surely an interesting subject of future investigations.

4.2.7. Outlook and conclusion

This study was aimed to characterize the consequences of hyperactive RAS-MAPK signaling on neuronal signaling and function. We found no substantial morphological changes in neurons expressing the Shp2^{D61Y} mutant, thus suggesting that the neurocognitive defects mediated by overactive Shp2 primarily affect functional properties. The key players identified in this study are summarized in Figure 4.1. Altogether, we identified profound alterations in two different compartments: first, the synaptic dysregulation likely leading to changes in neurotransmission and plasticity and second, the somato-nuclear alterations regarding ERK signaling and regulation of gene expression. We provide evidence for alterations in the vesicle cycling and SV pool size **(1)**. The surface expression of GluA1 is relatively increased **(2)**, while the GluN2B receptor surface level is decreased **(3)**. We could also show that the RAS-MAPK cascade is strongly upregulated **(4)** and the level of phosphorylated ERK is increased **(5)**, affecting the activity-induced regulation of gene transcription **(6)**. Additionally, our results suggest an increased network activity in cultured neurons from Shp2^{D61Y} animals. First, we found an increased network activity-driven recycling of SVs in in 14 DIV old Shp2^{D61Y} neurons. Second, our results demonstrated a consistent elevation of basal pERK level in samples from hippocampal slices that was investigated by Santosh Pothula in the frame of our joint publication (Altmuller et al. 2017b) and in dissociated cultures after different ways of synaptic stimulation. Finally, the lower level of nuclear CtBP1 as an activity-dependent transcriptional corepressor further supports this hypothesis.

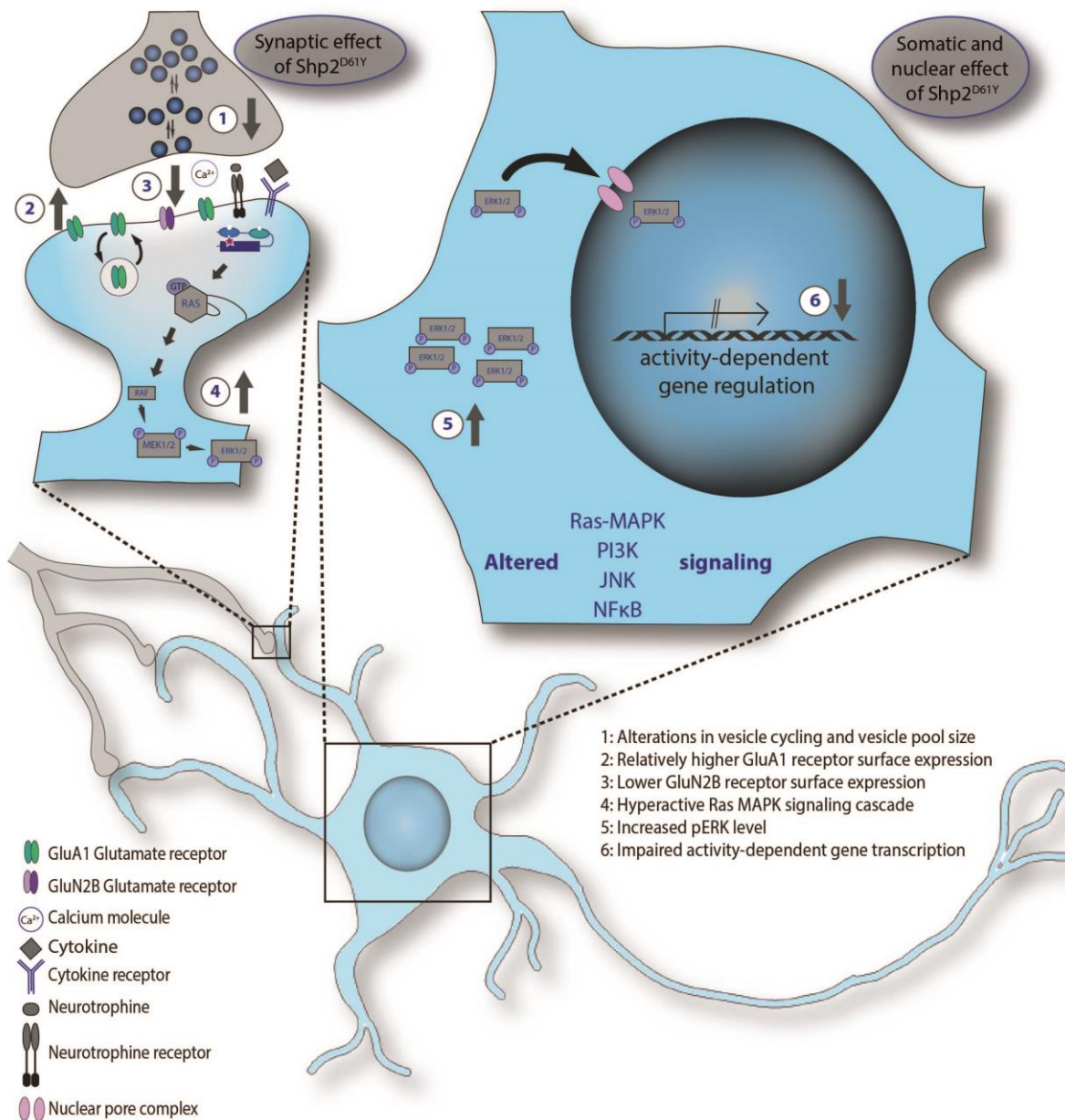


Figure 4.1: Schematic representation of the identified mechanisms probably contributing to the intellectual disability in NS.

Most importantly, our findings suggest that the loss of the dynamic regulation of RAS-MAPK signaling, rather than the elevated basal overactivation alone, is critical for the impact of hyperactive Shp2 on neuronal function. It is likely that this is a more general aspect of RASopathy-associated mutations, which may still be underestimated. The exact molecular mechanism underlying the impairments of dynamic regulation and its consequences demonstrate the need for further detailed investigations. Moreover, it might have important implications on treatment strategies, because the loss of the dynamic regulation can limit the efficacy of inhibitor treatment.

These findings are supported by the second part of our recent publication. Here, we made use of microarray-based hippocampal gene expression profiling and we compared the profile and the magnitude of gene expression under basal conditions and upon induction of neuronal activity using 4AP-Bic. We could show that indeed the consecutive regulation of gene expression is strongly perturbed in Shp2^{D61Y} neurons. The number of genes regulated in the mutant upon induction of activity was three times lower than in the control. Moreover, part of the genes that we found to be regulated in Shp2^{D61Y} neurons under unstimulated conditions greatly overlapped with genes regulated after induction of neuronal activity in control neurons. The subsequent *in silico* analysis further revealed changes in the cellular signaling network affecting PI3K/AKT/mTOR and JAK/STAT signaling cascades, which was confirmed by subsequent immunoblot analyses (Altmüller et al. 2017b).

Given the key role of activity-induced ERK signaling in learning and memory, we speculate that Shp2^{D61Y} expression potentially impairs synaptic transmission, gene regulation, and expression, thereby impairing important mechanisms of synaptic plasticity. Is it the perturbed gene regulation that causes the synaptic phenotype or is it vice versa? Many questions still remain. As already discussed above, the phosphorylation status of intracellular signaling molecules such as CaMKII might be of interest. As discussed the recycling of SVs, the activation of ERK, the function of CtBP1 as a transcriptional co-repressor as well as the synaptic abundance of AMPA and NMDA receptors all depend on neuronal activity and raise the need for electrophysiological experiments investigating alterations in future experiments. For example, multi-electrode arrays may be used to determine important network properties. This also represents an ideal model for pharmacological studies.

In summary, the increase in RAS-MAPK signaling caused by RASopathy-associated mutations leads to global changes affecting the sensitive neuronal functioning and severely disturbs the “happy-medium” dynamic regulation as shown in our study. It is of great importance to further investigate the ability of homeostatic adaptation in Shp2^{D61Y} neurons. We hypothesize that RASopathy-associated mutations still allow for homeostatic adaptations since the phenotype including cognitive impairments eases in adult RASopathy patients. Although adaptations might be still possible, there is a clear need for pharmacological treatment. The easiest way to counteract the hyperactive RAS-MAPK signaling cascade and to restore a physiological level of cellular signaling would be to target the cascade pharmacologically, e.g. by inhibiting MEK function using one of the common MEK inhibitors (Costa et al. 2002, Lee et al. 2014). Indeed, these treatments were initially promising and showed a reduction of abnormal RAS-MAPK signaling in animal models. Moreover, the use of statins as an inhibitor of RAS was also beneficial in the mouse model

and in small clinical studies (Mainberger et al. 2013, Bearden et al. 2016). Sadly, large-scale clinical trials failed to prove the positive effect of statin-treatment on cognitive impairment so far (Krab et al. 2008, van der Vaart et al. 2013), highlighting the importance of further studies to enable the treatment of cognitive impairments in RASopathies. Importantly, the pharmacological inhibition of RAS-MAPK signaling also impairs learning and memory (Stornetta and Zhu 2011, Ryu and Lee 2016). We suggest that possible treatment strategies should focus on the restoration of the dynamic regulation of neuronal RAS-MAPK signaling rather than the general dampening of this cascade.

5. Bibliography

5.1. References

- Adachi, M., Fukuda, M. and Nishida, E. (1999). "Two co-existing mechanisms for nuclear import of MAP kinase: passive diffusion of a monomer and active transport of a dimer." *EMBO J* **18**(19): 5347-5358.
- Adachi, M., Fukuda, M. and Nishida, E. (2000). "Nuclear export of MAP kinase (ERK) involves a MAP kinase kinase (MEK)-dependent active transport mechanism." *J Cell Biol* **148**(5): 849-856.
- Ahmadian, M. R., Zor, T., Vogt, D., Kabsch, W., Selinger, Z., Wittinghofer, A. and Scheffzek, K. (1999). "Guanosine triphosphatase stimulation of oncogenic Ras mutants." *Proc Natl Acad Sci U S A* **96**(12): 7065-7070.
- Ai, H., Lu, W., Ye, M. and Yang, W. (2013). "Synaptic non-GluN2B-containing NMDA receptors regulate tyrosine phosphorylation of GluN2B 1472 tyrosine site in rat brain slices." *Neurosci Bull* **29**(5): 614-620.
- Alabi, A. A. and Tsien, R. W. (2012). "Synaptic vesicle pools and dynamics." *Cold Spring Harb Perspect Biol* **4**(8): a013680.
- Alfieri, P., Cesarini, L., Mallardi, M., Piccini, G., Caciolo, C., Leoni, C., Mirante, N., Pantaleoni, F., Digilio, M. C., Gambardella, M. L., Tartaglia, M., Vicari, S., Mercuri, E. and Zampino, G. (2011). "Long term memory profile of disorders associated with dysregulation of the RAS-MAPK signaling cascade." *Behav Genet* **41**(3): 423-429.
- Allard, J. D., Chang, H. C., Herbst, R., McNeill, H. and Simon, M. A. (1996). "The SH2-containing tyrosine phosphatase corkscrew is required during signaling by sevenless, Ras1 and Raf." *Development* **122**(4): 1137-1146.
- Allison, M. B. and Myers, M. G., Jr. (2014). "20 years of leptin: connecting leptin signaling to biological function." *J Endocrinol* **223**(1): T25-35.
- Altmuller, F., Lissewski, C., Bertola, D., Flex, E., Stark, Z., Spranger, S., Baynam, G., Buscarilli, M., Dyack, S., Gillis, J., Yntema, H. G., Pantaleoni, F., van Loon, R. L., MacKay, S., Mina, K., Schanze, I., Tan, T. Y., Walsh, M., White, S. M., Niewisch, M. R., Garcia-Minaur, S., Plaza, D., Ahmadian, M. R., Cave, H., Tartaglia, M. and Zenker, M. (2017a). "Genotype and phenotype spectrum of NRAS germline variants." *Eur J Hum Genet* **25**(7): 823-831.
- Altmuller, F., Pothula, S., Annamneedi, A., Nakhaci-Rad, S., Montenegro-Venegas, C., Pina-Fernandez, E., Marini, C., Santos, M., Schanze, D., Montag, D., Ahmadian, M. R., Stork, O., Zenker, M. and Fejtova, A. (2017b). "Aberrant neuronal activity-induced signaling and gene expression in a mouse model of RASopathy." *PLoS Genet* **13**(3): e1006684.
- Aoki, Y., Niihori, T., Banjo, T., Okamoto, N., Mizuno, S., Kurosawa, K., Ogata, T., Takada, F., Yano, M., Ando, T., Hoshika, T., Barnett, C., Ohashi, H., Kawame, H., Hasegawa, T., Okutani, T., Nagashima, T., Hasegawa, S., Funayama, R., Nagashima, T., Nakayama, K., Inoue, S., Watanabe, Y., Ogura, T. and Matsubara, Y. (2013). "Gain-of-function mutations in RIT1 cause Noonan syndrome, a RAS/MAPK pathway syndrome." *Am J Hum Genet* **93**(1): 173-180.

- Aoki, Y., Niihori, T., Kawame, H., Kurosawa, K., Ohashi, H., Tanaka, Y., Filocamo, M., Kato, K., Suzuki, Y., Kure, S. and Matsubara, Y. (2005). "Germline mutations in HRAS proto-oncogene cause Costello syndrome." Nat Genet **37**(10): 1038-1040.
- Araki, T., Chan, G., Newbigging, S., Morikawa, L., Bronson, R. T. and Neel, B. G. (2009). "Noonan syndrome cardiac defects are caused by PTPN11 acting in endocardium to enhance endocardial-mesenchymal transformation." Proc Natl Acad Sci U S A **106**(12): 4736-4741.
- Araki, T., Mohi, M. G., Ismat, F. A., Bronson, R. T., Williams, I. R., Kutok, J. L., Yang, W., Pao, L. I., Gilliland, D. G., Epstein, J. A. and Neel, B. G. (2004). "Mouse model of Noonan syndrome reveals cell type- and gene dosage-dependent effects of Ptpn11 mutation." Nat Med **10**(8): 849-857.
- Araki, Y., Lin, D. T. and Huganir, R. L. (2010). "Plasma membrane insertion of the AMPA receptor GluA2 subunit is regulated by NSF binding and Q/R editing of the ion pore." Proc Natl Acad Sci U S A **107**(24): 11080-11085.
- Arendt, T., Gartner, U., Seeger, G., Barmashenko, G., Palm, K., Mittmann, T., Yan, L., Hummeke, M., Behrbohm, J., Bruckner, M. K., Holzer, M., Wahle, P. and Heumann, R. (2004). "Neuronal activation of Ras regulates synaptic connectivity." Eur J Neurosci **19**(11): 2953-2966.
- Atkins, C. M., Selcher, J. C., Petraitis, J. J., Trzaskos, J. M. and Sweatt, J. D. (1998). "The MAPK cascade is required for mammalian associative learning." Nat Neurosci **1**(7): 602-609.
- Baljuls, A., Kholodenko, B. N. and Kolch, W. (2013). "It takes two to tango--signalling by dimeric Raf kinases." Mol Biosyst **9**(4): 551-558.
- Barbacid, M. (1987). "ras genes." Annu Rev Biochem **56**: 779-827.
- Barford, D. and Neel, B. G. (1998). "Revealing mechanisms for SH2 domain mediated regulation of the protein tyrosine phosphatase SHP-2." Structure **6**(3): 249-254.
- Barrett, S. D., Bridges, A. J., Dudley, D. T., Saltiel, A. R., Fergus, J. H., Flamme, C. M., Delaney, A. M., Kaufman, M., LePage, S., Leopold, W. R., Przybranowski, S. A., Sebolt-Leopold, J., Van Becelaere, K., Doherty, A. M., Kennedy, R. M., Marston, D., Howard, W. A., Jr., Smith, Y., Warmus, J. S. and Tecle, H. (2008). "The discovery of the benzhydroxamate MEK inhibitors CI-1040 and PD 0325901." Bioorg Med Chem Lett **18**(24): 6501-6504.
- Barria, A. and Malinow, R. (2002). "Subunit-specific NMDA receptor trafficking to synapses." Neuron **35**(2): 345-353.
- Barria, A. and Malinow, R. (2005). "NMDA receptor subunit composition controls synaptic plasticity by regulating binding to CaMKII." Neuron **48**(2): 289-301.
- Bauler, T. J., Kamiya, N., Lapinski, P. E., Langewisch, E., Mishina, Y., Wilkinson, J. E., Feng, G. S. and King, P. D. (2011). "Development of severe skeletal defects in induced SHP-2-deficient adult mice: a model of skeletal malformation in humans with SHP-2 mutations." Dis Model Mech **4**(2): 228-239.
- Bayer, K. U., Lohler, J., Schulman, H. and Harbers, K. (1999). "Developmental expression of the CaM kinase II isoforms: ubiquitous gamma- and delta-CaM kinase II are the early isoforms and most abundant in the developing nervous system." Brain Res Mol Brain Res **70**(1): 147-154.

- Bearden, C. E., Helleman, G. S., Rosser, T., Montojo, C., Jonas, R., Enrique, N., Pacheco, L., Hussain, S. A., Wu, J. Y., Ho, J. S., McGough, J. J., Sugar, C. A. and Silva, A. J. (2016). "A randomized placebo-controlled lovastatin trial for neurobehavioral function in neurofibromatosis I." *Ann Clin Transl Neurol* **3**(4): 266-279.
- Bonetti, M., Rodriguez-Martinez, V., Paardekooper Overman, J., Overvoorde, J., van Eckelen, M., Jopling, C. and Hertog, J. (2014). "Distinct and overlapping functions of ptpn11 genes in Zebrafish development." *PLoS One* **9**(4): e94884.
- Bos, J. L. (1989). "ras oncogenes in human cancer: a review." *Cancer Res* **49**(17): 4682-4689.
- Brunet, A., Roux, D., Lenormand, P., Dowd, S., Keyse, S. and Pouyssegur, J. (1999). "Nuclear translocation of p42/p44 mitogen-activated protein kinase is required for growth factor-induced gene expression and cell cycle entry." *EMBO J* **18**(3): 664-674.
- Bunda, S., Burrell, K., Heir, P., Zeng, L., Alamsahebpour, A., Kano, Y., Raught, B., Zhang, Z. Y., Zadeh, G. and Ohh, M. (2015). "Inhibition of SHP2-mediated dephosphorylation of Ras suppresses oncogenesis." *Nat Commun* **6**: 8859.
- Burrone, J., Li, Z. and Murthy, V. N. (2006). "Studying vesicle cycling in presynaptic terminals using the genetically encoded probe synaptopHluorin." *Nat Protoc* **1**(6): 2970-2978.
- Busca, R., Pouyssegur, J. and Lenormand, P. (2016). "ERK1 and ERK2 Map Kinases: Specific Roles or Functional Redundancy?" *Front Cell Dev Biol* **4**: 53.
- Carta, C., Pantaleoni, F., Bocchinfuso, G., Stella, L., Vasta, I., Sarkozy, A., Digilio, C., Palleschi, A., Pizzuti, A., Grammatico, P., Zampino, G., Dallapiccola, B., Gelb, B. D. and Tartaglia, M. (2006). "Germline missense mutations affecting KRAS Isoform B are associated with a severe Noonan syndrome phenotype." *Am J Hum Genet* **79**(1): 129-135.
- Caunt, C. J. and McArdle, C. A. (2010). "Stimulus-induced uncoupling of extracellular signal-regulated kinase phosphorylation from nuclear localization is dependent on docking domain interactions." *J Cell Sci* **123**(Pt 24): 4310-4320.
- Caye, A., Strullu, M., Guidez, F., Cassinat, B., Gazal, S., Fenneteau, O., Lainey, E., Nouri, K., Nakhaei-Rad, S., Dvorsky, R., Lachenaud, J., Pereira, S., Vivent, J., Verger, E., Vidaud, D., Galambrun, C., Picard, C., Petit, A., Contet, A., Poiree, M., Sirvent, N., Mechinaud, F., Adjaoud, D., Paillard, C., Nelken, B., Reguerre, Y., Bertrand, Y., Haussinger, D., Dalle, J. H., Ahmadian, M. R., Baruchel, A., Chomienne, C. and Cave, H. (2015). "Juvenile myelomonocytic leukemia displays mutations in components of the RAS pathway and the PRC2 network." *Nat Genet* **47**(11): 1334-1340.
- Cesarini, L., Alfieri, P., Pantaleoni, F., Vasta, I., Cerutti, M., Petrangeli, V., Mariotti, P., Leoni, C., Ricci, D., Vicari, S., Selicorni, A., Tartaglia, M., Mercuri, E. and Zampino, G. (2009). "Cognitive profile of disorders associated with dysregulation of the RAS/MAPK signaling cascade." *Am J Med Genet A* **149A**(2): 140-146.
- Cesca, F., Baldelli, P., Valtorta, F. and Benfenati, F. (2010). "The synapsins: key actors of synapse function and plasticity." *Prog Neurobiol* **91**(4): 313-348.
- Chan, G., Kalaitzidis, D., Usenko, T., Kutok, J. L., Yang, W., Mohi, M. G. and Neel, B. G. (2009). "Leukemogenic Ptpn11 causes fatal myeloproliferative disorder via cell-autonomous effects on multiple stages of hematopoiesis." *Blood* **113**(18): 4414-4424.

Chang, J., Zhao, L., Chen, C., Peng, Y., Xia, Y., Tang, G., Bai, T., Zhang, Y., Ma, R., Guo, R., Mei, L., Liang, D., Cao, Q. and Wu, L. (2015). "Pachygyria, seizures, hypotonia, and growth retardation in a patient with an atypical 1.33Mb inherited microduplication at 22q11.23." *Gene* **569**(1): 46-50.

Chen, P. C., Wakimoto, H., Conner, D., Araki, T., Yuan, T., Roberts, A., Seidman, C., Bronson, R., Neel, B., Seidman, J. G. and Kucherlapati, R. (2010). "Activation of multiple signaling pathways causes developmental defects in mice with a Noonan syndrome-associated *Sos1* mutation." *J Clin Invest* **120**(12): 4353-4365.

Chi, P., Greengard, P. and Ryan, T. A. (2001). "Synapsin dispersion and reclustering during synaptic activity." *Nat Neurosci* **4**(12): 1187-1193.

Chung, H. J., Huang, Y. H., Lau, L. F. and Huganir, R. L. (2004). "Regulation of the NMDA receptor complex and trafficking by activity-dependent phosphorylation of the NR2B subunit PDZ ligand." *J Neurosci* **24**(45): 10248-10259.

Cirstea, I. C., Kutsche, K., Dvorsky, R., Gremer, L., Carta, C., Horn, D., Roberts, A. E., Lepri, F., Merbitz-Zahradnik, T., Konig, R., Kratz, C. P., Pantaleoni, F., Dentici, M. L., Joshi, V. A., Kucherlapati, R. S., Mazzanti, L., Mundlos, S., Patton, M. A., Silengo, M. C., Rossi, C., Zampino, G., Digilio, C., Stuppia, L., Seemanova, E., Pennacchio, L. A., Gelb, B. D., Dallapiccola, B., Wittinghofer, A., Ahmadian, M. R., Tartaglia, M. and Zenker, M. (2010). "A restricted spectrum of NRAS mutations causes Noonan syndrome." *Nat Genet* **42**(1): 27-29.

Coppinger, J., McDonald-McGinn, D., Zackai, E., Shane, K., Atkin, J. F., Asamoah, A., Leland, R., Weaver, D. D., Lansky-Shafer, S., Schmidt, K., Feldman, H., Cohen, W., Phalin, J., Powell, B., Ballif, B. C., Theisen, A., Geiger, E., Haldeman-Englert, C., Shaikh, T. H., Saitta, S., Bejjani, B. A. and Shaffer, L. G. (2009). "Identification of familial and de novo microduplications of 22q11.21-q11.23 distal to the 22q11.21 microdeletion syndrome region." *Hum Mol Genet* **18**(8): 1377-1383.

Cordeddu, V., Di Schiavi, E., Pennacchio, L. A., Ma'ayan, A., Sarkozy, A., Fodale, V., Cecchetti, S., Cardinale, A., Martin, J., Schackwitz, W., Lipzen, A., Zampino, G., Mazzanti, L., Digilio, M. C., Martinelli, S., Flex, E., Lepri, F., Bartholdi, D., Kutsche, K., Ferrero, G. B., Anichini, C., Selicorni, A., Rossi, C., Tenconi, R., Zenker, M., Merlo, D., Dallapiccola, B., Iyengar, R., Bazzicalupo, P., Gelb, B. D. and Tartaglia, M. (2009). "Mutation of SHOC2 promotes aberrant protein N-myristoylation and causes Noonan-like syndrome with loose anagen hair." *Nat Genet* **41**(9): 1022-1026.

Costa, R. M., Federov, N. B., Kogan, J. H., Murphy, G. G., Stern, J., Ohno, M., Kucherlapati, R., Jacks, T. and Silva, A. J. (2002). "Mechanism for the learning deficits in a mouse model of neurofibromatosis type 1." *Nature* **415**(6871): 526-530.

Cremers, C. W. and van der Burgt, C. J. (1992). "Hearing loss in Noonan syndrome." *Int J Pediatr Otorhinolaryngol* **23**(1): 81-84.

Davydova, D., Marini, C., King, C., Klueva, J., Bischof, F., Romorini, S., Montenegro-Venegas, C., Heine, M., Schneider, R., Schroder, M. S., Altmann, W. D., Henneberger, C., Rusakov, D. A., Gundelfinger, E. D. and Fejtova, A. (2014). "Bassoon specifically controls presynaptic P/Q-type Ca(2+) channels via RIM-binding protein." *Neuron* **82**(1): 181-194.

De Filippi, P., Zecca, M., Lisini, D., Rosti, V., Cagioni, C., Carlo-Stella, C., Radi, O., Veggiotti, P., Mastronuzzi, A., Acquaviva, A., D'Ambrosio, A., Locatelli, F. and Danesino, C. (2009). "Germline mutation of the NRAS gene may be responsible for the development of juvenile myelomonocytic leukaemia." *Br J Haematol* **147**(5): 706-709.

- De Rocca Serra-Nedelec, A., Edouard, T., Treguer, K., Tajan, M., Araki, T., Dance, M., Mus, M., Montagner, A., Tauber, M., Salles, J. P., Valet, P., Neel, B. G., Raynal, P. and Yart, A. (2012). "Noonan syndrome-causing SHP2 mutants inhibit insulin-like growth factor 1 release via growth hormone-induced ERK hyperactivation, which contributes to short stature." Proc Natl Acad Sci U S A **109**(11): 4257-4262.
- Denayer, E., Peeters, H., Sevenants, L., Derbent, M., Fryns, J. P. and Legius, E. (2012). "NRAS Mutations in Noonan Syndrome." Mol Syndromol **3**(1): 34-38.
- Dhillon, A. S., Hagan, S., Rath, O. and Kolch, W. (2007). "MAP kinase signalling pathways in cancer." Oncogene **26**(22): 3279-3290.
- Digilio, M. C., Lepri, F., Baban, A., Dentici, M. L., Versacci, P., Capolino, R., Ferese, R., De Luca, A., Tartaglia, M., Marino, B. and Dallapiccola, B. (2011). "RASopathies: Clinical Diagnosis in the First Year of Life." Mol Syndromol **1**(6): 282-289.
- Easton, J. B., Royer, A. R. and Middlemas, D. S. (2006). "The protein tyrosine phosphatase, Shp2, is required for the complete activation of the RAS/MAPK pathway by brain-derived neurotrophic factor." J Neurochem **97**(3): 834-845.
- Ekvall, S., Wilbe, M., Dahlgren, J., Legius, E., van Haeringen, A., Westphal, O., Anneren, G. and Bondeson, M. L. (2015). "Mutation in NRAS in familial Noonan syndrome--case report and review of the literature." BMC Med Genet **16**: 95.
- El Gaamouch, F., Buisson, A., Moustie, O., Lemieux, M., Labrecque, S., Bontempi, B., De Koninck, P. and Nicole, O. (2012). "Interaction between alphaCaMKII and GluN2B controls ERK-dependent plasticity." J Neurosci **32**(31): 10767-10779.
- English, J. D. and Sweatt, J. D. (1997). "A requirement for the mitogen-activated protein kinase cascade in hippocampal long term potentiation." J Biol Chem **272**(31): 19103-19106.
- Fasano, O., Aldrich, T., Tamanoi, F., Taparowsky, E., Furth, M. and Wigler, M. (1984). "Analysis of the transforming potential of the human H-ras gene by random mutagenesis." Proc Natl Acad Sci U S A **81**(13): 4008-4012.
- Flavell, S. W. and Greenberg, M. E. (2008). "Signaling mechanisms linking neuronal activity to gene expression and plasticity of the nervous system." Annu Rev Neurosci **31**: 563-590.
- Flex, E., Jaiswal, M., Pantaleoni, F., Martinelli, S., Strullu, M., Fansa, E. K., Caye, A., De Luca, A., Lepri, F., Dvorsky, R., Pannone, L., Paolacci, S., Zhang, S. C., Fodale, V., Bocchinfuso, G., Rossi, C., Burkitt-Wright, E. M., Farrotti, A., Stellacci, E., Cecchetti, S., Ferese, R., Bottero, L., Castro, S., Fenneteau, O., Brethon, B., Sanchez, M., Roberts, A. E., Yntema, H. G., Van Der Burgt, I., Cianci, P., Bondeson, M. L., Cristina Digilio, M., Zampino, G., Kerr, B., Aoki, Y., Loh, M. L., Palleschi, A., Di Schiavi, E., Care, A., Selicorni, A., Dallapiccola, B., Cirstea, I. C., Stella, L., Zenker, M., Gelb, B. D., Cave, H., Ahmadian, M. R. and Tartaglia, M. (2014). "Activating mutations in RRAS underlie a phenotype within the RASopathy spectrum and contribute to leukaemogenesis." Hum Mol Genet **23**(16): 4315-4327.
- Flotho, C., Valcamonica, S., Mach-Pascual, S., Schmahl, G., Corral, L., Ritterbach, J., Hasle, H., Arico, M., Biondi, A. and Niemeyer, C. M. (1999). "RAS mutations and clonality analysis in children with juvenile myelomonocytic leukemia (JMML)." Leukemia **13**(1): 32-37.

- Forbes, S. A., Beare, D., Gunasekaran, P., Leung, K., Bindal, N., Boutselakis, H., Ding, M., Bamford, S., Cole, C., Ward, S., Kok, C. Y., Jia, M., De, T., Teague, J. W., Stratton, M. R., McDermott, U. and Campbell, P. J. (2015). "COSMIC: exploring the world's knowledge of somatic mutations in human cancer." Nucleic Acids Res **43**(Database issue): D805-811.
- Fragale, A., Tartaglia, M., Wu, J. and Gelb, B. D. (2004). "Noonan syndrome-associated SHP2/PTPN11 mutants cause EGF-dependent prolonged GAB1 binding and sustained ERK2/MAPK1 activation." Hum Mutat **23**(3): 267-277.
- Friedman, J. M. (1993). Neurofibromatosis 1. GeneReviews(R). R. A. Pagon, M. P. Adam, H. H. Ardinger et al. Seattle (WA).
- Fukuda, M., Gotoh, Y. and Nishida, E. (1997). "Interaction of MAP kinase with MAP kinase kinase: its possible role in the control of nucleocytoplasmic transport of MAP kinase." EMBO J **16**(8): 1901-1908.
- Gauthier, A. S., Furstoss, O., Araki, T., Chan, R., Neel, B. G., Kaplan, D. R. and Miller, F. D. (2007). "Control of CNS cell-fate decisions by SHP-2 and its dysregulation in Noonan syndrome." Neuron **54**(2): 245-262.
- Gelb, B. D. and Tartaglia, M. (1993). Noonan Syndrome with Multiple Lentiginos. GeneReviews(R). R. A. Pagon, M. P. Adam, H. H. Ardinger et al. Seattle (WA).
- Gorski, J. A., Talley, T., Qiu, M., Puellas, L., Rubenstein, J. L. and Jones, K. R. (2002). "Cortical excitatory neurons and glia, but not GABAergic neurons, are produced in the Emx1-expressing lineage." J Neurosci **22**(15): 6309-6314.
- Gremer, L., De Luca, A., Merbitz-Zahradnik, T., Dallapiccola, B., Morlot, S., Tartaglia, M., Kutsche, K., Ahmadian, M. R. and Rosenberger, G. (2010). "Duplication of Glu37 in the switch I region of HRAS impairs effector/GAP binding and underlies Costello syndrome by promoting enhanced growth factor-dependent MAPK and AKT activation." Hum Mol Genet **19**(5): 790-802.
- Gremer, L., Merbitz-Zahradnik, T., Dvorsky, R., Cirstea, I. C., Kratz, C. P., Zenker, M., Wittinghofer, A. and Ahmadian, M. R. (2011). "Germline KRAS mutations cause aberrant biochemical and physical properties leading to developmental disorders." Hum Mutat **32**(1): 33-43.
- Gripp, K. W. (2005). "Tumor predisposition in Costello syndrome." Am J Med Genet C Semin Med Genet **137C**(1): 72-77.
- Gripp, K. W. and Lin, A. E. (1993). Costello Syndrome. GeneReviews(R). R. A. Pagon, M. P. Adam, H. H. Ardinger et al. Seattle (WA).
- Grossmann, K. S., Rosario, M., Birchmeier, C. and Birchmeier, W. (2010). "The tyrosine phosphatase Shp2 in development and cancer." Adv Cancer Res **106**: 53-89.
- Gutch, M. J., Flint, A. J., Keller, J., Tonks, N. K. and Hengartner, M. O. (1998). "The *Caenorhabditis elegans* SH2 domain-containing protein tyrosine phosphatase PTP-2 participates in signal transduction during oogenesis and vulval development." Genes Dev **12**(4): 571-585.
- Hagihara, K., Zhang, E. E., Ke, Y. H., Liu, G., Liu, J. J., Rao, Y. and Feng, G. S. (2009). "Shp2 acts downstream of SDF-1alpha/CXCR4 in guiding granule cell migration during cerebellar development." Dev Biol **334**(1): 276-284.

- Halt, A. R., Dallapiazza, R. F., Zhou, Y., Stein, I. S., Qian, H., Juntti, S., Wojcik, S., Brose, N., Silva, A. J. and Hell, J. W. (2012). "CaMKII binding to GluN2B is critical during memory consolidation." *EMBO J* **31**(5): 1203-1216.
- Hara, D., Fukuchi, M., Miyashita, T., Tabuchi, A., Takasaki, I., Naruse, Y., Mori, N., Kondo, T. and Tsuda, M. (2009). "Remote control of activity-dependent BDNF gene promoter-I transcription mediated by REST/NRSF." *Biochem Biophys Res Commun* **384**(4): 506-511.
- Hardingham, G. E., Arnold, F. J. and Bading, H. (2001). "A calcium microdomain near NMDA receptors: on switch for ERK-dependent synapse-to-nucleus communication." *Nat Neurosci* **4**(6): 565-566.
- Hardingham, G. E. and Bading, H. (2010). "Synaptic versus extrasynaptic NMDA receptor signalling: implications for neurodegenerative disorders." *Nat Rev Neurosci* **11**(10): 682-696.
- Hardingham, G. E., Fukunaga, Y. and Bading, H. (2002). "Extrasynaptic NMDARs oppose synaptic NMDARs by triggering CREB shut-off and cell death pathways." *Nat Neurosci* **5**(5): 405-414.
- Hayashi, T. and Huganir, R. L. (2004). "Tyrosine phosphorylation and regulation of the AMPA receptor by SRC family tyrosine kinases." *J Neurosci* **24**(27): 6152-6160.
- Henley, J. M. and Wilkinson, K. A. (2013). "AMPA receptor trafficking and the mechanisms underlying synaptic plasticity and cognitive aging." *Dialogues Clin Neurosci* **15**(1): 11-27.
- Herbst, R., Carroll, P. M., Allard, J. D., Schilling, J., Raabe, T. and Simon, M. A. (1996). "Daughter of sevenless is a substrate of the phosphotyrosine phosphatase Corkscrew and functions during sevenless signaling." *Cell* **85**(6): 899-909.
- Hernandez-Porrás, I., Fabbiano, S., Schuhmacher, A. J., Aicher, A., Canamero, M., Camara, J. A., Cusso, L., Desco, M., Heesch, C., Mulero, F., Bustelo, X. R., Guerra, C. and Barbacid, M. (2014). "K-RasV14I recapitulates Noonan syndrome in mice." *Proc Natl Acad Sci U S A* **111**(46): 16395-16400.
- Hiramoto, R., Imamura, T., Muramatsu, H., Wang, X., Kanayama, T., Zuiki, M., Yoshida, H., Moroto, M., Fujiki, A., Chiyonobu, T., Osone, S., Ishida, H., Kojima, S. and Hosoi, H. (2015). "Serial investigation of PTPN11 mutation in nonhematopoietic tissues in a patient with juvenile myelomonocytic leukemia who was treated with unrelated cord blood transplantation." *Int J Hematol* **102**(6): 719-722.
- Hof, P., Pluskey, S., Dhe-Paganon, S., Eck, M. J. and Shoelson, S. E. (1998). "Crystal structure of the tyrosine phosphatase SHP-2." *Cell* **92**(4): 441-450.
- Husi, H., Ward, M. A., Choudhary, J. S., Blackstock, W. P. and Grant, S. G. (2000). "Proteomic analysis of NMDA receptor-adhesion protein signaling complexes." *Nat Neurosci* **3**(7): 661-669.
- Imanishi, D., Miyazaki, Y., Yamasaki, R., Sawayama, Y., Taguchi, J., Tsushima, H., Fukushima, T., Yoshida, S., Sasaki, H., Hata, T. and Tomonaga, M. (2007). "Donor-derived DNA in fingernails among recipients of allogeneic hematopoietic stem-cell transplants." *Blood* **110**(7): 2231-2234.
- Ivanova, D., Dirks, A., Montenegro-Venegas, C., Schone, C., Altrock, W. D., Marini, C., Frischknecht, R., Schanze, D., Zenker, M., Gundelfinger, E. D. and Fejtova, A. (2015). "Synaptic

activity controls localization and function of CtBP1 via binding to Bassoon and Piccolo." EMBO J **34**(8): 1056-1077.

Jopling, C., van Geemen, D. and den Hertog, J. (2007). "Shp2 knockdown and Noonan/LEOPARD mutant Shp2-induced gastrulation defects." PLoS Genet **3**(12): e225.

Jovanovic, J. N., Benfenati, F., Siow, Y. L., Sihra, T. S., Sanghera, J. S., Pelech, S. L., Greengard, P. and Czernik, A. J. (1996). "Neurotrophins stimulate phosphorylation of synapsin I by MAP kinase and regulate synapsin I-actin interactions." Proc Natl Acad Sci U S A **93**(8): 3679-3683.

Jovanovic, J. N., Czernik, A. J., Fienberg, A. A., Greengard, P. and Sihra, T. S. (2000). "Synapsins as mediators of BDNF-enhanced neurotransmitter release." Nat Neurosci **3**(4): 323-329.

Kaech, S. and Banker, G. (2006). "Culturing hippocampal neurons." Nat Protoc **1**(5): 2406-2415.

Kamiya, N., Kim, H. K. and King, P. D. (2014). "Regulation of bone and skeletal development by the SHP-2 protein tyrosine phosphatase." Bone **69**: 55-60.

Kaplan, M. S., Opitz, J. M. and Gosset, F. R. (1968). "Noonan's syndrome. A case with elevated serum alkaline phosphatase levels and malignant schwannoma of the left forearm." Am J Dis Child **116**(4): 359-366.

Ke, Y., Zhang, E. E., Hagihara, K., Wu, D., Pang, Y., Klein, R., Curran, T., Ranscht, B. and Feng, G. S. (2007). "Deletion of Shp2 in the brain leads to defective proliferation and differentiation in neural stem cells and early postnatal lethality." Mol Cell Biol **27**(19): 6706-6717.

Keilhack, H., David, F. S., McGregor, M., Cantley, L. C. and Neel, B. G. (2005). "Diverse biochemical properties of Shp2 mutants. Implications for disease phenotypes." J Biol Chem **280**(35): 30984-30993.

Kerchner, G. A. and Nicoll, R. A. (2008). "Silent synapses and the emergence of a postsynaptic mechanism for LTP." Nat Rev Neurosci **9**(11): 813-825.

Kim, H. J. and Bar-Sagi, D. (2004). "Modulation of signalling by Sprouty: a developing story." Nat Rev Mol Cell Biol **5**(6): 441-450.

Kim, J. H., Lee, H. K., Takamiya, K. and Huganir, R. L. (2003). "The role of synaptic GTPase-activating protein in neuronal development and synaptic plasticity." J Neurosci **23**(4): 1119-1124.

Kim, M. J., Dunah, A. W., Wang, Y. T. and Sheng, M. (2005). "Differential roles of NR2A- and NR2B-containing NMDA receptors in Ras-ERK signaling and AMPA receptor trafficking." Neuron **46**(5): 745-760.

Kinsler, V. A., Thomas, A. C., Ishida, M., Bulstrode, N. W., Loughlin, S., Hing, S., Chalker, J., McKenzie, K., Abu-Amero, S., Slater, O., Chanudet, E., Palmer, R., Morrogh, D., Stanier, P., Healy, E., Sebire, N. J. and Moore, G. E. (2013). "Multiple congenital melanocytic nevi and neurocutaneous melanosis are caused by postzygotic mutations in codon 61 of NRAS." J Invest Dermatol **133**(9): 2229-2236.

Kontaridis, M. I., Eminaga, S., Fornaro, M., Zito, C. I., Sordella, R., Settleman, J. and Bennett, A. M. (2004). "SHP-2 positively regulates myogenesis by coupling to the Rho GTPase signaling pathway." Mol Cell Biol **24**(12): 5340-5352.

- Krab, L. C., de Goede-Bolder, A., Aarsen, F. K., Pluijm, S. M., Bouman, M. J., van der Geest, J. N., Lequin, M., Catsman, C. E., Arts, W. F., Kushner, S. A., Silva, A. J., de Zeeuw, C. I., Moll, H. A. and Elgersma, Y. (2008). "Effect of simvastatin on cognitive functioning in children with neurofibromatosis type 1: a randomized controlled trial." *JAMA* **300**(3): 287-294.
- Kraoua, L., Journal, H., Bonnet, P., Amiel, J., Pouvreau, N., Baumann, C., Verloes, A. and Cave, H. (2012). "Constitutional NRAS mutations are rare among patients with Noonan syndrome or juvenile myelomonocytic leukemia." *Am J Med Genet A* **158A**(10): 2407-2411.
- Krapivinsky, G., Krapivinsky, L., Manasian, Y., Ivanov, A., Tyzio, R., Pellegrino, C., Ben-Ari, Y., Clapham, D. E. and Medina, I. (2003). "The NMDA receptor is coupled to the ERK pathway by a direct interaction between NR2B and RasGRF1." *Neuron* **40**(4): 775-784.
- Kraszewski, K., Mundigl, O., Daniell, L., Verderio, C., Matteoli, M. and De Camilli, P. (1995). "Synaptic vesicle dynamics in living cultured hippocampal neurons visualized with CY3-conjugated antibodies directed against the luminal domain of synaptotagmin." *J Neurosci* **15**(6): 4328-4342.
- Kratz, C. P., Franke, L., Peters, H., Kohlschmidt, N., Kazmierczak, B., Finckh, U., Bier, A., Eichhorn, B., Blank, C., Kraus, C., Kohlhase, J., Pauli, S., Wildhardt, G., Kutsche, K., Auber, B., Christmann, A., Bachmann, N., Mitter, D., Cremer, F. W., Mayer, K., Daumer-Haas, C., Nevinny-Stickel-Hinzpeter, C., Oeffner, F., Schluter, G., Gencik, M., Uberlacker, B., Lissewski, C., Schanze, I., Greene, M. H., Spix, C. and Zenker, M. (2015). "Cancer spectrum and frequency among children with Noonan, Costello, and cardio-facio-cutaneous syndromes." *Br J Cancer* **112**(8): 1392-1397.
- Kratz, C. P., Niemeyer, C. M., Castleberry, R. P., Cetin, M., Bergstrasser, E., Emanuel, P. D., Hasle, H., Kardos, G., Klein, C., Kojima, S., Sary, J., Trebo, M., Zecca, M., Gelb, B. D., Tartaglia, M. and Loh, M. L. (2005). "The mutational spectrum of PTPN11 in juvenile myelomonocytic leukemia and Noonan syndrome/myeloproliferative disease." *Blood* **106**(6): 2183-2185.
- Kratz, C. P., Rapisuwon, S., Reed, H., Hasle, H. and Rosenberg, P. S. (2011). "Cancer in Noonan, Costello, cardiofaciocutaneous and LEOPARD syndromes." *Am J Med Genet C Semin Med Genet* **157C**(2): 83-89.
- Krenz, M., Gulick, J., Osinska, H. E., Colbert, M. C., Molkenin, J. D. and Robbins, J. (2008). "Role of ERK1/2 signaling in congenital valve malformations in Noonan syndrome." *Proc Natl Acad Sci U S A* **105**(48): 18930-18935.
- Kusakari, S., Saitow, F., Ago, Y., Shibasaki, K., Sato-Hashimoto, M., Matsuzaki, Y., Kotani, T., Murata, Y., Hirai, H., Matsuda, T., Suzuki, H., Matozaki, T. and Ohnishi, H. (2015). "Shp2 in forebrain neurons regulates synaptic plasticity, locomotion, and memory formation in mice." *Mol Cell Biol* **35**(9): 1557-1572.
- Kushner, S. A., Elgersma, Y., Murphy, G. G., Jaarsma, D., van Woerden, G. M., Hojjati, M. R., Cui, Y., LeBoutillier, J. C., Marrone, D. F., Choi, E. S., De Zeeuw, C. I., Petit, T. L., Pozzo-Miller, L. and Silva, A. J. (2005). "Modulation of presynaptic plasticity and learning by the H-ras/extracellular signal-regulated kinase/synapsin I signaling pathway." *J Neurosci* **25**(42): 9721-9734.
- Lauchle, J. O., Braun, B. S., Loh, M. L. and Shannon, K. (2006). "Inherited predispositions and hyperactive Ras in myeloid leukemogenesis." *Pediatr Blood Cancer* **46**(5): 579-585.
- Lauriol, J., Jaffre, F. and Kontaridis, M. I. (2015). "The role of the protein tyrosine phosphatase SHP2 in cardiac development and disease." *Semin Cell Dev Biol* **37**: 73-81.

- Lavoie, H. and Therrien, M. (2015). "Regulation of RAF protein kinases in ERK signalling." Nat Rev Mol Cell Biol **16**(5): 281-298.
- Lazarevic, V., Pothula, S., Andres-Alonso, M. and Fejtova, A. (2013). "Molecular mechanisms driving homeostatic plasticity of neurotransmitter release." Front Cell Neurosci **7**: 244.
- Leal, G., Comprido, D. and Duarte, C. B. (2014). "BDNF-induced local protein synthesis and synaptic plasticity." Neuropharmacology **76 Pt C**: 639-656.
- Lee, B. H., Kim, J. M., Jin, H. Y., Kim, G. H., Choi, J. H. and Yoo, H. W. (2011). "Spectrum of mutations in Noonan syndrome and their correlation with phenotypes." J Pediatr **159**(6): 1029-1035.
- Lee, D. A., Portnoy, S., Hill, P., Gillberg, C. and Patton, M. A. (2005). "Psychological profile of children with Noonan syndrome." Dev Med Child Neurol **47**(1): 35-38.
- Lee, Y. S., Ehninger, D., Zhou, M., Oh, J. Y., Kang, M., Kwak, C., Ryu, H. H., Butz, D., Araki, T., Cai, Y., Balaji, J., Sano, Y., Nam, C. I., Kim, H. K., Kaang, B. K., Burger, C., Neel, B. G. and Silva, A. J. (2014). "Mechanism and treatment for learning and memory deficits in mouse models of Noonan syndrome." Nat Neurosci **17**(12): 1736-1743.
- Lepri, F., De Luca, A., Stella, L., Rossi, C., Baldassarre, G., Pantaleoni, F., Cordeddu, V., Williams, B. J., Dentici, M. L., Caputo, V., Venanzi, S., Bonaguro, M., Kavamura, I., Faienza, M. F., Pilotta, A., Stanzial, F., Faravelli, F., Gabrielli, O., Marino, B., Neri, G., Silengo, M. C., Ferrero, G. B., Torrente, I., Selicorni, A., Mazzanti, L., Digilio, M. C., Zampino, G., Dallapiccola, B., Gelb, B. D. and Tartaglia, M. (2011). "SOS1 mutations in Noonan syndrome: molecular spectrum, structural insights on pathogenic effects, and genotype-phenotype correlations." Hum Mutat **32**(7): 760-772.
- Liu, S. Q. and Cull-Candy, S. G. (2000). "Synaptic activity at calcium-permeable AMPA receptors induces a switch in receptor subtype." Nature **405**(6785): 454-458.
- Lois, C., Hong, E. J., Pease, S., Brown, E. J. and Baltimore, D. (2002). "Germline transmission and tissue-specific expression of transgenes delivered by lentiviral vectors." Science **295**(5556): 868-872.
- Lorenz, S., Petersen, C., Kordass, U., Seidel, H., Zenker, M. and Kutsche, K. (2012). "Two cases with severe lethal course of Costello syndrome associated with HRAS p.G12C and p.G12D." Eur J Med Genet **55**(11): 615-619.
- Luscher, C. and Malenka, R. C. (2012). "NMDA receptor-dependent long-term potentiation and long-term depression (LTP/LTD)." Cold Spring Harb Perspect Biol **4**(6).
- Mainberger, F., Jung, N. H., Zenker, M., Wahllander, U., Freudenberg, L., Langer, S., Berweck, S., Winkler, T., Straube, A., Heinen, F., Granstrom, S., Mautner, V. F., Lidzba, K. and Mall, V. (2013). "Lovastatin improves impaired synaptic plasticity and phasic alertness in patients with neurofibromatosis type 1." BMC Neurol **13**: 131.
- Makhinson, M., Chotiner, J. K., Watson, J. B. and O'Dell, T. J. (1999). "Adenylyl cyclase activation modulates activity-dependent changes in synaptic strength and Ca²⁺/calmodulin-dependent kinase II autophosphorylation." J Neurosci **19**(7): 2500-2510.
- Malinow, R. and Malenka, R. C. (2002). "AMPA receptor trafficking and synaptic plasticity." Annu Rev Neurosci **25**: 103-126.

- Marino, B., Digilio, M. C., Toscano, A., Giannotti, A. and Dallapiccola, B. (1999). "Congenital heart diseases in children with Noonan syndrome: An expanded cardiac spectrum with high prevalence of atrioventricular canal." *J Pediatr* **135**(6): 703-706.
- Matsubara, M., Kusubata, M., Ishiguro, K., Uchida, T., Titani, K. and Taniguchi, H. (1996). "Site-specific phosphorylation of synapsin I by mitogen-activated protein kinase and Cdk5 and its effects on physiological functions." *J Biol Chem* **271**(35): 21108-21113.
- Mazzanti, L., Cacciari, E., Cicognani, A., Bergamaschi, R., Scarano, E. and Forabosco, A. (2003). "Noonan-like syndrome with loose anagen hair: a new syndrome?" *Am J Med Genet A* **118A**(3): 279-286.
- Mozhayeva, M. G., Sara, Y., Liu, X. and Kavalali, E. T. (2002). "Development of vesicle pools during maturation of hippocampal synapses." *J Neurosci* **22**(3): 654-665.
- Nakamura, T., Gulick, J., Pratt, R. and Robbins, J. (2009). "Noonan syndrome is associated with enhanced pERK activity, the repression of which can prevent craniofacial malformations." *Proc Natl Acad Sci U S A* **106**(36): 15436-15441.
- Nava, C., Hanna, N., Michot, C., Pereira, S., Pouvreau, N., Niihori, T., Aoki, Y., Matsubara, Y., Arveiler, B., Lacombe, D., Pasmant, E., Parfait, B., Baumann, C., Heron, D., Sigaudy, S., Toutain, A., Rio, M., Goldenberg, A., Leheup, B., Verloes, A. and Cave, H. (2007). "Cardio-facio-cutaneous and Noonan syndromes due to mutations in the RAS/MAPK signalling pathway: genotype-phenotype relationships and overlap with Costello syndrome." *J Med Genet* **44**(12): 763-771.
- Neel, B. G., Gu, H. and Pao, L. (2003). "The 'Shp'ing news: SH2 domain-containing tyrosine phosphatases in cell signaling." *Trends Biochem Sci* **28**(6): 284-293.
- Niemeyer, C. M. (2014). "RAS diseases in children." *Haematologica* **99**(11): 1653-1662.
- Niihori, T., Aoki, Y., Ohashi, H., Kurosawa, K., Kondoh, T., Ishikiriya, S., Kawame, H., Kamasaki, H., Yamanaka, T., Takada, F., Nishio, K., Sakurai, M., Tamai, H., Nagashima, T., Suzuki, Y., Kure, S., Fujii, K., Imaizumi, M. and Matsubara, Y. (2005). "Functional analysis of PTPN11/SHP-2 mutants identified in Noonan syndrome and childhood leukemia." *J Hum Genet* **50**(4): 192-202.
- Noonan, J. A. (1968). "Hypertelorism with Turner phenotype. A new syndrome with associated congenital heart disease." *Am J Dis Child* **116**(4): 373-380.
- Noonan, J. A. and Kappelgaard, A. M. (2015). "The efficacy and safety of growth hormone therapy in children with noonan syndrome: a review of the evidence." *Horm Res Paediatr* **83**(3): 157-166.
- Oishi, K., Gaengel, K., Krishnamoorthy, S., Kamiya, K., Kim, I. K., Ying, H., Weber, U., Perkins, L. A., Tartaglia, M., Mlodzik, M., Pick, L. and Gelb, B. D. (2006). "Transgenic Drosophila models of Noonan syndrome causing PTPN11 gain-of-function mutations." *Hum Mol Genet* **15**(4): 543-553.
- Oishi, K., Zhang, H., Gault, W. J., Wang, C. J., Tan, C. C., Kim, I. K., Ying, H., Rahman, T., Pica, N., Tartaglia, M., Mlodzik, M. and Gelb, B. D. (2009). "Phosphatase-defective LEOPARD syndrome mutations in PTPN11 gene have gain-of-function effects during Drosophila development." *Hum Mol Genet* **18**(1): 193-201.

- Oliveira, J. B., Bidere, N., Niemela, J. E., Zheng, L., Sakai, K., Nix, C. P., Danner, R. L., Barb, J., Munson, P. J., Puck, J. M., Dale, J., Straus, S. E., Fleisher, T. A. and Lenardo, M. J. (2007). "NRAS mutation causes a human autoimmune lymphoproliferative syndrome." Proc Natl Acad Sci U S A **104**(21): 8953-8958.
- Pagani, M. R., Oishi, K., Gelb, B. D. and Zhong, Y. (2009). "The phosphatase SHP2 regulates the spacing effect for long-term memory induction." Cell **139**(1): 186-198.
- Pandit, B., Sarkozy, A., Pennacchio, L. A., Carta, C., Oishi, K., Martinelli, S., Pogna, E. A., Schackwitz, W., Ustaszewska, A., Landstrom, A., Bos, J. M., Ommen, S. R., Esposito, G., Lepri, F., Faul, C., Mundel, P., Lopez Siguero, J. P., Tenconi, R., Selicorni, A., Rossi, C., Mazzanti, L., Torrente, I., Marino, B., Digilio, M. C., Zampino, G., Ackerman, M. J., Dallapiccola, B., Tartaglia, M. and Gelb, B. D. (2007). "Gain-of-function RAF1 mutations cause Noonan and LEOPARD syndromes with hypertrophic cardiomyopathy." Nat Genet **39**(8): 1007-1012.
- Paoletti, P., Bellone, C. and Zhou, Q. (2013). "NMDA receptor subunit diversity: impact on receptor properties, synaptic plasticity and disease." Nat Rev Neurosci **14**(6): 383-400.
- Passafaro, M., Piech, V. and Sheng, M. (2001). "Subunit-specific temporal and spatial patterns of AMPA receptor exocytosis in hippocampal neurons." Nat Neurosci **4**(9): 917-926.
- Patterson, M. A., Szatmari, E. M. and Yasuda, R. (2010). "AMPA receptors are exocytosed in stimulated spines and adjacent dendrites in a Ras-ERK-dependent manner during long-term potentiation." Proc Natl Acad Sci U S A **107**(36): 15951-15956.
- Pearson, G., Robinson, F., Beers Gibson, T., Xu, B. E., Karandikar, M., Berman, K. and Cobb, M. H. (2001). "Mitogen-activated protein (MAP) kinase pathways: regulation and physiological functions." Endocr Rev **22**(2): 153-183.
- Pierpont, E. I., Pierpont, M. E., Mendelsohn, N. J., Roberts, A. E., Tworog-Dube, E. and Seidenberg, M. S. (2009). "Genotype differences in cognitive functioning in Noonan syndrome." Genes Brain Behav **8**(3): 275-282.
- Pierpont, E. I., Tworog-Dube, E. and Roberts, A. E. (2013). "Learning and memory in children with Noonan syndrome." Am J Med Genet A **161A**(9): 2250-2257.
- Prendiville, T. W., Gauvreau, K., Tworog-Dube, E., Patkin, L., Kucherlapati, R. S., Roberts, A. E. and Lacro, R. V. (2014). "Cardiovascular disease in Noonan syndrome." Arch Dis Child **99**(7): 629-634.
- Qiu, W. W., Yin, S. S. and Stucker, F. J. (1998). "Audiologic manifestations of Noonan syndrome." Otolaryngol Head Neck Surg **118**(3 Pt 1): 319-323.
- Quilliam, L. A., Khosravi-Far, R., Huff, S. Y. and Der, C. J. (1995). "Guanine nucleotide exchange factors: activators of the Ras superfamily of proteins." Bioessays **17**(5): 395-404.
- Raman, M., Chen, W. and Cobb, M. H. (2007). "Differential regulation and properties of MAPKs." Oncogene **26**(22): 3100-3112.
- Rauen, K. A. (1993). Cardiofaciocutaneous Syndrome. GeneReviews(R). R. A. Pagon, M. P. Adam, H. H. Ardinger et al. Seattle (WA).
- Rauen, K. A. (2013). "The RASopathies." Annu Rev Genomics Hum Genet **14**: 355-369.

- Rizzoli, S. O. and Betz, W. J. (2005). "Synaptic vesicle pools." Nat Rev Neurosci **6**(1): 57-69.
- Roberts, A. E., Allanson, J. E., Tartaglia, M. and Gelb, B. D. (2013). "Noonan syndrome." Lancet **381**(9863): 333-342.
- Roelofs, R. L., Janssen, N., Wingbermuhle, E., Kessels, R. P. and Egger, J. I. (2016). "Intellectual development in Noonan syndrome: a longitudinal study." Brain Behav: e00479.
- Romano, A. A., Allanson, J. E., Dahlgren, J., Gelb, B. D., Hall, B., Pierpont, M. E., Roberts, A. E., Robinson, W., Takemoto, C. M. and Noonan, J. A. (2010). "Noonan syndrome: clinical features, diagnosis, and management guidelines." Pediatrics **126**(4): 746-759.
- Rosario, M., Franke, R., Bednarski, C. and Birchmeier, W. (2007). "The neurite outgrowth multiadapter RhoGAP, NOMA-GAP, regulates neurite extension through SHP2 and Cdc42." J Cell Biol **178**(3): 503-516.
- Rose, T., Schoenenberger, P., Jezek, K. and Oertner, T. G. (2013). "Developmental refinement of vesicle cycling at Schaffer collateral synapses." Neuron **77**(6): 1109-1121.
- Runtuwene, V., van Eekelen, M., Overvoorde, J., Rehmann, H., Yntema, H. G., Nillesen, W. M., van Haeringen, A., van der Burgt, I., Burgering, B. and den Hertog, J. (2011). "Noonan syndrome gain-of-function mutations in NRAS cause zebrafish gastrulation defects." Dis Model Mech **4**(3): 393-399.
- Ryu, H. H. and Lee, Y. S. (2016). "Cell type-specific roles of RAS-MAPK signaling in learning and memory: Implications in neurodevelopmental disorders." Neurobiol Learn Mem.
- Sarkozy, A., Carta, C., Moretti, S., Zampino, G., Digilio, M. C., Pantaleoni, F., Scioletti, A. P., Esposito, G., Cordeddu, V., Lepri, F., Petrangeli, V., Dentici, M. L., Mancini, G. M., Selicorni, A., Rossi, C., Mazzanti, L., Marino, B., Ferrero, G. B., Silengo, M. C., Memo, L., Stanzial, F., Faravelli, F., Stuppia, L., Puxeddu, E., Gelb, B. D., Dallapiccola, B. and Tartaglia, M. (2009). "Germline BRAF mutations in Noonan, LEOPARD, and cardiofaciocutaneous syndromes: molecular diversity and associated phenotypic spectrum." Hum Mutat **30**(4): 695-702.
- Scannevin, R. H. and Haganir, R. L. (2000). "Postsynaptic organization and regulation of excitatory synapses." Nat Rev Neurosci **1**(2): 133-141.
- Schenk, U., Menna, E., Kim, T., Passafaro, M., Chang, S., De Camilli, P. and Matteoli, M. (2005). "A novel pathway for presynaptic mitogen-activated kinase activation via AMPA receptors." J Neurosci **25**(7): 1654-1663.
- Schubbert, S., Zenker, M., Rowe, S. L., Boll, S., Klein, C., Bollag, G., van der Burgt, I., Musante, L., Kalscheuer, V., Wehner, L. E., Nguyen, H., West, B., Zhang, K. Y., Sisternans, E., Rauch, A., Niemeyer, C. M., Shannon, K. and Kratz, C. P. (2006). "Germline KRAS mutations cause Noonan syndrome." Nat Genet **38**(3): 331-336.
- Seeger, G., Yan, L., Gartner, U., Huemmeke, M., Barmashenko, G., Mittmann, T., Heumann, R. and Arendt, T. (2004). "Activation of Ras in neurons modifies synaptic vesicle docking and release." Neuroreport **15**(17): 2651-2654.
- Sharland, M., Burch, M., McKenna, W. M. and Paton, M. A. (1992). "A clinical study of Noonan syndrome." Arch Dis Child **67**(2): 178-183.

- Shaul, Y. D. and Seger, R. (2007). "The MEK/ERK cascade: from signaling specificity to diverse functions." *Biochim Biophys Acta* **1773**(8): 1213-1226.
- Shaw, A. C., Kalidas, K., Crosby, A. H., Jeffery, S. and Patton, M. A. (2007). "The natural history of Noonan syndrome: a long-term follow-up study." *Arch Dis Child* **92**(2): 128-132.
- Sheng, M. and Kim, E. (2011). "The postsynaptic organization of synapses." *Cold Spring Harb Perspect Biol* **3**(12).
- Sheng, M. and Lee, S. H. (2001). "AMPA receptor trafficking and the control of synaptic transmission." *Cell* **105**(7): 825-828.
- Shi, S., Hayashi, Y., Esteban, J. A. and Malinow, R. (2001). "Subunit-specific rules governing AMPA receptor trafficking to synapses in hippocampal pyramidal neurons." *Cell* **105**(3): 331-343.
- Shipton, O. A. and Paulsen, O. (2014). "GluN2A and GluN2B subunit-containing NMDA receptors in hippocampal plasticity." *Philos Trans R Soc Lond B Biol Sci* **369**(1633): 20130163.
- Stevenson, D., Viskochil, D. and Mao, R. (1993). Legius Syndrome. *GeneReviews*(R). R. A. Pagon, M. P. Adam, H. H. Ardinger et al. Seattle (WA).
- Stieglitz, E., Taylor-Weiner, A. N., Chang, T. Y., Gelston, L. C., Wang, Y. D., Mazor, T., Esquivel, E., Yu, A., Seepo, S., Olsen, S. R., Rosenberg, M., Archambeault, S. L., Abusin, G., Beckman, K., Brown, P. A., Briones, M., Carcamo, B., Cooper, T., Dahl, G. V., Emanuel, P. D., Fluchel, M. N., Goyal, R. K., Hayashi, R. J., Hitzler, J., Hugge, C., Liu, Y. L., Messinger, Y. H., Mahoney, D. H., Jr., Monteleone, P., Nemecek, E. R., Roehrs, P. A., Schore, R. J., Stine, K. C., Takemoto, C. M., Toretzky, J. A., Costello, J. F., Olshen, A. B., Stewart, C., Li, Y., Ma, J., Gerbing, R. B., Alonzo, T. A., Getz, G., Gruber, T. A., Golub, T. R., Stegmaier, K. and Loh, M. L. (2015). "The genomic landscape of juvenile myelomonocytic leukemia." *Nat Genet* **47**(11): 1326-1333.
- Stornetta, R. L. and Zhu, J. J. (2011). "Ras and Rap signaling in synaptic plasticity and mental disorders." *Neuroscientist* **17**(1): 54-78.
- Strullu, M., Caye, A., Lachenaud, J., Cassinat, B., Gazal, S., Fenneteau, O., Pouvreau, N., Pereira, S., Baumann, C., Contet, A., Sirvent, N., Mechinaud, F., Guellec, I., Adjaoud, D., Paillard, C., Alberti, C., Zenker, M., Chomienne, C., Bertrand, Y., Baruchel, A., Verloes, A. and Cave, H. (2014). "Juvenile myelomonocytic leukaemia and Noonan syndrome." *J Med Genet* **51**(10): 689-697.
- Sweatt, J. D. (2004). "Mitogen-activated protein kinases in synaptic plasticity and memory." *Curr Opin Neurobiol* **14**(3): 311-317.
- Tajan, M., de Rocca Serra, A., Valet, P., Edouard, T. and Yart, A. (2015). "SHP2 sails from physiology to pathology." *Eur J Med Genet* **58**(10): 509-525.
- Tartaglia, M. and Gelb, B. D. (2010). "Disorders of dysregulated signal traffic through the RAS-MAPK pathway: phenotypic spectrum and molecular mechanisms." *Ann N Y Acad Sci* **1214**: 99-121.
- Tartaglia, M., Gelb, B. D. and Zenker, M. (2011). "Noonan syndrome and clinically related disorders." *Best Pract Res Clin Endocrinol Metab* **25**(1): 161-179.
- Tartaglia, M., Martinelli, S., Stella, L., Bocchinfuso, G., Flex, E., Cordeddu, V., Zampino, G., Burgt, I., Palleschi, A., Petrucci, T. C., Sorcini, M., Schoch, C., Foa, R., Emanuel, P. D. and Gelb, B. D.

- (2006). "Diversity and functional consequences of germline and somatic PTPN11 mutations in human disease." *Am J Hum Genet* **78**(2): 279-290.
- Tartaglia, M., Niemeyer, C. M., Fragale, A., Song, X., Buechner, J., Jung, A., Hahlen, K., Hasle, H., Licht, J. D. and Gelb, B. D. (2003). "Somatic mutations in PTPN11 in juvenile myelomonocytic leukemia, myelodysplastic syndromes and acute myeloid leukemia." *Nat Genet* **34**(2): 148-150.
- Tartaglia, M., Pennacchio, L. A., Zhao, C., Yadav, K. K., Fodale, V., Sarkozy, A., Pandit, B., Oishi, K., Martinelli, S., Schackwitz, W., Ustaszewska, A., Martin, J., Bristow, J., Carta, C., Lepri, F., Neri, C., Vasta, I., Gibson, K., Curry, C. J., Sigüero, J. P., Digilio, M. C., Zampino, G., Dallapiccola, B., Bar-Sagi, D. and Gelb, B. D. (2007). "Gain-of-function SOS1 mutations cause a distinctive form of Noonan syndrome." *Nat Genet* **39**(1): 75-79.
- Tartaglia, M., Zampino, G. and Gelb, B. D. (2010). "Noonan syndrome: clinical aspects and molecular pathogenesis." *Mol Syndromol* **1**(1): 2-26.
- Terashima, A., Cotton, L., Dev, K. K., Meyer, G., Zaman, S., Duprat, F., Henley, J. M., Collingridge, G. L. and Isaac, J. T. (2004). "Regulation of synaptic strength and AMPA receptor subunit composition by PICK1." *J Neurosci* **24**(23): 5381-5390.
- Thomas, G. M. and Huganir, R. L. (2004). "MAPK cascade signalling and synaptic plasticity." *Nat Rev Neurosci* **5**(3): 173-183.
- Tian, X., Gotoh, T., Tsuji, K., Lo, E. H., Huang, S. and Feig, L. A. (2004). "Developmentally regulated role for Ras-GRFs in coupling NMDA glutamate receptors to Ras, Erk and CREB." *EMBO J* **23**(7): 1567-1575.
- Tidyman, W. E. and Rauen, K. A. (2009). "The RASopathies: developmental syndromes of Ras/MAPK pathway dysregulation." *Curr Opin Genet Dev* **19**(3): 230-236.
- Torii, S., Nakayama, K., Yamamoto, T. and Nishida, E. (2004). "Regulatory mechanisms and function of ERK MAP kinases." *J Biochem* **136**(5): 557-561.
- Traynelis, S. F., Wollmuth, L. P., McBain, C. J., Menniti, F. S., Vance, K. M., Ogden, K. K., Hansen, K. B., Yuan, H., Myers, S. J. and Dingledine, R. (2010). "Glutamate receptor ion channels: structure, regulation, and function." *Pharmacol Rev* **62**(3): 405-496.
- Trifilieff, P., Calandrea, L., Herry, C., Mons, N. and Micheau, J. (2007). "Biphasic ERK1/2 activation in both the hippocampus and amygdala may reveal a system consolidation of contextual fear memory." *Neurobiol Learn Mem* **88**(4): 424-434.
- Trifilieff, P., Herry, C., Vanhoutte, P., Caboche, J., Desmedt, A., Riedel, G., Mons, N. and Micheau, J. (2006). "Foreground contextual fear memory consolidation requires two independent phases of hippocampal ERK/CREB activation." *Learn Mem* **13**(3): 349-358.
- Trovo-Marqui, A. B. and Tajara, E. H. (2006). "Neurofibromin: a general outlook." *Clin Genet* **70**(1): 1-13.
- Tsuriel, S., Geva, R., Zamorano, P., Dresbach, T., Boeckers, T., Gundelfinger, E. D., Garner, C. C. and Ziv, N. E. (2006). "Local sharing as a predominant determinant of synaptic matrix molecular dynamics." *PLoS Biol* **4**(9): e271.

- van der Burgt, I., Thoonen, G., Roosenboom, N., Assman-Hulsmans, C., Gabreels, F., Otten, B. and Brunner, H. G. (1999). "Patterns of cognitive functioning in school-aged children with Noonan syndrome associated with variability in phenotypic expression." *J Pediatr* **135**(6): 707-713.
- van der Vaart, T., Plasschaert, E., Rietman, A. B., Renard, M., Oostenbrink, R., Vogels, A., de Wit, M. C., Descheemaeker, M. J., Vergouwe, Y., Catsman-Berrevoets, C. E., Legius, E., Elgersma, Y. and Moll, H. A. (2013). "Simvastatin for cognitive deficits and behavioural problems in patients with neurofibromatosis type 1 (NF1-SIMCODA): a randomised, placebo-controlled trial." *Lancet Neurol* **12**(11): 1076-1083.
- Vara, H., Onofri, F., Benfenati, F., Sassoe-Pognetto, M. and Giustetto, M. (2009). "ERK activation in axonal varicosities modulates presynaptic plasticity in the CA3 region of the hippocampus through synapsin I." *Proc Natl Acad Sci U S A* **106**(24): 9872-9877.
- Vashishta, A., Habas, A., Pruunsild, P., Zheng, J. J., Timmusk, T. and Hetman, M. (2009). "Nuclear factor of activated T-cells isoform c4 (NFATc4/NFAT3) as a mediator of antiapoptotic transcription in NMDA receptor-stimulated cortical neurons." *J Neurosci* **29**(48): 15331-15340.
- Verhoeven, W., Wingbermuhle, E., Egger, J., Van der Burgt, I. and Tuinier, S. (2008). "Noonan syndrome: psychological and psychiatric aspects." *Am J Med Genet A* **146A**(2): 191-196.
- Vetter, I. R. and Wittinghofer, A. (2001). "The guanine nucleotide-binding switch in three dimensions." *Science* **294**(5545): 1299-1304.
- von Kriegsheim, A., Baiocchi, D., Birtwistle, M., Sumpton, D., Bienvenut, W., Morrice, N., Yamada, K., Lamond, A., Kalna, G., Orton, R., Gilbert, D. and Kolch, W. (2009). "Cell fate decisions are specified by the dynamic ERK interactome." *Nat Cell Biol* **11**(12): 1458-1464.
- Voronin, L. L. and Cherubini, E. (2004). "'Deaf, mute and whispering' silent synapses: their role in synaptic plasticity." *J Physiol* **557**(Pt 1): 3-12.
- Wakioka, T., Sasaki, A., Kato, R., Shouda, T., Matsumoto, A., Miyoshi, K., Tsuneoka, M., Komiya, S., Baron, R. and Yoshimura, A. (2001). "Sprad is a Sprouty-related suppressor of Ras signalling." *Nature* **412**(6847): 647-651.
- Wennerberg, K., Rossman, K. L. and Der, C. J. (2005). "The Ras superfamily at a glance." *J Cell Sci* **118**(Pt 5): 843-846.
- West, A. E., Griffith, E. C. and Greenberg, M. E. (2002). "Regulation of transcription factors by neuronal activity." *Nat Rev Neurosci* **3**(12): 921-931.
- Wey, M., Lee, J., Jeong, S. S., Kim, J. and Heo, J. (2013). "Kinetic mechanisms of mutation-dependent Harvey Ras activation and their relevance for the development of Costello syndrome." *Biochemistry* **52**(47): 8465-8479.
- Wiegert, J. S. and Bading, H. (2011). "Activity-dependent calcium signaling and ERK-MAP kinases in neurons: a link to structural plasticity of the nucleus and gene transcription regulation." *Cell Calcium* **49**(5): 296-305.
- Wood, A., Massarano, A., Super, M. and Harrington, R. (1995). "Behavioural aspects and psychiatric findings in Noonan's syndrome." *Arch Dis Child* **72**(2): 153-155.

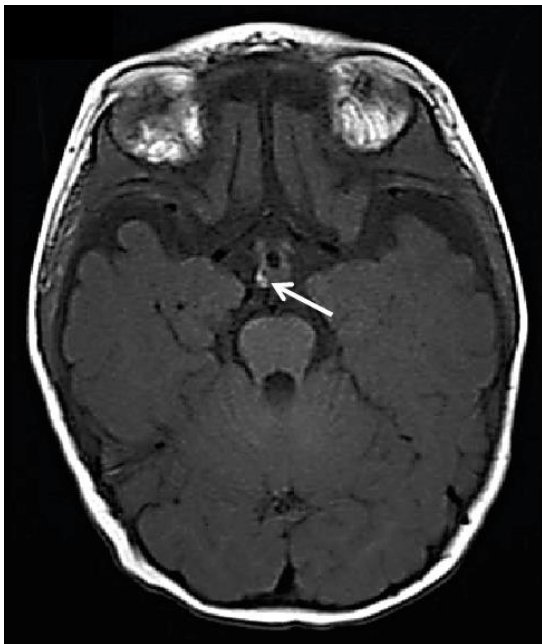
- Wu, G. Y., Deisseroth, K. and Tsien, R. W. (2001a). "Activity-dependent CREB phosphorylation: convergence of a fast, sensitive calmodulin kinase pathway and a slow, less sensitive mitogen-activated protein kinase pathway." Proc Natl Acad Sci U S A **98**(5): 2808-2813.
- Wu, G. Y., Deisseroth, K. and Tsien, R. W. (2001b). "Spaced stimuli stabilize MAPK pathway activation and its effects on dendritic morphology." Nat Neurosci **4**(2): 151-158.
- Wu, X., Simpson, J., Hong, J. H., Kim, K. H., Thavarajah, N. K., Backx, P. H., Neel, B. G. and Araki, T. (2011). "MEK-ERK pathway modulation ameliorates disease phenotypes in a mouse model of Noonan syndrome associated with the Raf1(L613V) mutation." J Clin Invest **121**(3): 1009-1025.
- Xiang, G., Pan, L., Xing, W., Zhang, L., Huang, L., Yu, J., Zhang, R., Wu, J., Cheng, J. and Zhou, Y. (2007). "Identification of activity-dependent gene expression profiles reveals specific subsets of genes induced by different routes of Ca(2+) entry in cultured rat cortical neurons." J Cell Physiol **212**(1): 126-136.
- Yamamoto, G. L., Agüena, M., Gos, M., Hung, C., Pilch, J., Fahiminiya, S., Abramowicz, A., Cristian, I., Buscarilli, M., Naslavsky, M. S., Malaquias, A. C., Zatz, M., Bodamer, O., Majewski, J., Jorge, A. A., Pereira, A. C., Kim, C. A., Passos-Bueno, M. R. and Bertola, D. R. (2015). "Rare variants in SOS2 and LZTR1 are associated with Noonan syndrome." J Med Genet **52**(6): 413-421.
- Ye, X. and Carew, T. J. (2010). "Small G protein signaling in neuronal plasticity and memory formation: the specific role of ras family proteins." Neuron **68**(3): 340-361.
- Zenker, M. (2011). "Clinical manifestations of mutations in RAS and related intracellular signal transduction factors." Curr Opin Pediatr **23**(4): 443-451.
- Zenker, M., Lehmann, K., Schulz, A. L., Barth, H., Hansmann, D., Koenig, R., Korinthenberg, R., Kreiss-Nachtsheim, M., Meinecke, P., Morlot, S., Mundlos, S., Quante, A. S., Raskin, S., Schnabel, D., Wehner, L. E., Kratz, C. P., Horn, D. and Kutsche, K. (2007). "Expansion of the genotypic and phenotypic spectrum in patients with KRAS germline mutations." J Med Genet **44**(2): 131-135.
- Zhou, L., Talebian, A. and Meakin, S. O. (2015). "The signaling adapter, FRS2, facilitates neuronal branching in primary cortical neurons via both Grb2- and Shp2-dependent mechanisms." J Mol Neurosci **55**(3): 663-677.
- Zhu, J. J., Qin, Y., Zhao, M., Van Aelst, L. and Malinow, R. (2002). "Ras and Rap control AMPA receptor trafficking during synaptic plasticity." Cell **110**(4): 443-455.

5.2. Online references

- NSEuroNet Database, European Network on Noonan syndrome and Related Disorders: <https://nseuro.net.com/php/index.php>
- COSMIC, Catalogue of somatic mutations in cancer (Forbes et al. 2015): <http://cancer.sanger.ac.uk/cosmic>
- LightCycler480 instrument, instructions, and applications: www.lightcycler.com
- Clinical trials: <https://clinicaltrials.gov/>

6. Supplements

6.1. Supplementary figure



Supplementary Figure 6.1: Brain MRI scan of patient 12 at the age of 8 months. The lesion of 0.8 x 0.7 x 0.6 cm in the hypothalamus is depicted by the white arrow. This figure is adopted from Altmüller et al. (2017a).

6.2. Supplementary table

Supplementary Table 6.1: Frequency of clinical findings in patients with a *NRAS* mutation

	Cirstea, 2010	Runtuwene, 2011	Digilio, 2011	Denayer, 2012	Kraoua, 2012	Ekvall, 2015	Present Study	Total	%
Males/Females	3/2	1/0	0/1	4/3	1/1	1/1	9/10	19/18	
Median age (in years)	14	30	2	20	10,5	45	7,1	14	
Prenatal abnormalities	3/5	ND	0/1	ND	2/2	0/2	10/14	15/24	63
Polyhydramnios	2/5	ND	0/1	ND	1/2	0/2	7/14	10/24	42
Nuchal edema	1/5	ND	0/1	ND	0/2	0/2	3/14	4/24	17
Fetal chylothorax/hydrops	0/5	ND	0/1	ND	0/2	0/2	3/14	3/24	13
Feeding difficulties	ND	ND	0/1	1/7	2/2	ND	5/14	8/24	33
Cardiac anomaly	3/5	0/1	1/1	1/7	1/2	2/2	11/18	19/36	53
PST	2/5	0/1	1/1	0/7	1/2	0/2	1/18	5/36	14
ASD/VSD	0/5	0/1	0/1	0/7	0/2	1/2	3/18	4/36	11
HCM	2/5	0/1	1/1	0/7	0/2	1/2	6/18	10/36	28
Acquired lymphatic disorder	0/5	ND	ND	ND	ND	ND	0/18	0/23	0
Short stature	3/5	1/1	1/1	4/7	1/2	0/2	5/16	15/33	45
Motor delay	5/5	ND	1/1	1/2	1/2	ND	6/14	14/24	58
Intellectual/learning disabilities	2/5	1/1	0/1	0/7	0/2	0/2	6/13	9/31	29
Cryptorchidism in males	2/3	1/1	NA	2/2	0/1	0/1	5/8	10/16	63
Curly Hair	3/5	ND	0/1	ND	1/2	1/2	2/16	7/26	27
Keratosis pilaris	4/5	ND	0/1	ND	1/2	0/2	4/17	9/27	33
Scoliosis	1/5	ND	ND	ND	1/2	ND	0/17	2/24	8
Pectus deformity	4/5	1/1	1/1	2/7	2/2	0/2	6/18	16/36	44
Short/broad/webbed neck	4/5	1/1	1/1	2/2	2/2	2/2	16/17	28/30	93
Ocular ptosis	1/5	ND	0/1	ND	2/2	0/2	14/18	17/28	61
Bleeding diathesis	0/5	ND	ND	2/7	1/2	1/2	3/16	7/32	22
Neoplasia (benign and malignant)	0/5	0/1	0/1	0/7	0/2	0/2	2/17	2/35	6

Previously reported individuals with *NRAS* mutation-associated Noonan syndrome include patients reported by Cirstea et al. (2010)(n=5), Runtuwene et al. (2011) (n=1), Digilio et al. (2011) (n=1), Denayer et al. (2012) (n=7), Kraoua et al. (2012) (n=2), and Ekvall et al. (2015) (n=2). ASD: atrial septal defect; HCM: hypertrophic cardiomyopathy; ND: no data; PST: pulmonary/pulmonary valve stenosis; VSD: ventricular septal defect. This table is adopted from (Altmüller et al. 2017a).

6.3. List of abbreviations

°C	degree Celsius	csw	Corkscrew
+	present	CTRL	control
-	absent	CtBP1	C-terminal Binding Protein 1
%	Percent	DAPI	4',6-Diamidin-2-phenylindol
A	Adenine	DIV	days <i>in vitro</i>
4AP	4-Aminopyridine	DMEM	Dulbecco's Modified Eagle Medium
ACSF	Artificial cerebrospinal fluid	DMSO	Dimethyl sulfoxide
AKT	Protein kinase B	EGF	Epidermal growth factor
ALPS	Autoimmune lymphoproliferative syndrome	EGFP	Enhanced green fluorescent protein
AMPA	α -amino-3-hydroxy-5-methyl-4- isoxazolepropionic acid receptor	ERK	Extracellular signal-regulated kinase
APV	(2R)-amino-5-phosphonovaleric acid	FA	fetal ascites
AraC	Cytosine β -D-arabinofuranoside	FCS	Fetal calf serum
ASD	Atrial septal defect	f	female
AVS	atrial valve stenosis	FRS2	fibroblast growth factor receptor substrate 2
bp	base pairs	Fwd	forward
BDNF	Brain derived neurotrophic factor	G	Guanine
Bic	Bicuculline	g	gravitational force
BSA	Bovine serum albumin	GAB1	GRB2-associated binding protein
C	Cytosine	GAD65	Glutamate decarboxylase 65
CaS	Café au lait spots	GAP	GTPase-activating protein
CaMKII	Ca ²⁺ /Calmodulin-dependent protein kinase II	GFP	Green fluorescent protein
cAMP	cyclic adenosine monophosphate	GDP	Guanosin diphosphate
CFCS	Cardiofaciocutaneous syndrome	GH	Growth hormone
CH	curly hair	GluA1	Glutamate-binding AMPA receptor subunit 1
CNS	Central nervous system	GluA2	Glutamate-binding AMPA receptor subunit 2
Cond.	Conditional	GluN1	Glutamate-binding NMDA receptor subunit 1
Const.	Constitutive	GluN2A	Glutamate-binding NMDA receptor subunit 2B
CREB	cAMP response element-binding protein	GluN2B	Glutamate-binding NMDA receptor subunit 2B
C-SH2	C-terminal Src homology 2	GOF	Gain of function
CS	Costello syndrome	GTP	Guanosine triphosphate
CSK	C-terminal Src kinase		

gr	Gramm	MEK	Mitogen-activated protein kinase kinase
GRB2	Growth factor receptor-bound protein 2	MD	motor delay
h	hour	min	Minutes
HA	haemangioma	ML	multiple lentigines
HBSS	Hank's balanced salt solution	ml	Milliliter
HCM	Hypertrophic cardiomyopathy	μl	Microliter
HD	prenatal heart defect	μM	micromolar
HF	hydrops fetalis	μm	Micrometer
HRAS	v-Ha-ras Harvey rat sarcoma viral oncogene homolog	MN	multiple nevi
HVR	Hypervariable region	mo	month
ID (m)	intellectual disability (mild)	MS	Microsoft
ID (s)	intellectual disability (severe)	MSK	mitogen- and stress-activated kinase
IEGs	immediate early genes	mTOR	mammalian Target of Rapamycin
IF	Immunofluorescence	MVP	mitral valve
IGF1	Insulin-like growth factor 1	n	number
IQ	Intelligence quotient	NA	not applicable
IRS1	Insulin receptor substrate1	nCT	neonatal chylothorax
IUFD	intrauterine fetal death	ND	No data
JAK/STAT	Janus Kinase/Signal Transducer and Activator of Transcription	NE	fetal nuchal edema
JMML	Juvenile myelomonocytic leukemia	NF1	Neurofibromatosis type 1
JNK	c-Jun N-terminal Kinase	nLE	neonatal lymphatic edema
KCl	Potassium Chloride	NMDA	N-methyl-D-aspartic acid
KI	knock in	NRAS	Neuroblastoma Rat sarcoma viral oncogene homolog
KO	knock out	N-SH2	N-terminal Src homology 2
KP	keratosis pilaris	NS	Noonan syndrome
KRAS	V-Ki-ras2 Kirsten rat sarcoma viral oncogene homolog	p	p-value
LOF	Loss of function	pl	Promoter 1
LTD	Long-term depression	pll	Promoter 2
LTP	Long-term potentiation	pat. Inherit	paternally inherited
m	male	panGluA	Antibody recognizing all GluA receptor subunits
mat. Inherit	maternally inherited	PBS	Phosphate buffered saline
MAP2	Microtubule-associated protein2	PDA	persistent ductus arteriosus
MAPK	Mitogen-activated protein kinase	PDGFR	Platelet-derived growth factor receptor

PE	fetal pleural effusions	ST	strabismus
PFA	Paraformaldehyde	SV	Synaptic vesicle
PH	polyhydramnios	SW I	Switch I region
PI3K	Phosphatidylinositol-4,5- bisphosphate 3-kinase	SW II	Switch II region
PICK1	Protein Interacting with C Kinase-1	T	Thymine
P-L	P-Loop	TH	thorax anomaly
PTK	Protein tyrosine kinase	TRP	Total recycling pool
P/S	Penicillin-Streptomycin- Fungizone antibiotic- antimycotic solution	VM	ventriculomegaly
PST	pulmonary/pulmonary valve stenosis	VSD	ventricular septal defect
PT	ocular ptosis	VW	von Willebrand syndrome
PTP	Protein tyrosine phosphatase	WT	wild type
ptp-2	<i>PTPN11</i> -orthologue in worms	WH	wooly hair
<i>PTPN11</i>	Tyrosine-protein phosphatase non-receptor type 11	y	year(s)
Ras	Rat sarcoma protein		
RE	refractive error		
rev	reverse		
ROCK	Rho-associated Kinase		
RP	Recycling pool		
RRP	Readily releasable pool		
RSK	p90 ribosomal s6 kinase		
RTK	Receptor Tyrosine Kinase		
SE	sparse eyebrows		
SEM	Standard Error of the Mean		
SDS	Sodium dodecyl sulfate		
sec	seconds		
SNPs	Single nucleotide polymorphisms		
SH	sparse hair		
SH2	Src homology 2		
SHP2	Protein encoded by <i>PTPN11</i>		
SN	short neck /webbed neck		
SRC	Sarcoma proto-oncogene tyrosine kinase		

6.4. List of Publications

Parts of this thesis were published in the following articles:

Altmüller, F.*, Lissewski, C.*, Bertola, D., Flex, E., Stark, Z., Spranger, S., Baynam, G., Buscarilli de Moraes, M., Dyack, S., Gillis, J., Yntema, H.G., Pantaleoni, F., van Loon, R.L.E., MacKay, S., Mina, K., Schanze, I., Tan, T.Y., Walsh, M., White, S.M., Niewisch, M.R., García-Miñaur, S., Plaza, D., Ahmadian, M.R., Cavé, H., Tartaglia, M., Zenker, M. (2017) “Genotype and phenotype spectrum of NRAS germline variants.” *European Journal of Human Genetics*; advanced online publication on May 3rd 2017, *shared first authorship

Altmüller, F.*, Pothula, S.*, Annamneedi, A., Montenegro-Venegas, C., Nakhei-Rad, S., Pina-Fernández, E., Marini, C., Santos, M., Schanze, D., Ahmadian, M.R., Montag, D., Stork, O., Zenker, M., Fejtova, A. (2017) “Aberrant neuronal activity-induced signaling and gene expression in a mouse model of RASopathy.” *PLoS Genet* 13(3): e1006684. <https://doi.org/10.1371/journal.pgen.1006684>; published on March 27th 2017, *shared first authorship

Former publication:

Damman, G.*, Teschler, S.*, Haag, T.*, **Altmüller, F.***, Tuzek, F., und Damman, R. H. (2011) “Increased DNA methylation of neuropsychiatric genes occurs in borderline personality disorder.” *Epigenetics* 6: 12, 1454-1462; <http://dx.doi.org/10.4161/epi.6.12.18363>; published on December 1st 2011, *shared first authorship

6.5. Erklärung zur eigenständigen Verfassung der Arbeit

Hiermit erkläre ich, dass ich die von mir eingereichte Dissertation zu dem Thema “ Variability and Pathogenesis of Neurodevelopmental Deficits in Noonan Syndrome” selbständig verfasst, nicht schon als Dissertation verwendet habe und die benutzten Hilfsmittel und Quellen vollständig angegeben wurden.

Weiterhin erkläre ich, dass ich weder diese noch eine andere Arbeit zur Erlangung des akademischen Grades doctor rerum naturalium (Dr. rer. nat.) an anderen Einrichtungen eingereicht habe.

Magdeburg, den 19. Mai 2017

M. Sc. Franziska Altmüller